DESIGN & FABRICATION OF MICROFLUIDIC DNA EXTRACTION DEVICE FOR WATER QUALITY MONITORING

DESIGN & FABRICATION OF MICROFLUIDIC DNA EXTRACTION DEVICE FOR WATER QUALITY MONITORING

By

Bo Dang, B.ENG.

B. Eng. (McMaster University, Ontario, Canada)

A Thesis

Submitted to the School of Graduate Studies

In Partial Fulfillment of the Requirements

For the Degree

Master of Applied Science

McMaster University

MASTER OF APPLIED SCIENCE (2012) McMaster University

(Mechanical Engineering) Hamilton, Ontario, Canada

TITLE	DESIGN & FABRICATION OF A MICROFLUIDIC DNA EXTRACTION DEVICE FOR WATER QUALITY MONITORING
AUTHOR	Bo Dang, B.Eng.
SUPERVISOR	Professor P. R. Selvaganapathy Department of Mechanical Engineering
NUMBER OF PAGES	XIX, 119

ABSTRACT

Continuous monitoring of pathogens that may be present in water is one of the key preventive measures that can be used in rural areas of developed countries and developing countries to reduce chances of the water borne diseases outbreak. Off-site testing of microbiological contamination of water is conventionally done for monitoring water quality. However, such a process is time consuming and involves using a variety of hazardous reagents. To address these issues, a portable device for rapid detection of unsafe water is needed.

One of the key components in this system is to extract DNA from the pathogens. The primary consideration for DNA extraction is to separate DNA from proteins and other cell debris in the lysate solution. The pure population of DNA molecules are then sent downstream for subsequent processing such as real-time PCR (Polymerase Chain Reaction) and BioFET sensors for further identification and analysis.

The focus of the thesis will be on the fabrication of a microfluidic DNA extraction system that can achieve high DNA extraction efficiency and a good repeatability. It can also be easily automated, and integrated with other components of the DNA analysis system. The high surface-to-volume macro/mesoporous silica DNA binding column was synthesized using sol-gel silica technology and triblock copolymer F127 was added to form a crack-free mesoporous silica network. Furthermore, a monodispersed polystyrene microspheres soft-template was assembled using a simple but novel technique that

employs controlled suction to enhance self-assembly into a periodically patterned structure in the extraction chamber/chambers. In combination of heat annealing treatment of this assembled polystyrene template, one can easily control the size of the macropores in the final macro/mesoporous silica structure to allow a lower pressure resistance for DNA sample flow at elution stage. The final macro/mesoporous silica structure synthesized using heat annealing temperature of 115^{o}C for 10 minutes was determined to have a porosity of 83.6%. Mesopores of this silica monolith was determined by BET test to be 3.65 nm and the macroporous ranging from 0.5μm to 0.86μm were observed. In addition, the fabrication of porous silica monolith can be easily integrated with the microfluidic system for achieving DNA extraction purposes

ACKNOWLEDGMENTS

Foremost, I would like to express my sincere gratitude to my supervisor, Dr. P. Ravi Selvaganapathy, for giving me the opportunity to be involved in such an interesting topic of research. I would like to thank him for his patience, enthusiasm and continuous support of my research. Dr. Ravi has been nothing short of a great mentor to me, offering his excellent guidance throughout the intricacies of this research. I am deeply grateful for his phenomenal assistance and feel very fortunate to have been paired with such an outstanding faculty member. Next, I would like to thank Dr. C. Y. Ching for his critical comments and suggestions that helped me overcome many difficulties in my research.

I thank my fellow labmates in Center for Advanced Micro-Electro-Fluidics laboratory: Leo Hsu, Wen-I Wu, Pouya Rezai for the stimulating discussions and invaluable assistances. Shehad, Ali, and Peter for the sleepless night we were working together before deadlines. Also, big thanks to Siawash, Chao, Russel, Reza for providing an engaging and fun working environment. Additionally, I would like to thank Doris Stevanovic, Zhilin Peng, Jingfeng Yang from CEDT and Ron Lodewyks, Mark Mackenzie, Jim McLaren and Joe Verhaeghe from Mechanical Engineering machine shop for providing valuable help and suggestions.

I would like to thank Fangfang Zhang, Hanjiang Dong, Jim Garrett, Hongyu Lu, Yujie Zhu, Songtao Yang, Yuguo Cui, Wenhe Gong, Jieyi Liu for their help on my research, and I would also like to thank my friend Rahul Sadavarte, who has been an

extraordinary help by providing me feedback in the thesis process. I am humbled by his intelligence and generosity and appreciate the wisdom he shared.

Last but not least, I would like to thank my family, my parents for their love, support, encouragement and advice. You have always been there for me, and I am forever in your debt.

ABBREVIATIONS

µTAS	Miniaturized Total Analysis Systems
AAO	Anodic Aluminum Oxide
BET	Brunauer, Emmett and Teller
BPO	Benzoyl Peroxide
BSA	Bovine Serum Albumin
CsCl	Cesium Chloride
DEAE	Diethylaminoethanol
DLS	Dynamic Light Scattering
DNA	Deoxyribonucleic acid
DRIE	Deep Reactive Ion Etching
EDX	Energy Dispersive X-ray
E.coli	Escherichia coli
F127	Pluronic F127
FISH	Fluorescent in situ Hybridization

GuSCN	Guanidine Thiocyanate
IUPAC	International Union of Pure and Applied Chemistry
LOAC/LoC	Lab-On-A-Chip
NFSTC	National Forensic Science Technology Center
PC	Polycarbonate
PCR	Polymerase Chain Reaction
PCTE	Polycarbonate Track Etch
PDMS	Polydimethylsiloxane
PoC	Point-of-Care
PS	Polystyrene
PVP	Polyvinylpyrrolidone
RNA	Ribonucleic acid
SBA	Santa Barbara Amorphous
SEM	Scanning Electron Microscopy
SPE	Solid Phase Extraction
ssDNA	Single Stranded DNA

TEOS	Tetraethyl Orthosilicate
TGA	Thermogravimetric Analysis
TMOS	Tetramethyl Orthosilicate

TABLE OF CONTENTS

LIST OF FIGURES

LIST OF TABLES

Chapter 1 Motivation & Organization

1.1Motivation

Former Secretary-General of the United Nations Kofi Annan stated in a press release for the World Environment Day in 2003 that "Water related diseases are responsible for 80% of all diseases and deaths in developing countries" [1]. Based on another research done by *Prüss et al.* from the World Health Organization in 2002, waterborne diseases cause an estimated 4% of all deaths and 5.7% of the total disease burden worldwide [2]. Although developing countries account for a major portion of those statistics, developed countries are not immune to these infections either. Examples of water borne disease outbreak in developed countries include the Milwaukee, Wisconsin *Cryptosporidium parvum* outbreak in 1993 [3]and the Walkerton, Ontario *Escherichia coli* outbreak in 2000 [4]. It indicates the importance of continuously monitoring water quality as one of the key preventive measures for water treatment process.

Continuous monitoring of pathogens that may be present in water can effectively reduce chance of water borne disease outbreak in rural areas of developed countries and developing countries. This preventive measure is generally accomplished by off-site testing of microbiological contamination of water. However, such processes require centralized laboratories for analyses. The time delay associated with this procedure is

frequently unacceptable. To address this issue, a portable and low-cost device for rapid detection of unsafe water on-site is needed.

Conventional monitoring of water for many different human pathogens can be done using culture methods, but it is time consuming (at least 48 hours [5]), labour intensive and cannot be used for the detection of active but nonculturable cells [6]. In contrast, molecular techniques, especially nucleic acid-based methods are able to detect pathogens or microorganisms with high sensitivity and within a few hours of time frame [6]. Microfluidic platform provides precise sampling control, parallel fabrication for low-cost manufacturing process, and has been proven to be an ideal technology for miniaturization of biological assays. In this case, a microfluidic nucleic acid diagnostic/monitoring device will have the capability to continuously accumulate and collect pathogen samples from water and quantitatively detect their presence. As shown in Figure 1-1, the system starting from the sample preparation step, filters out unwanted particles/cells and increases the concentration of the target pathogens or indicator organisms such as *E. coli* from a 100ml water sample, and all target organisms are collected in 1ml of solution and send to the lysis stage to release the nucleic acid from the cells into the lysate solution, 10μl of lysate collected from lysis stage will be used in DNA extraction device and nucleic acid will then be isolated from proteins and other cell debris. Polymerase Chain Reaction (PCR) will be carried out in the amplification stage in order to achieve the desired concentration for detection. Finally, the identification of the nucleic acid will be done by using a biosensor. All individual components are connected

through microfluidic channels and flow control will be achieved by a micropump or external pneumatic system.

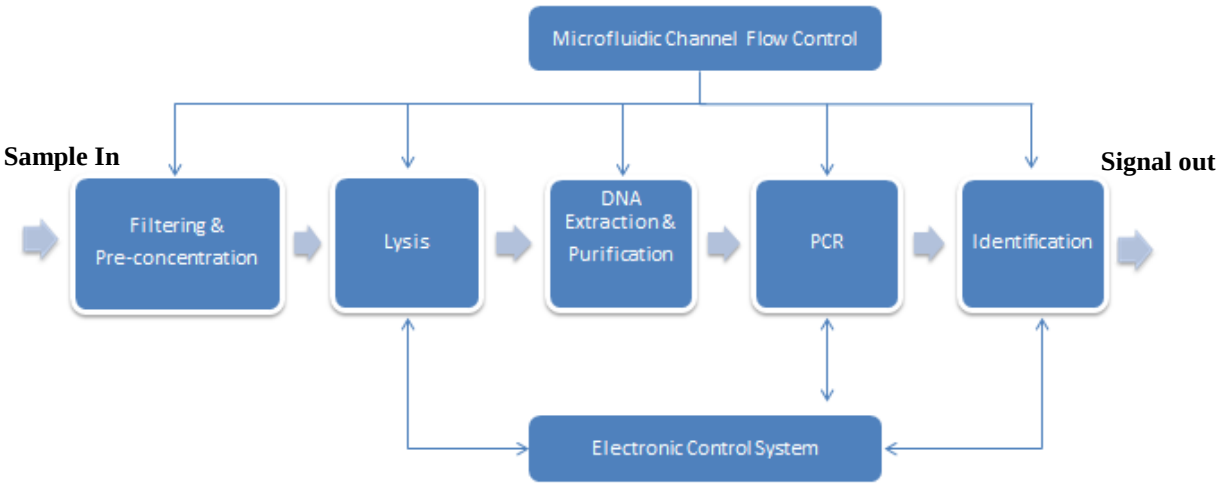

Figure 1-1 Block diagram for components of a microfluidic diagnostic/monitoring device

One of the key components in this system is the DNA extraction and purification device. The presence of lipids, proteins and other cell debris in lysate will interfere with the operation of the biosensor downstream and lead to erroneous results. Thus the primary consideration for DNA extraction is to separate nucleic acid from proteins, lipid and other cell debris after the cell lysis process. The purified sample of nucleic acid molecules where there has no humic acid contamination are then sent downstream for subsequent processing such as real-time Polymerase Chain Reaction (PCR) and BioFET sensors for further identification and analysis.

This thesis will focus on the design and engineering aspects of a microfluidic DNA extraction system. To yield high purity and efficiency of DNA for downstream

PCR application, a highly uniform macro/mesoporous silica monolith is synthesized and integrated into a single extraction chamber microfluidic device. In addition, the simple but novel suction assisted assembly approach is tested to demonstrate the feasibility of multiple chamber assembly for fabricating multiple extraction columns simultaneously.

1.2 Sequence of Chapters

The organization of the thesis is outlined as following:

Chapter 2 provides an overview that outlines the overall focus of the thesis. Following introduction of Lab-On-A-Chip microfluidic devices and their suitability for the automation and miniaturization of DNA extraction process, various traditional DNA extraction methods are reviewed and discussed. Finally, several microfluidic DNA extraction techniques that have been published in the literature are compared and weighted.

Chapter 3 presents the design of the microfluidic device for DNA extraction, brief introduction to self-assembly of polystyrene microspheres, sol-gel processes and use of polystyrene microspheres soft-template method for synthesizing a controllable macro/mesoporous silica monolith. The overall schematics for device fabrication are illustrated at the end of chapter.

Chapter 4 includes the fabrication details for using a rapid prototyping mold to make a through-hole PDMS, soft-lithography technique to create PDMS channels and the process of synthesizing monodispersed polystyrene microspheres. The procedure for

preparing polystyrene microspheres assembly template and the sol-gel matrix integration is also illustrated. Finally, the characterization of the macro/mesoporous silica monolith is presented. And the concept for simultaneous assembly in multiple chambers is demonstrated for the case where there are multiple columns in a single device.

Chapter 5 concludes the thesis by highlighting the contribution, namely, the Lab-On-A-Chip format DNA extraction chip. It also provides suggestions for future device testing and improvement.

Chapter 2 Introduction and Literature Review

2.1 Introduction

The vision of a lab-on-a-chip real time monitoring system requires integration of sample pre-concentration, cell lysis, DNA extraction, polymerase chain reaction (PCR) and detection component. DNA extraction and purification is the first step in many molecular diagnostic methods such as PCR, fluorescent in situ hybridization (FISH) and DNA microarrays [7]. It essentially determines the reliability and sensitivity of the downstream application. This thesis will focus on the DNA extraction and purification part of the overall system. Various traditional benchtop DNA extraction methods and different microfluidic technologies will be compared and evaluated in order to design and construct an automated and miniaturized system for extraction of DNA.

2.2Traditional DNA extraction methods

2.2.1 Salting-out Method

This method is based on differentially precipitating cellular components [8] due to solubility differences between nucleic acids and contaminants [9], [10] . When a high concentration of salt such as potassium acetate, lithium chloride or ammonium acetate is used, proteins and other contaminants precipitate from the cell lysate because of their lower solubility at that high salt concentration. The precipitate containing proteins can be subsequently removed by centrifugation. Finally, DNA can be recovered by using alcohol

precipitation as detailed in Section 2.2.7 of this thesis. This procedure for extracting DNA is very simple [11] however, yield and purity of extracted DNA is highly variable [12].

2.2.2 Phenol/Chloroform Extraction

Phenol/chloroform extraction protocol was first developed by *Chomczynski et al*. in 1987 [13], and it has been widely considered as a gold-standard for producing high-purity DNA [14]. Equal volume of phenol/chloroform is mixed with aqueous cell lysate, resulting in separation of upper aqueous phase and lower organic phase rich in phenol. The nucleic acid (DNA, RNA) remains in aqueous phase while protein and other cellular contaminants are denatured and become less polar, thus dissolving in the organic phase. Nucleic acids from aqueous phase can then be re-extracted by repeating the process until high-purity of DNA is obtained. Finally the DNA is isolated using alcohol precipitation. Even though the phenol/chloroform extraction method has greater than 90% recovery efficiency [15] and is very reliable for any downstream molecular diagnostic assays, it is normally limited for laboratory environment because both phenol and chloroform are hazardous. In addition, it is very labour-intensive, time consuming (roughly 2 hours process [16]) and require user expertise [14]. The miniaturization of the process using microfluidic can potentially solve all above listed disadvantages, and an existing microfluidic device using phenol/chloroform extraction principle will be reviewed in section 2.3.2.

2.2.3 Anion-Exchange

Anion exchange method for DNA extraction is based on the principle ion exchange chromatography to separate the ions and polar molecules based on differences in their charge [17] at physiologic condition. Solid phase anion exchange is performed wherein the positively charged surface molecules are attracted to the negatively charged phosphates of the nucleic acid. DNA binds to the substrate under low salt conditions, impurities such as RNA and cellular proteins are washed away using medium salt buffers [12]. High salt buffer is used to elute the DNA. Finally, DNA can be recovered from eluted solution by alcohol precipitation.

Chelex® 100 extraction is one example of the anion exchange DNA extraction technique, and it is one of the mainstays of forensic science [18]. It has been used for extracting DNA from many different type of forensic samples [19–22]. Based on the DNA Analyst Online Training manual provided by National Forensic Science Technology Center (NFSTC) in United States, this method is fast, simple, inexpensive and does not involve any harzardous chemicals. But the trade off is harsh extraction environment, faster rate of DNA degradation [23], posibility of inhibition of subsequent amplification(PCR) process and inconsistency of extraction efficiencies based on different samples and resins. Resins also can lose its chelating capability after few hours in suspension.

Another example of anion exchange resin is QIAGEN Resin. Its chemical structure is shown in Figure 2-1A. This resin is a macroporous silica material with a high

density of diethylaminoethanol (DEAE). By adjusting the salt concentration and pH conditions, the positively charged DEAE group on the surface of resin will interact differently with the negatively charged nucleic acid backbone (see Figure 2-1B) [24] thus achieving binding and elution of nucleic acids. This product developed by QIAGEN is able to deliver ultrapure, transfection grade DNA for downstream applications. However, the process is labour intensive (roughly 1 hour process based on the recommended protocol) the resin chemistry and process of binding/elution at different buffer conditions is not publicly known and so will not be considered as an suitable technology for miniaturization.

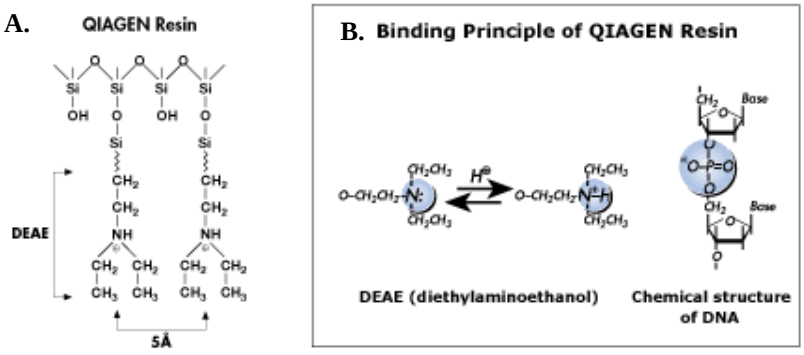

Figure 2-1 A) QIAGEN Resin Chemical Structures B) Binding principle (positively charged DEAE groups interact with negatively charged phosphate group of the DNA backbone[24]

2.2.4 Silica Beads Extraction

The chaotropic salt induced adsorption of DNA onto silica surface is sometimes referred as *Boom* method. Nucleic acid extraction was performed by activated diatomaceous earth (86% silica) absorption, as described by *Boom et al* [25] in 1991. This

method makes use of a chaotropic agent to disrupt and denature macromolecules such as proteins, while at the same time promote nucleic acids binding to silica surface [25].

Guanidine thiocyanate is the most commonly used chaotropic salt in DNA extraction process [26]. It also has the beneficial property of lysing viruses [27][28]. With the presence of high concentrations of chaotropic salts like Guanidine thiocyanate, the nucleic acids are selectively attached to the surface of silica while the cellular proteins and other debris remains in the solution and can be subsequently washed away. Ready to use DNA is then eluted from the silica column using a lower salt buffer/water, and there is no alcohol precipitation required.

The most common commercial available extraction kit is based on *Boom* extraction method where silica material is integrated with a spin column. The procedure is illustrated bellow in Figure 2-2 (NORGEN Bacterial Genomic DNA Isolation Kit), it is a three-step procedure: binding, washing and eluting. The hands on preparation time is typically 20 minutes, it is only a fraction of time spent for phenol/chloroform extraction and can yield high-purity (90-95% [29]) nucleic acid consistently and economically and no hazardous chemicals are used during the process. The only disadvantage is that the process requires laboratory centrifugation machine for binding and elution, which makes it very hard to miniaturize to a portable rapid detection device.

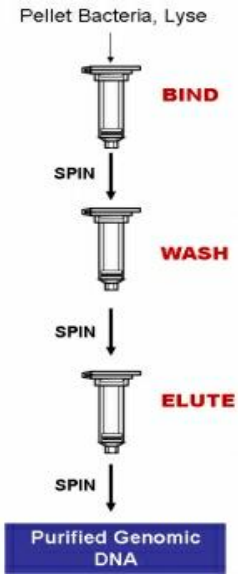

Figure 2-2 Commercial DNA extraction column extraction procedure (http://www.norgenbiotek.com)

2.2.5 Magnetic Beads Extraction

Principle of working of Magnetic Beads Extraction is same as the silica affinity extraction. The bead normally comprises of an iron oxide core with layers of silica coating on the surface as shown in Figure 2-3. The only difference between magnetic beads extraction and silica beads extraction is that there is no need of centrifugation step to separate particles and lysate solution. As shown in Figure 2-4, Magnetic force is used to separate DNA from contaminates. Only DNA binds to the silica surface of the magnetic particles, and the magnetic particles are collected along with nucleic acid. Finally the nucleic acids are extracted by standard wash and elute procedure. And 84% of recovery efficiency was reported by *Yoza et al*.[30]by using this technique.

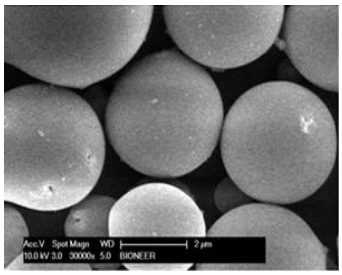

Figure 2-3 "AccuBead™ magnetic beads, silica coating of the iron oxide[31]

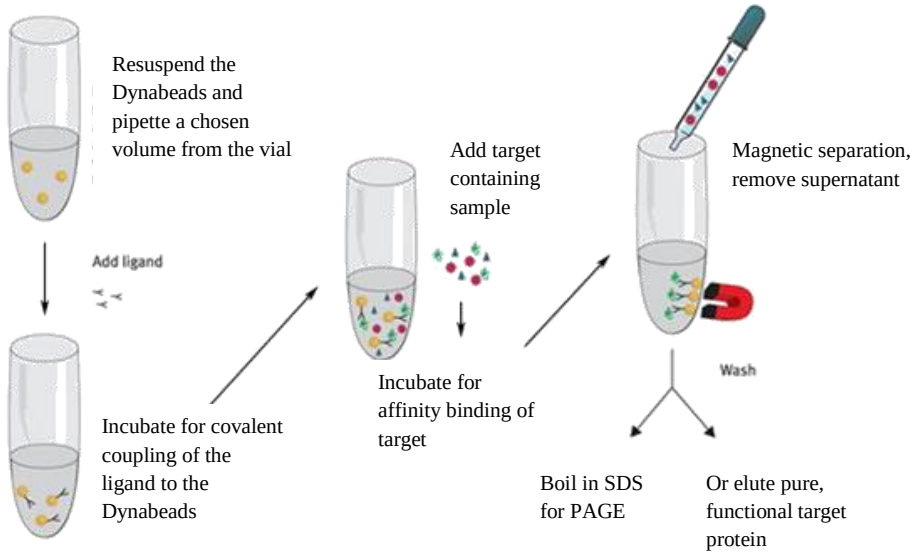

Figure 2-4 Surface-Activated Dynabeads extraction procedure[32]

2.2.6 Cesium Chloride (CsCl) Purification

Cesium chloride (CsCl) and CsTFA are used as a gradient media for density gradient ultracentrifugation to separate nucleic acids and other macromolecules [33]. DNA, RNA, proteins, and lipid have different buoyant-densities and can be separated in equilibrium buoyant-density gradients in an ultracentrifuge [34]. RNA has a high buoyant density and will pellet in CsCl gradients [35] whereas DNA band formed can be collected from the centrifuge tube and extracted by alcohol precipitation.

Despite high quality and high extraction efficiency of this method, CsCl gradient centrifugation is a labour-intensive, expensive and time consuming (up to 24-48 hours) method [36]. The relative centrifugal force (RCF) required can be up to 308,941 g-force (57,000 rpm) [37] and it is impossible to achieve based on current microfluidic technology.

2.2.7 Alcohol Precipitation of DNA

Most of bench-top DNA extraction technique list above includes an alcohol precipitation step at the end of the protocol to re-suspend nucleic acids in a more suitable buffer, solvents such as ethanol (75–80%) or isopropanol (final concentration of 40–50%) are commonly used in the presence of salt to precipitate nucleic acids [8].

The precipitation protocol normally uses salt like sodium acetate to neutralize the negatively charged DNA phosphate backbone. DNA becomes less soluble in water. According to coulomb's law (Equation 2-1), with a much lower dielectric constant alcohol added, the overall dielectric constant become smaller and the force between phosphate groups and the positive ions from the salt added become stronger. This allows positive ions from salt added to interact with the negatively charged DNA phosphate backbone much easier and forming stable ionic bonds due to electrostatic attraction between two oppositely charged ions. This causes nucleic acids to precipitate from the sample solution [38].

$$F = \frac{1}{4\pi\varepsilon_r\varepsilon_0}\frac{q_1 q_2}{r^2}$$

Equation 2-1 Coulomb's law. q1,q2: phosphate backbone and positive ion charge; r: separation distance; ε_0: electric constant; ε_r:dielectric constant

2.2.8 Other Extraction Methods

There are also few other different extraction methods such as Hydroxyapatite (HA) based extraction [39] , ionic liquid direct (BmimPF6) extraction [40], Proteinase K extraction method [41], Alkaline Lysis and boiling method [42]. These methods are not discussed here either due to the low/inconsistent nucleic acids yield/quality or because the extraction procedure might leave behind many potential inhibitors that affects downstream applications [43].

2.3 Microfluidic devices for Sample Preparation

2.3.1 µTAS & Lab on a chip

The concept of lab on a chip (LOAC/LoC) or miniaturized total analysis systems (µTAS) as it is known today was first developed by *Manz et al.* [44] in early 1900s. *Manz* and his co-workers successfully fabricated a completed chemical analysis system which incorporated sample treatment, separation and detection into a portable platform.

µTAS was envisioned as a new way of chemical sensing [45] but this technique gradually gained more attention and branched off into several new fields and applications. The µTAS has been implementing in genomics, medical diagnostics [46], drug discovery

[47], biological [48][49], bio-chemical analysis [50], point-of-care testing [51] and many other different areas.

The μTAS can precisely handle and analyse flow streams having microliter and even sub-microliter volumes [52] and has the advantage of minimal consumption of reagents, shorter reaction times, increased automation and reduced manufacturing costs [49]. The possibility of parallel operation, miniaturization of traditional large scale laboratory and automate the whole analysis process make this technology appealing to many researchers [49].

LoC technology has attracted a lot of attention from pharmaceutical industries in drug screening processes. Large quantities of enzymes/chemicals are used for experimenting the functionality and effectiveness of the substance against various diseases. These screening processes have to go through a very long development cycle and are normally very expensive. By the use of parallel processing and small quantities of drug candidates, LoC devices not only can speed up the drug discovery cycles but also can dramatically reduce the development cost in comparison with the traditional methods.

Microfluidic technology as part of LoC technology also gained significant interest from both academia and industry for the sensing and diagnostic purposes. The intrinsic features of microfluidics make it a perfect LoC format to use as a Point-of-Care (PoC) diagnostic device (*i.e.* the medical testing at or near the location of patient without needing a clinical lab). Such microfluidic diagnostic devices will provide patients and

medical professionals a portable, affordable device with fast turnaround time of analysis, among other advantages [53] over traditional benchtop instrument.

There have been many companies that have introduced products to address different PoC disease diagnostics based on microfluidic technology. The microfluidic PoC product can be found for analysing Blood chemistries, respiratory infections, pathogen identifications, and HIV/AIDS related detection. There are also many more products focusing on different areas of interests that are currently under development [54]. Figure 2-5 shows few different portable microfluidic based PoC products for clinical tests.

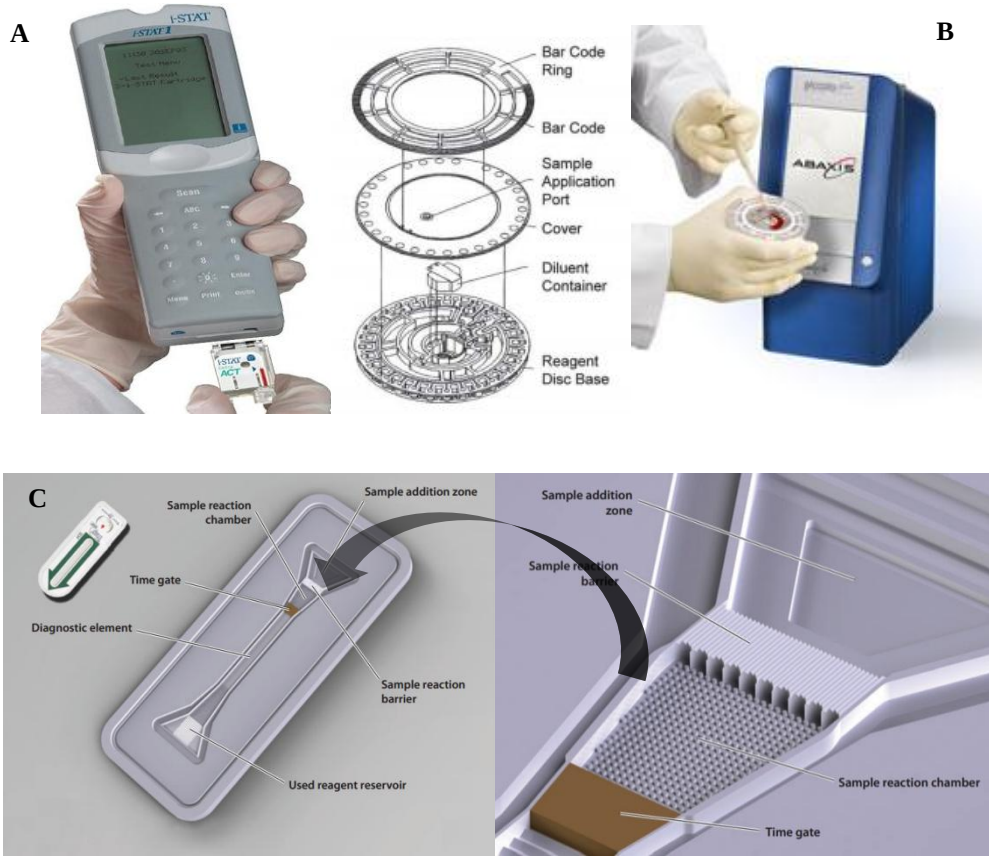

Figure 2-5 Images of microfluidics based PoC test devices: A) i-STAT portable clinical analyzer taken from http://www.abbottpointofcare.com/ B) Abaxis Xpress, taken from http://www.abaxis.com C) Biosite point-of-care testing test strip[55]

2.3.2 Microfluidic chips for DNA Extraction

In order to develop a nucleic-acid (molecular diagnostics) PoC microfluidic device and to be able to eliminate the interference of proteins and other cell debris on biosensor and achieve a reliable result, it is very important to have good quality and high purity of the DNA sample. There are many significant advances in development of DNA extraction device integrated with microfluidic technologies in order to address this issue. Various types of microfluidic DNA extraction chip published will be categorized and reviewed in this section.

Liquid/Liquid Extraction

Liquid-liquid extraction in microfluidic device is done using phenol-chloroform extraction principle. A microfluidic Y junction configuration was proposed by *Reddy et al*. [56] to create a two phase flow. As shown in Figure 2-6A, a two phase flow between organic stream with phenol/ chloroform and an aqueous stream containing cell lysates was achieved through two inlet design. The protein and other cell debris partition to the interface between the organic and aqueous phases while the DNA stayed in the aqueous phase. Bovine serum albumin (BSA) was fluorescence tagged in order to visualize this precipitation (shown in Figure 2-6B).

This technique proved the concept of microfluidic device for DNA extraction using organic extraction. However, *Reddy et al*. indicated that the complete removal of protein is not possible using this configuration due to limited interfacial area in the channel [56]. In addition, the intrinsic nature of phenol-chloroform extraction has determined the slow speed of extraction, and it would not be an efficient extraction process to use in a LoC microfluidic format.

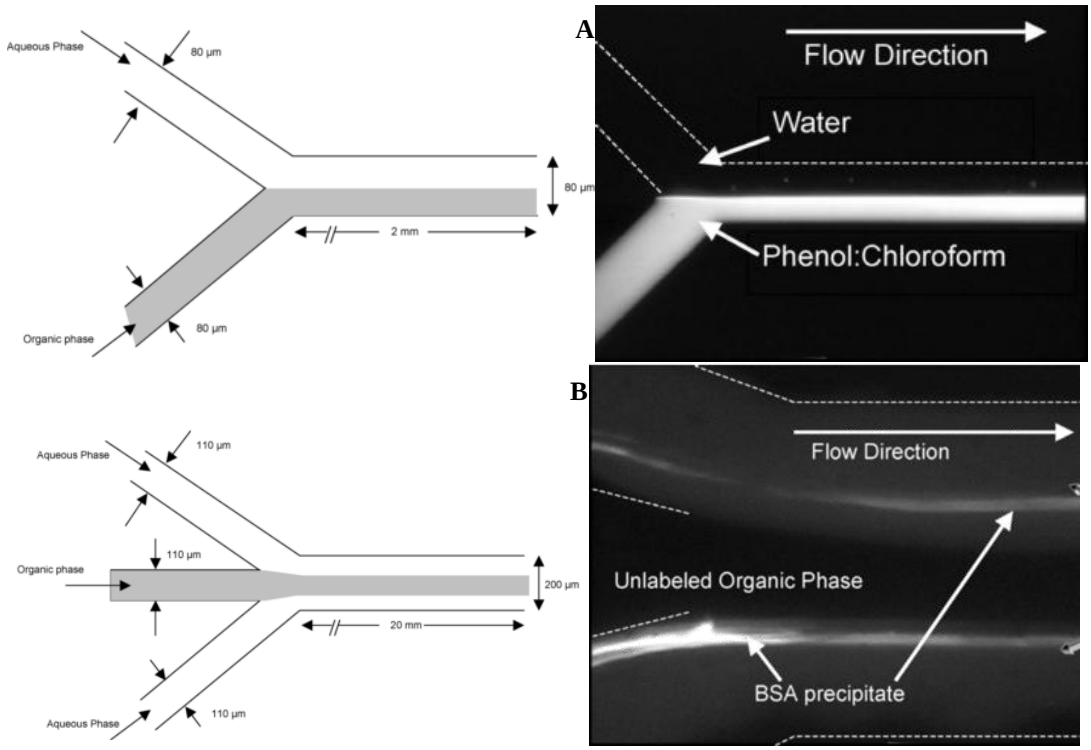

Figure 2-6 A) Two inlet design of two phase flow B) Two-phase flow DNA extraction [56]

Solid Support Extraction

Solid Support Extraction (SPE) or sometimes called Solid Phase Extraction (SPE) of nucleic acids has also been demonstrated in a microfluidic device. In this device the

principle of high affinity of nucleic acid to silica surface is used to extract DNA from other materials present in cell lysate. There are four different ways to achieve high contact surface areas between lysate solution and silica surface in a microfluidic device. Namely: (i) use of silica pillar structures, (ii) silica beads, (iii) magnetic beads and (iv) silica sol-gel matrix to increase surface-to-volume ratio of silica surface and achieve high extraction efficiency of DNA.

Silica Pillar Structure

Figure 2-7A shows the features of silica pillars in the DNA extraction chamber that were created by using deep reactive ion etching (DRIE) of oxidized silicon wafer. By comparing DNA extraction quantity with a un-etched chip, *Christel et al.* [57] demonstrated that there is a direct correlation between the silica surface area and the binding capability of the device. They also confirmed the maximum DNA binding efficiency to the glass as 40 ng/cm^2 reported by *Vogelstein et al.* [58]. In Figure 2-7B, similar techniques were employed in order to increase the silica surface areas further, thus increasing the capacity of the extraction chip [59]. One can also increase the surface to volume ratio by creating a more complex PMMA pillar structure using LIGA (lithography, electroplating and molding) process [60](Figure 2-7C), during this process, X-ray lithography is used to transfer designed pattern to PMMA photoresist on top of a conductive titanium layer deposited on the glass substrate. And the microposts are functionalized with chitosan and allow DNA binding in a pH-dependent manner [61].

Both DRIE and LIGA fabrication process are robust and the pattern can be precisely controlled thus having high reproducibility. However, the processes are expensive as increasing silica surface is limited by the capability of micromachining process and which limits the efficiency of DNA extraction (<50% DNA recovery efficiency). In addition, the extraction efficiency is also limited by how well the lysate solution is in contact with pillars' surface. In other words, for better extraction capability and extraction efficiency, this device should pack as many pillars as possible and the spacing between pillars should be as small as possible. Thus it will not be considered as a favorable technology due to its low yield and high cost.

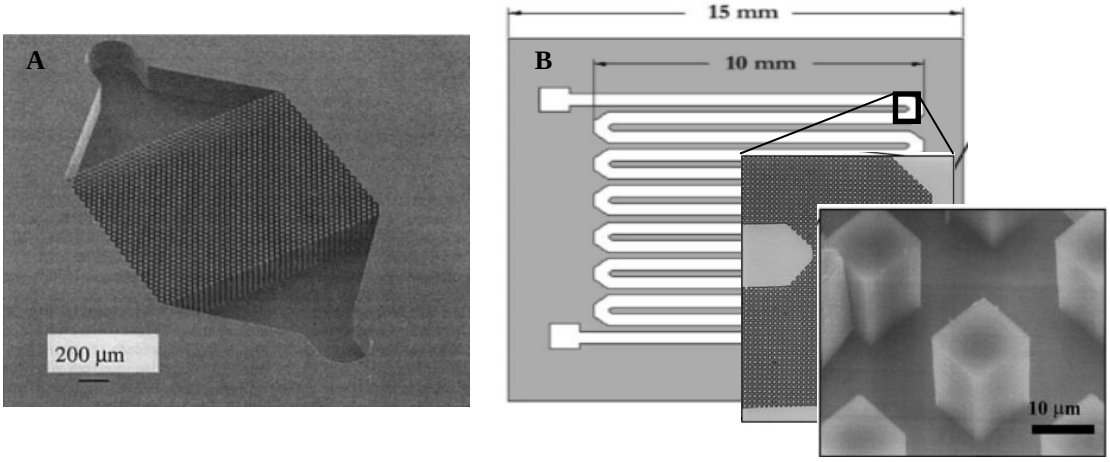

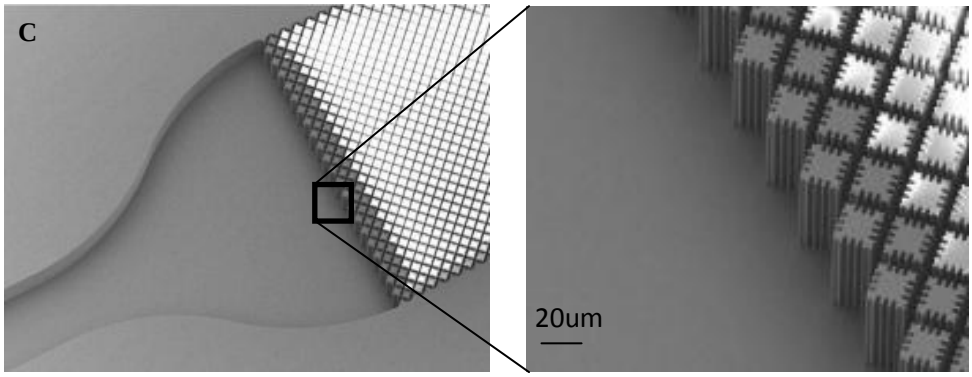

Figure 2-7 A) Pillar structure created using DRIE in a DNA extraction chamber[57] **B) Silica pillars in microfluidic channels**[59] **C) Micro pillars created using LIGA on a silicon chip**[60]

Silica Beads

The idea behind packing silica particles into an extraction chamber is to achieve higher DNA extraction efficiency by dramatically increasing the silica surface area in contact with lysate solution. Packed silica particle for DNA extraction was first demonstrated by *Tian et al*. [62] by packing silica particles into a 500nL of capillary, roughly 70% of DNA is recovered from white blood cells and more than 80% of the protein is removed in less than 10 minutes [62]. Their experiment also indicated that the DNA extracted using this method was free of PCR-inhibiting contaminants. *Breadmore et al*, [63] later demonstrated integration of silica particles with a microfluidic channel and immobilized using sol-gel method for DNA extraction (Shown in Figure 2-8) and achieved 67±10% recovery efficiency for λ-phage DNA.

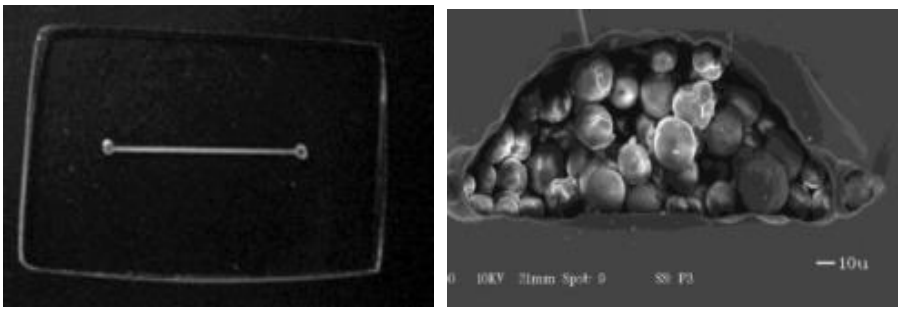

Figure 2-8 Silica particle immobilized with sol-gel in microfluidic channel [63]

It is also important to note that there are significant differences in DNA extraction efficiency between the design of immobilized silica beads and free moving beads inside a microfluidic channel. *Chung et al.* observed that the extraction efficiency increased two-fold in the immobilized silica beads set-up comparing with the free moving beads set-up. With the addition of serum (protein) mixed with DNA as input sample, the amount of DNA extracted in immobilized silica beads set-up was an astonishing 88-fold higher than the one with the free moving silica beads [64]. The conclusion they draw from the experiments was that the free moving silica beads reduce the chance of interaction between DNA and the silica surface, thus the extraction efficiency decreases. With the addition of proteins, it further reduces the chance of DNA collision/binding with silica surface if the silica particles were not fixed. Also, the phenomenon was more evident when using the diluted/low concentration of DNA sample. This offers a guideline for designing of an ideal LoC device for performing DNA extraction: This device has to contain stationary silica support surfaces.

Other than sol-gel immobilization of particles another common practice, as shown in Figure 2-9, is to create physical barriers to retain silica beads into one specific chamber [65][66], and allowing the reagents to flow freely. Similar to silica pillar structure fabrication process, the device can be created by deep reactive ion etching (DRIE).

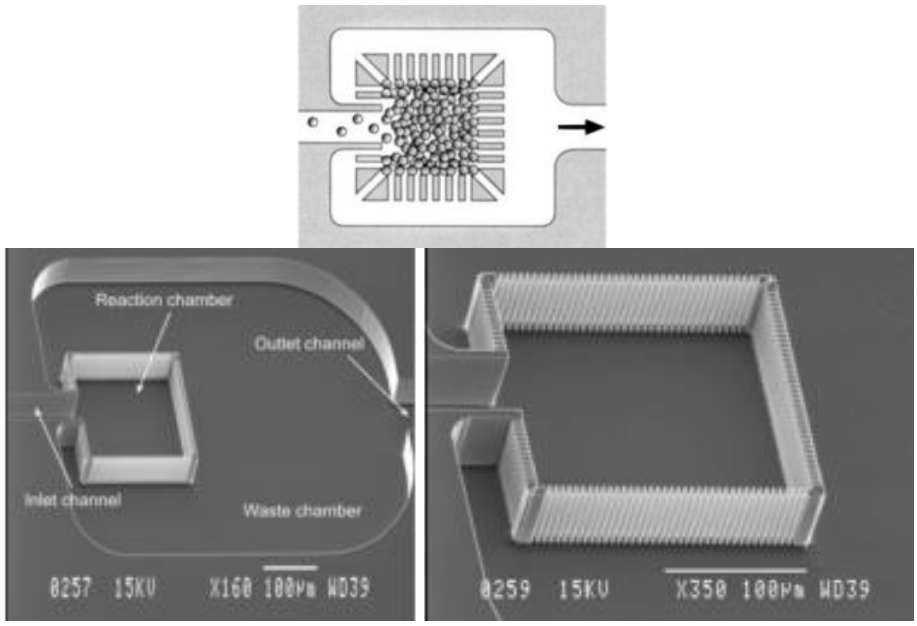

Figure 2-9 Microfilter design for packing beads[65][66]

Silica Matrix

Instead of packing silica particles into a confined space for performing DNA extraction, *Shaw et al.* [67] injected potassium silicate into a glass capillary, and the sol-gel process formed a porous silica monolith after solidification. The network of silica monolith shows in Figure 2-10A has demonstrated ability of performing DNA extraction tasks. Later *Wu et al.*[68]improved the technique and

packed the sol-gel silica into a microchip to utilize the high surface area-to-volume of silica sol-gel matrix for DNA extraction (Figure 2-10B). And the device was able to achieve 85 ± 7% of λ-phage DNA extraction efficiency and 68 ± 3% of genomic DNA extraction efficiency.

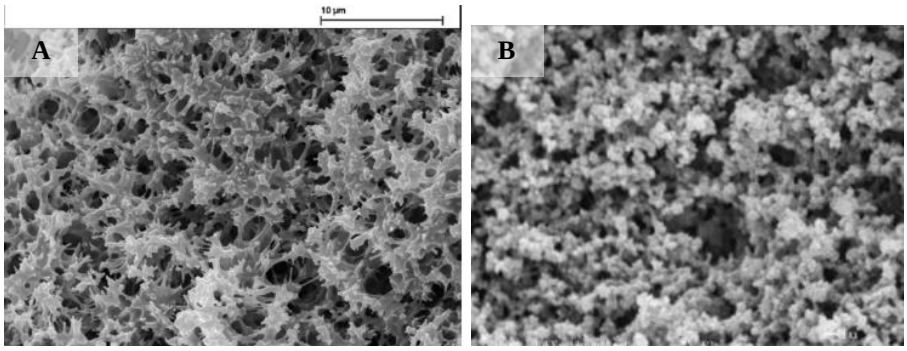

Figure 2-10 A) Silica porous monolith[67] **in a capillary tube B) silica porous network in a microchip**[69]

Other than using sol-gel to create a network of porous silica structure, researchers also explored the use of anodization technology to create porous silica structure on top of a silicon micro-channel (Figure 2-11). Various pore geometries, surface morphology and porosity can be achieved by adjusting the HF concentration, current density and etching time [70]. The microfluidic channel pattern is first defined using DRIE, a porous silica layer then is fabricated by anodizing the silicon channel surface in HF electrolyte. Finally glass wafer is anodically bonded with glass cover using silicon wafer bonder to enclose the microfluidic channel [70]. *Chen et al* demonstrated an average of 83±11.6% λ-phage DNA extraction using this technique. But their result also indicated 15% of extraction performance

drop after 5th repetition. Considering that these devices are constructed on silicon substrate and cannot be reused after few times of use, they are significantly more expensive than a polymeric extraction device.

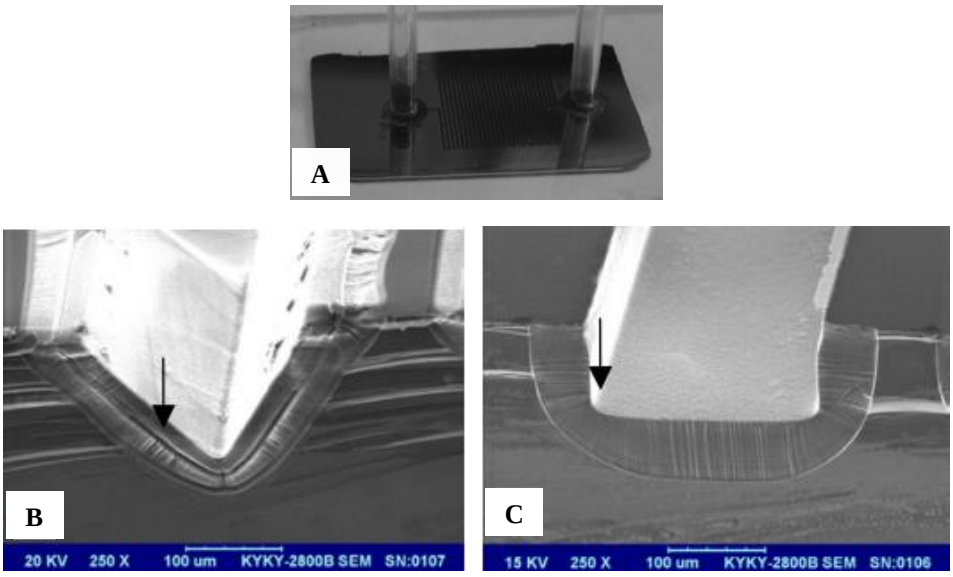

Figure 2-11 A) Microfluidic porous channel device; B) Porous V channel, 80 mAcm^{-2} , Anodized in 30% HF, 15min C)Porous rectangle channel, 80mAcm^{-2} , Anodized in 30% HF, 15min [71]

Magnetic Beads

Instead of stationary solid silica phase, magnetic beads coated with silica were used to move DNA with lysate solution controlled by the movement of magnetic force. The microfluidic device constructed by *Karle et al* [72] shown in Figure 2-12 is a great way to illustrate this dynamic solid phase extraction process. The lysed sample with beads and binding buffer are continuously injected into microfluidic channel, at this time DNA is bonded with the superparamagnetic

beads. Washing buffer is then used to wash the protein and other debris into the parallel channel. The last step is addition of eluting buffer that allows DNA dissociation from the beads and is further collected for downstream applications.

Unlike benchtop magnetic beads extraction, the magnetic beads are flowing with the lysate solution in a typical magnetic beads microfluidic extraction device, and it is very challenging to mix beads with lysate solution properly in a simple microfluidic configuration due to which this technique normally has very limited extraction rate. *Karle et al* only achieved 25% of extraction rate in their device. Additionally, generation of the magnetic field that controls the extraction process will be difficult to integrate with the microfluidic device.

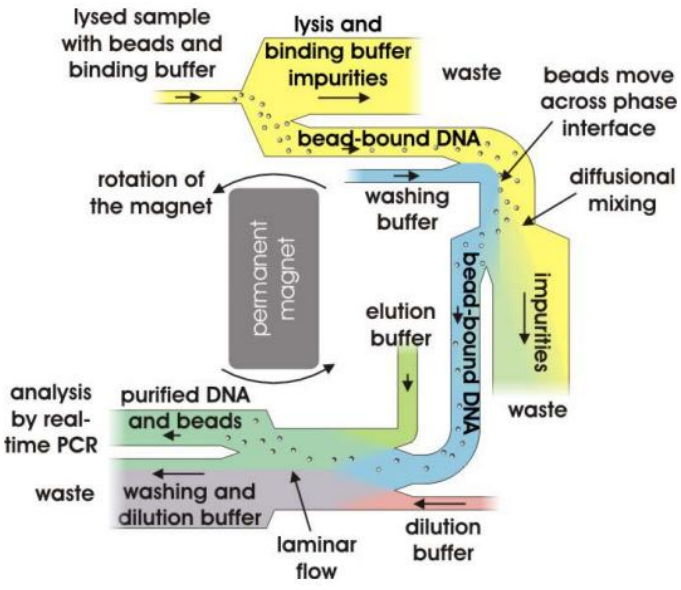

Figure 2-12 Schematic view of a continuous DNA extraction flow by using superparamagnetic beads[72]

2.3Summary

In this chapter, various traditional benchtop and miniaturized platforms for DNA extraction were studied. All these platforms have their own advantages and disadvantages which make it difficult to choose a particular platform as ideal for all applications. To choose the proper technology for building a microfluidic device that fits our design criteria, all the advantages and disadvantages of different technologies are compared and weighted based on the following criteria: toxicity of chemicals involved, ease of automation and miniaturization, and extraction efficiency. Table 1 provides a summary of some of the advantages and disadvantages. The fact that silica solid phase extraction is very easy for LoC integration, high extraction efficiency, low cost and it does not require extra ethanol precipitation step makes it an ideal candidate.

TABLE 2-1 Comparison of Nucleic Acid Extraction Techniques

Technique	Advantages	Disadvantages	Automation& Miniaturization
Salting-out	Quick, easy, low cost	Efficiency & quality highly variable	Easy
CsCl	High quality extraction	Very time intensive, expensive	Very Difficult
Ion Exchange (Chelex)	Quick, easy	Consistency, Only extract ssDNA	Easy
Magnetic beads(silica)	Low cost, high efficiency, PCR compatible	Low extraction efficiency if uses LoC format	Difficult
Phenol & Chloroform	Effective, reliable	Toxicity, time consuming, require user expertise.	Medium (low efficiency & not possible for complete removal of protein)
Silica solid support	Low cost, high efficiency, PCR compatible, one step extraction	Centrifugation machine is normally required	Easy

A comparison table for different existing microfluidic extraction devices using SPE is summarized and shown in Table 2-2 below, which includes the DNA recovery efficiency and time required for different methods.

Table 2-2 Microfluidic Silica Affinity Extraction Comparisons

Technique	Recovery Efficiency	Time	Reference
Silica resin	70%	10min	[62]
Magnetic particles	25%	1min	[73]
Silica micropillars	21%,50%	15min	[74], [57]
Silica beads, TEOS sol-gel	50-77%	15min	[63], [75], [76]
TMOS sol-gel	70-85%	30min	[69]
Porous Channel	83%	15min	[71]

It is easily seen that silica beads, silica beads/sol-gel hybrid, porous silica sol-gel and porous silica channel all can integrate into a microfluidic device and achieve high extraction efficiency. Compared with packed silica columns, the silica beads/sol-gel hybrid tends to be more stable over time, and therefore yields better reproducibility under optimized loading conditions. Thus focus will be given to silica sol-gel methodology to fabricate a microfluidic device that is cheap, disposable, reliable and has high extraction efficiency.

In the next chapter, the top-down flow design configuration and polystyrene template method for creating macro/mesoporous silica monolith will be described in detail in order to optimize the silica surface-to-volume ratio for maximizing DNA extraction efficiency.

Chapter 3 Device Design and Principle

3.1 Design Overview

Health Canada's guideline suggests that the Total Coliform Bacterial concentration in drinking water should bellow 10 cells per 100ml [77]. In recreational waters where the "primary contact" is through activities such as swimming, windsurfing and waterskiing, the maximum permissible *E. coli* concentration is 200 cells per 100ml. For "secondary contact" activities such as canoeing or fishing, the *E. Coli* concentration should below 1000 *E. coli* per 100ml [78]. It is also reported by *Matthews et al* that the typical concentration of pathogenic indicator microorganism (*E. coli*) in raw sewage is in between 10^5 to 10^{10} cells per liter, *Enterococci* (indicator) is 10^6 to 10^7 cells per liter and *Clostridium perfringens* (indicator) is 10^5 to 10^6 cells per liter [79]. Any device used for monitoring water quality would be required to detect bacterial populations in the wide range as indicated above, spanning from close to drinking water level to the worst scenario - sewage water. And ideally it should be able to identify cells ranging from 10s of cells to $10^{5\text{ to }9}$ cells in a 100ml of water sample. That means the device should have a detection range from pictograms to micrograms of nucleic acid, assuming the weight of nucleic acid in all indicator cells is the same as *E. coli* cells (0.117 pg per cell).

Therefore the design criteria for the extraction unit is set for up to one microgram of nucleic acid extraction first and once the concept has been tested using biological samples, it will then be modified and optimized for achieving our detection goals.

Typical microfluidic extraction devices uses an elution buffer size of 10µl -15µl and the elution buffer volume can vary from 2µl to 250µl depend on the technology used [60]. In order to reduce the time required for the whole extraction process and the chemical reagent consumption, the extraction chip has to be designed with a small dead volume that requires minimal elution buffer and other chemical reagents.

3.2 Extraction Procedures

Solid Support Extraction of DNA using silica has been chosen in this thesis as it offers a high DNA extraction efficiency, does not require any toxic chemicals and also is easy to automate and miniaturize in a microfluidic format as compared to other extraction processes. The microfluidic device for DNA extraction is illustrated in Figure 3.1. The chaotropic salt guanidine thiocyanate (GuSCN) is used as DNA binding buffer as it can achieve good DNA purification, where humic acid contaminant residual is very low comparing with other extraction & purification protocols [80], and it does not inhibit downstream PCR process. The cell lysate which contains DNA, protein and cell debris are mixed with GuSCN binding buffer and flowed through the porous silica monolith in the extraction chamber. The optimal DNA binding affinity with silica surface is created by controlling of the binding buffer pH under acidic conditions, where researches had found that the DNA adsorption rate increases significantly with the decreases of pH level

[81–83]. DNA attaches to the surface of silica while protein and other cell debris will continuously flow pass through the silica monolith and subsequently be collected at the outlet as waste. Finally, low concentration salt or water is infused through the main horizontal microfluidic channel wherein DNA will then detach from silica surface and be collected in the next chamber for uses in the downstream application like DNA amplification.

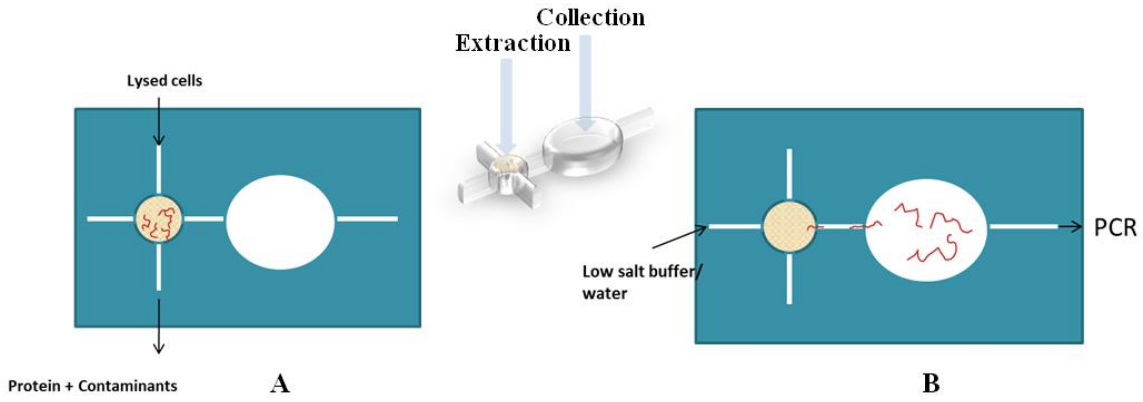

Figure 3-1 Schematics of two step DNA extraction process, A) DNA Extraction B) DNA collection

3.3 Sol-Gel Synthesis of Mesoporous Silica

As explained in Chapter 2, the silica monolith created using TEOS sol-gel method can achieve high extraction efficiency similar to silica resins. With the addition of triblock copolymer, the crack-free silica structure allows yield better reproducibility comparing with packed silica column. This method is chosen here for synthesizing of mesoporous silica material.

3.3.1 Silica Extraction Principle

In understanding the driving force and mechanism behind the DNA adsorption to silica surface, *Melzak et al.* [82] determined that there are three different competing effects, namely: (i) shielded intermolecular electrostatic force, (ii) dehydration of the DNA (iii) intermolecular hydrogen bond formation [82] that contribute to the overall driving force for adsorption.

DNA and silica surface are both highly negatively charged, when high concentration of salt is added to the system, the ionic strength in the aqueous solution increases and the Debye length of the DNA and the surface decreases (Figure 3-2), and bulk of the liquid can gradually get closer to the charged surface. When the salt concentration reaches a critical level, the sorbent and adsorbent can get close enough and form intermolecular hydrogen bonds [81]. Decreasing pH value can also promote the binding between DNA and silica surface. Effect of decrease in pH value is equivalent to the protonation of both DNA phosphate backbone and the silanol groups on silica [82], and it significantly increases the binding sites for DNA interaction with the silica surface[81], that's also why acidic condition was found to be optimal binding pH level instead of alkaline condition.

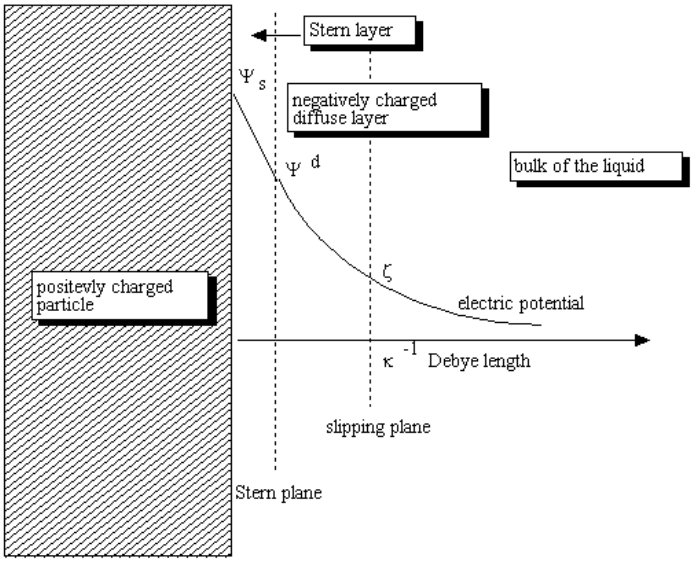

Figure 3-2 Illustration of the structure of the electric double layer and Debye length[84]

As per the dehydration effect, *Melzak et al.* proposed the following equation for representing interaction between the DNA and silica surface:

DNA (hydrated) + silica (hydrated) + conterions ⇌ neutral DNA- silica complex+ water

With the addition of guanidine-HCl, the free water molecules in the solution decreases due to the formation of hydrated ions from the salt, and driven the reaction to the right direction, thereby increasing the affinity capability [81] of silica.

When adding chaotropic salt such as guanidine thiocyanate into the cell lysate, the ionic strength increases and Debye length decreases between bulk solution and silica surface, and DNA in the bulk solution get close to the silica surface and forms hydrogen bonding when the salt concentration reaches a critical level. The addition of chaotropic

ions also destroys structure of hydrated shell consisting of water molecules and with the cation bridge formation that binds DNA molecules with silica surface. At the meantime, proteins are denaturized by chaotropic salt and subsequently washed away along with other contaminants.

3.3.2 TEOS & Silica sol-gel

The silica sol-gel process is a chemical hydrolysis and poly-condensation reaction from silicon alkoxide such as Tetraethyl orthosilicate ($Si(OC_2H_5)_4$) to form SiO_2 as the final reaction product. It essentially describes the change from dispersions of colloidal particles in a liquid solution (sol) state to a porous, interconnected, rigid silica network [85]. Tetraethyl orthosilicate (TEOS) consists of four ethyl groups attached to SiO_4^{4-} ion and the chemical structure is shown in Figure 3-3. It is mainly used as a crosslinking agent in silicone polymers and as a precursor to silicon dioxide in the semiconductor industry [86]. Silica aerogel is another material developed via silica sol-gel process that attracts many researchers due to its excellent insulating, light weight and high specific surface area [87]. It is also used in the fabrication of hybrid material such as the inorganic/organic composite - TEOS/PDMS [88]. In addition, the sol-gel process is starting to gain more attention in DNA extraction and has been integrated with microfluidic device for DNA extraction purposes [68][63].

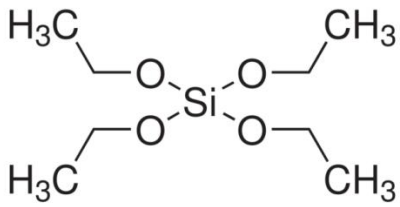

Figure 3-3 Chemical structure of TEOS [Sigma Aldrich]

3.3.3 Sol-Gel Chemistry

TEOS (Tetraethyl Orthosilicate) is prone to being converted into silicon dioxide through hydrolysis and condensation reactions. The sol-gel process is initiated upon the addition of water, and resulting products are silica (SiO_2) and ethanol.

$$Si(OC_2H_5)_4 + 2\ H_2O \rightarrow SiO_2 + 4\ C_2H_5OH \qquad \text{Equation 3-1}$$

The first step of the reaction is the formation of silanol groups by hydrolysis of the alkoxide precursors, and a silica network is formed through the polymerization that occurs during alcohol condensation and water condensation. The polycondensation reaction leads to cross linked polysilicates which precipitate during the reaction [89].

$$\text{Hydrolysis: } \equiv Si - OR + H_2O \leftrightarrow \equiv Si - OH + ROH \qquad \text{Equation 3-2}$$

$$\text{Alcohol condensation: } \equiv Si - OR + HO - Si \equiv \leftrightarrow \equiv Si - O - Si \equiv + ROH \qquad \text{Equation 3-3}$$

$$\text{Water condensation: } \equiv Si - OH + HO - Si \equiv \leftrightarrow \equiv Si - O - Si \equiv + H_2O \qquad \text{Equation 3-4}$$

The alcohol condensation and water condensation processes are uncontrolled and leads to poor ordered structure with broad range of pore sizes. In addition, *Wolfe et al.* found that the sol-gels alone did not yield good DNA extraction efficiency [63] as the sol-

gel shrinks and forms a flow channel between the silica monolith and the channel wall (illustrated in Figure 3-4-B) and it can result cell lysate flow around the sol-gel structure instead of flow through it. *Wu et al.* explored the methodology to solve this problem by using Tetramethyl-Orthosilicate (TMOS) based sol-gel with polyethylene glycol as the porogen, but the pores created using this method are small (1.863nm to 3.324nm [90]) and *Wu et al.* observed that the pores can be easily blocked by cell debris in lysate solution and it can significantly reduce the DNA extraction efficiency of the device, especially when repeat extractions were performed in a single device [69].

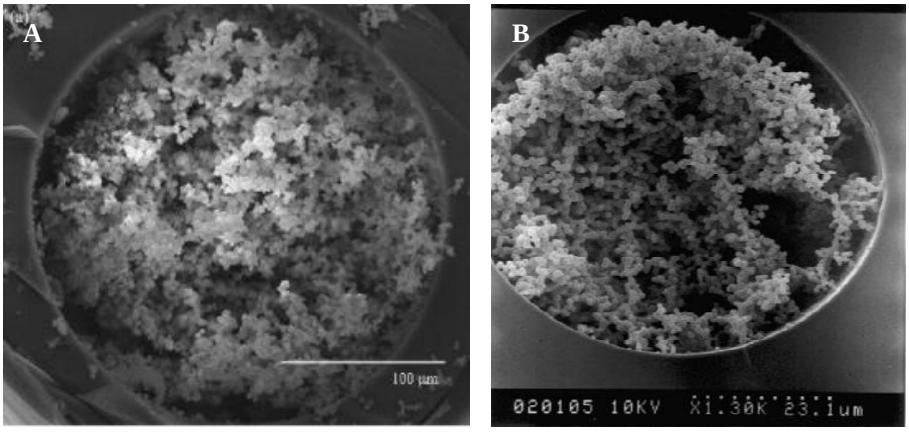

Figure 3-4 A) monolith completely filled the capillary [91] **B) Spacing between monolith and capillary formed a flow channel** [92]

Similar to *Wu et al.*'s methodology, a surfactant (Pluronic F127) template polymerization method can be used to control and guide the reaction in order to obtain well-ordered polysilicate structure [93], also minimize the effect of crack and shrinkage of silica sol-gel process.

3.3.4 Triblock Copolymer & Mesoporous Silica Structure

Based on the International Union of Pure and Applied Chemistry (IUPAC) classification, microporous material have pore diameters smaller than 2 nm, mesoporous materials have pore diameters in between 2 nm and 50 nm and macroporous materials have pores with diameter larger than 50 nm [94].

Zhao et al. first synthesized mesoporous silica by using non-ionic triblock polymers in 1997 [95], [96]. The material was characterized and using the naming convention abbreviation SBA-X (Santa Barbara Amorphous), where X corresponds to a specific pore structure and surfactant used.

Non-ionic triblock copolymer, Pluronic F127 can be used as the structure directing surfactant for forming a well-ordered mesoporous silica structure. It consists of hydrophilic polyethylene oxide chains (PEO) and hydrophobic polypropylene oxide chains (PPO) shows in Figure 3-4.

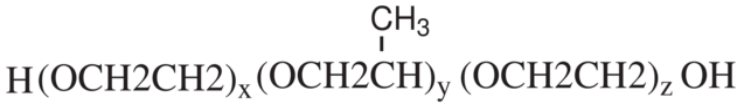

Figure 3-5 Chemical formula and properties of copolymer Pluronic F-127 (surfactant) [Sigma Aldrich]

By carefully selecting the molar ratio of the water, butanol, Pluronic F127 system one could synthesize silica material with different periodic mesoporous structures such as two dimensional hexagonal and three dimensional cubic symmetry[97](Figure 3-5). The

molar ratio for this work is chosen to synthesize spherical pores in a body cubic center structure (SBA-160) [95].

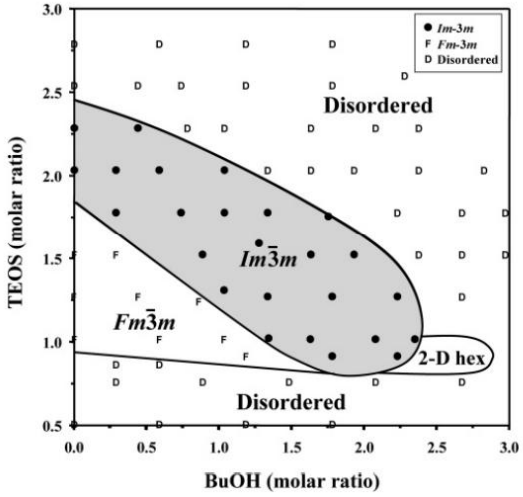

Figure 3-6 Diagram of mesophase structures established based on XRD measurements by Kleitz et al[97] **, the molar ratio Kleitz et al used is 0.0035 F127/x TEOS/y BuOH/0.91 HCl/117 H2O**

It is shown by *Sakamoto et al.* [98] that the pores in the SBA-16 mesoporous silica material were periodically ordered and it has the cage-like mesopores arranged in a three dimensional cubic body centered symmetry shown in Figure 3-6 [95], [98].

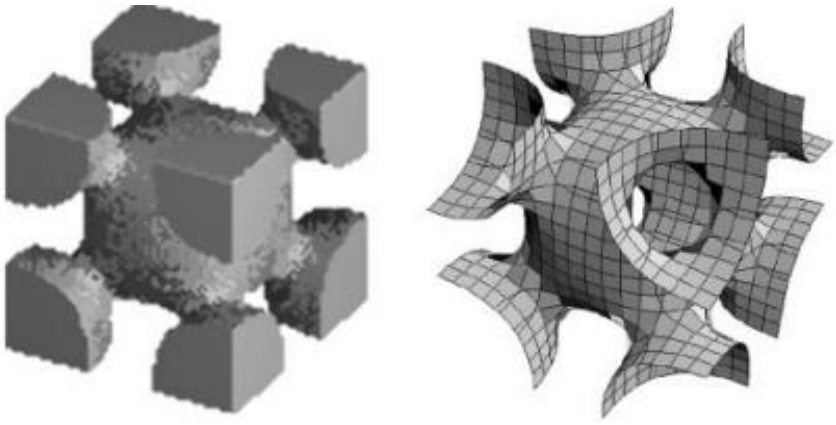

Figure 3-7 3D arrangement of cavities and interconnection of SBA-16 [98], **Structure of periodic minimal surface of SBA-16 material**[98]

3.4 Colloidal Template (Soft-Template) Method

The triblock copolymer mesoporous silica synthesis method however can create cubic body centered pores sizes ranging only from 2.1 -5.4 nm [99], which is difficult for 2nm diameter DNA molecules to maneuver inside the porous media. And similar to polyethylene glycol synthesis method, the small sized pores can easily blocked by components in the lysate [69] and the small cavities also can potentially trap DNA and reduces the recovery efficiency. In addition, such extraction media also introduces high pressure resistance in the flow system.

Colloidal template (soft-template) method for synthesizing macro/mesoporous silica material is used here to create a high surface-to-volume ratio silica surface for good extraction efficiency, and the ordered macroporous network formed can significantly

reduce the pressure resistance of the flow and allow easy attachment and elution of the DNA sample.

The soft-template method for synthesizing porous silica material can preserve the long range periodicity of the negative replica structure from the soft-template [100], and the size of the uniform hexagonally structured pores can be easily controlled by varying the size of template particles. In addition, the size of macropores can be easily adjusted by heat annealing of the polystyrene template to form interconnections between particles. The highly ordered and controllable periodically arranged silica structures created can potentially enhance the repeatability and efficiency of DNA extraction process comparing with other sol-gel silica method, and enables the DNA extraction device for multiple time uses. This method however has never been integrated with any microfluidic system or for DNA extraction. In the following sections, a simple but novel technique to create and integrate the porous silica cartridge with a microfluidic chip for DNA extraction will be outlined.

Porous silica filling material obtained via colloidal crystal template is achieved by first packing monodispersed polystyrene particles tightly together, and then filling the silica sol-gel in the space between the particles. After the solidification of the gel, the polystyrene template will be removed to form high degree of interconnected pores with periodicity.

3.4.1 Filtration Assembly

Self-assembly is a process where disordered components spontaneously form a well-defined three dimensional ordered geometry [101] and it is described by *Grzybowski et al.* as *the ultimate dream for lazy scientist* to let the forces of nature to assemble components into a desired structure [102].

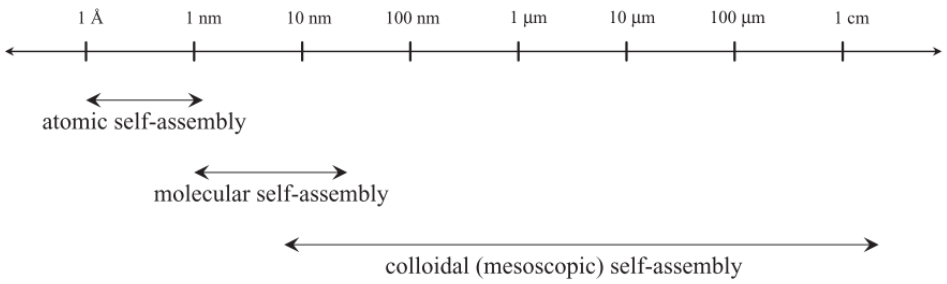

Figure 3-8 Classification of self-assemblies based on the size or nature of building blocks[103]

Self-assembly can be categorized by the size/nature of the building block as shown in Figure 3-7, there is atomic self-assembly that describes the phenomena of self-assembly at atomic level, molecular self-assembly such as DNA self-assembly and colloidal self-assembly which is deals with self-assembly of larger building unit [103]. The initial testing has indicated that with the use of 2.8µm polystyrene template one can

create silica interconnect pore sizes of 100 nm, which is well above the physical size of DNA (2 nm in diameter). In other words, micrometer sized polystyrene can be used as template for creating a porous silica structure that allows the free movement of DNA inside the monolith during elution step. The method for colloidal self-assembly and the soft-template creation and synthesize of macro/mesoporous silica will be explored in the following sections.

Development of the self-assembly approach to construct a new, functional material and device is based on the bottom-up approach, unlike the top-down approach which start from a complex structure and dismantle it into smaller components (Photolithography) [104]. The bottom-up approach will be starting from the self-assembly of building block and eventually build towards a more complex structure. The bottom-up approach is chosen due to its advantages of experimental simplicity, possibility of three dimensional assembly and potential for inexpensive mass production [105].

Two dimensional ordered patterns of particles can be created by utilizing the attractive capillary forces between substrate and particles, examples are: Dip coating/float transferring [106], electrophoretic deposition [107], [108], physical and chemical template [109], spin coating [110], [111] and Langmuir-Blodgett [112–114].

The patterning of long range periodic three dimensional structures can be done through different types of techniques, such as sedimentation, filtration, centrifugation and slit filling as illustrated in Figure 3-8. Sedimentation of the particle is the easiest and the slowest process among different assembly methods. Filtration and centrifugation

processes are utilized to speed up the sedimentation process. Slit filling is also very effective way to pack particles into a thin slit between two plates by filtering particle suspension [115].

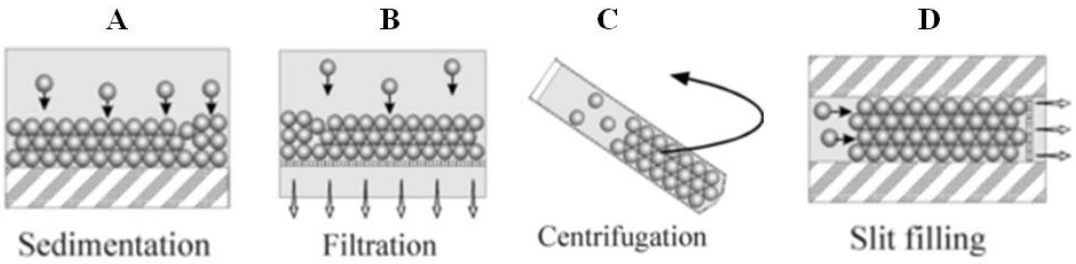

Figure 3-9 Schematics representation of different 3D colloidal crystalline methods[116]

The design criteria for this assembly device is to be able to simultaneously assemble particles in multiple chambers, allow wash and easy infusion of different media (i.e. silica sol-gel) material and should be able to easily integrate with different parts of microfluidic device components. Filtration fits all the above design criteria and therefore was chosen.

In order to test this concept, a single filtration assembly chamber will be fabricated, which is comprised of a through-hole PDMS chamber and a porous polycarbonate membrane (shown in Figure 3-9). The chamber formed can accumulate particles and the membrane at the bottom allows pressurized removal of the liquid.

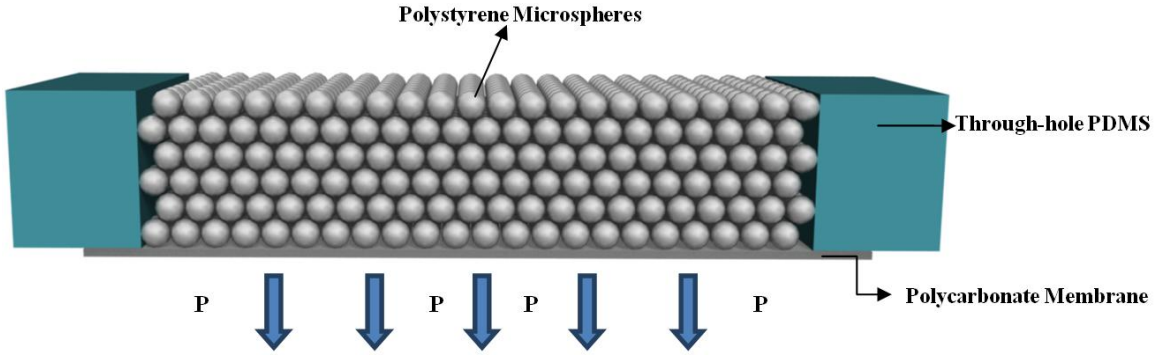

Figure 3-10 Filtration chamber

A single chamber assembly and integration will be demonstrated in the Chapter 4 of this thesis, and the concept of multiple chamber assembly will also be tested as proof of concept at the end of Chapter 4.

3.4.2 PDMS Mold Design & Suction Device Design

PDMS through-hole (Figure 3-10-B) can be fabricated by using a rapid prototyped mold (Figure 3-10-A). PDMS is cast into a mold and the inverse feature is transferred to the PDMS once it is cured. Another rapid prototyping mold is also created to apply suction pressure uniformly over the entire assembly chamber as shown in Figure 3-11. The process of assembly is as follows, the through-hole PDMS piece is first bonded with porous polycarbonate membrane to form the particle assembly chamber, and it is tightly secured in between a rapid prototyped suction mold and a cap to create a good contact of two surfaces. The rectangular 1mm by 1mm pressure channel inside the suction device is split into four smaller circular channels with diameter of 0.6mm to allow uniform pressure distribution to the opening area of through-hole PDMS when suction is applied

using a syringe pump. Details fabrication process of through-hole PDMS and assembly experiment set-up will be discussed further in Chapter 4.

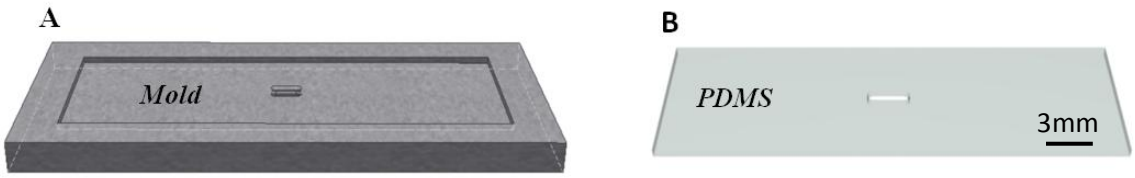

Figure 3-11 PDMS through-hole mold and PDMS through hole replicate

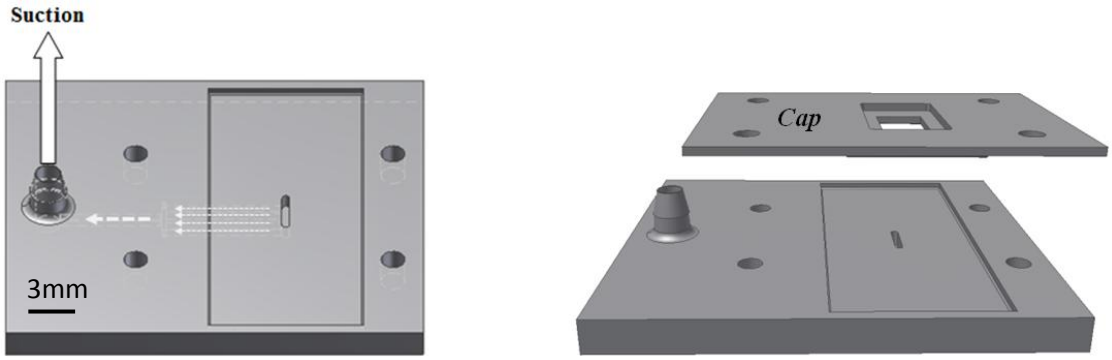

Figure 3-12 Suction device for corresponding through-hold PDMS piece

3.4.3 Macro/mesoporous Material: Soft-Template Method

The soft-template method will be used to create highly ordered macropores on top of mesoporous material to form a macro/mesoporous material. As shown in Figure 3-12, polystyrene particles in ethanol solvent are first assembled inside the PDMS through-hole chamber. The silica sol-gel solution contains surfactant can fills the space in between polystyrene microspheres with the help of polystyrene microspheres acting as the templates. Finally the polystyrene template is removed after the infiltration and solidification of the silica gel and the inversed silica skeleton is left behind which contains mesoporous features defined by the triblock copolymer Pluoronic F127

surfactant, and the macroporous features which results after the removal of polystyrene templates.

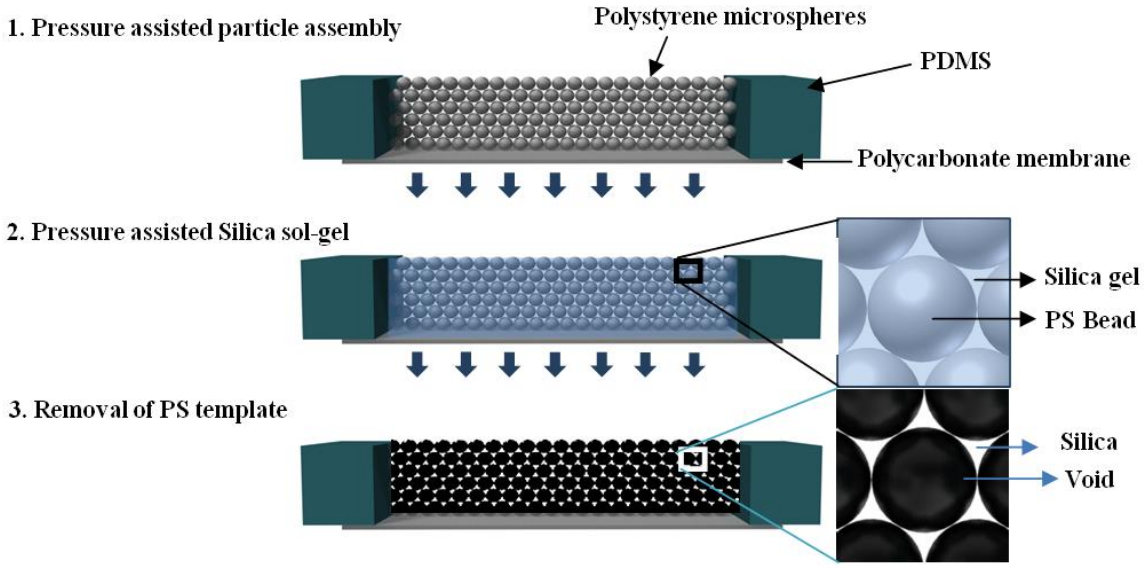

Figure 3-13 Schematics of template method for making porous silica monolith

3.5 Microsphere Size & Total DNA Binding Capability

The device is also designed to be able to continuously collect large amount of DNA sample. The total silica contact surface area has to be large enough to capture 1μg of DNA as explained at the outset. Based on the maximum binding efficiency of 40ng/cm^2 [58][117] to glass, the total silica surface inside the extraction chamber has to be larger than 25 cm^2 to achieve the 1μg of DNA extraction goal.

In order to have a small elution volume and a faster extraction speed, the corresponding extraction chamber should be also small. Our design uses 1.8 mm^3 extraction chamber sizes with dimension of 3mm ×1mm ×0.65mm. As we can see from

Table 3-1, with the decrease of the assembled particle size from 9μm to 1μm, the theoretical maximum packing fraction (porosity) and the dead volume of the device remains constant. However, the number of particles that can be packed in one extraction chamber significantly increased, thus the total available silica surface for DNA binding increased significantly. Any monodispersed polystyrene microsphere smaller than 9μm can be used as soft-template for synthesizing porous silica monolith that's capable of 1 μg DNA extraction, the particles also need to be larger than 1μm for easy visualization of self-assembly during development stage of design. In this thesis, 3μm polystyrene microspheres were chosen as it offers a total of 75.8 cm^2 silica surface for 3μg of DNA binding (factor of safety: 3). The top-down flow configuration is illustrated in Figure 3-13, two separate microfluidic channels are placed on top and connected to the extraction chamber to form a complete microfluidic system. The total combined dead volume of extraction chamber and microfluidic channel is calculated to be 0.87 mm^3 (0.87 μl). Typical dead volume/elution volume required for commercial available silica based extraction kit can ranges from 2ml to 24ml or even higher (Norgenbiotek kits). In contrast, 5-10 μl of elution buffer should be sufficient for flushing DNA out of our microfluidic system at the end.

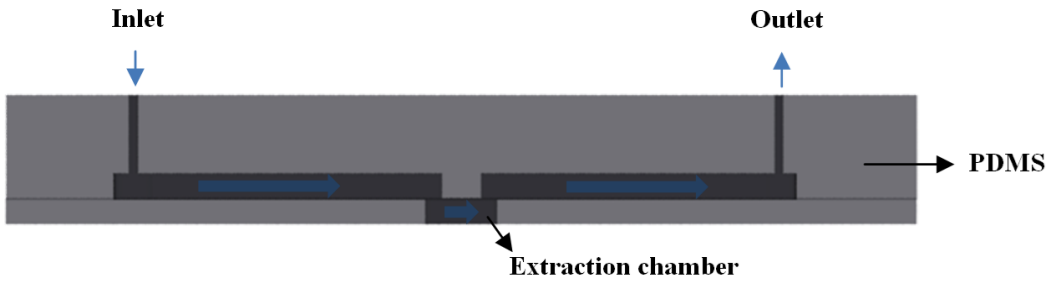

Figure 3-14 Illustration of top-down flow configuration (not to scale)

Table 3-1 Relation between PS particle size, total silica surface, total DNA binding capability and dead volume

Size (µm)	Porosity	No. of Particle	Silica surface (cm^2)	Total DNA(µg)	Dead volume(mm^3)
1	0.74	1.81E+09	22.7	9.10	0.87
3	0.74	6.70E+07	75.8	3.03	0.87
5	0.74	1.45E+07	45.5	1.82	0.87
7	0.74	5.28E+06	32.5	1.30	0.87
9	0.74	2.48E+06	25.3	1.01	0.87

3.6 Synthesis of Polystyrene Microsphere: Dispersion Polymerization

Highly monodispersed polystyrene particle size ranging from 1 to 10 micrometers can be synthesized by using dispersion polymerization process [118]. Figure 3-14 shows a schematic for the particle growth from a nucleus due to reaction between initiator and monomer molecules, which reaches a stable spherical state in the presence of polymeric stabilizers [119]. Initiator decomposes at the right temperature and the free radicals are formed that react with styrene monomers and form oligomers. The growing oligomer chains then aggregate and absorb stabilizer until a stable particle nucleus is formed. The polymerization and the growth of particles continue until all surrounding monomers are consumed [120].

The synthesis process normally comprise of the following chemical components: monomers, water-insoluble initiator and stabilizer, and all components should be dissolved in the polymerization medium such as alcohol. The experimental procedures for

creating monodispersed polystyrene microspheres and the recipe used will be detailed and listed in Chapter 4.

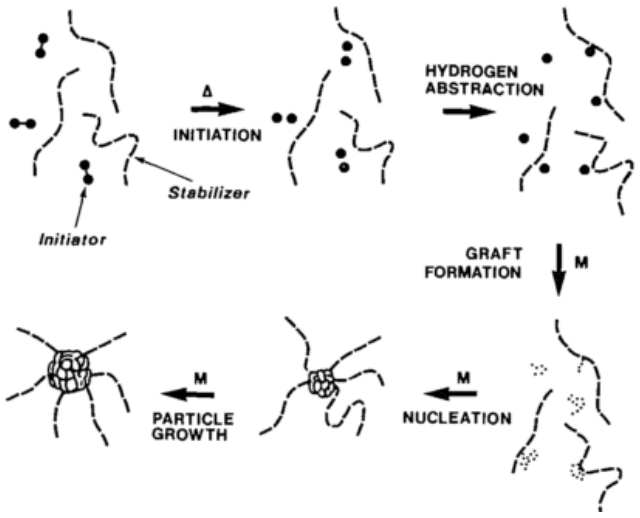

Figure 3-15 Schematic representation of nucleation and growth in a dispersion polymerization [121]

3.7 Size Control of Macro-pores

The monolith can be considered as a macroporous material due to the fact that larger than 50nm interconnected pores are present. However, the process cannot guarantee a complete interconnection everywhere as shown by initial tests (section 4.7.2). Heat treatment can be performed before the infiltration of silica sol-gel step in order to control interconnect pore size and to ensure interconnects are present throughout the monolith.

As illustrated in Figure 3-15, polystyrene particles become soft when the annealing temperature exceed its glass transition temperature of 95^{o}C [122] and the particle contact spot eventually melt and forms connection between particles when

temperature increases further. As a result, the macro pore size increases after removal of template due to the silica sol-gel solution can no longer infiltrate the merged part of the polystyrene particles. The process of identifying the appropriate temperature and annealing duration for achieving interconnected pores throughout silica monolith will be presented in next chapter.

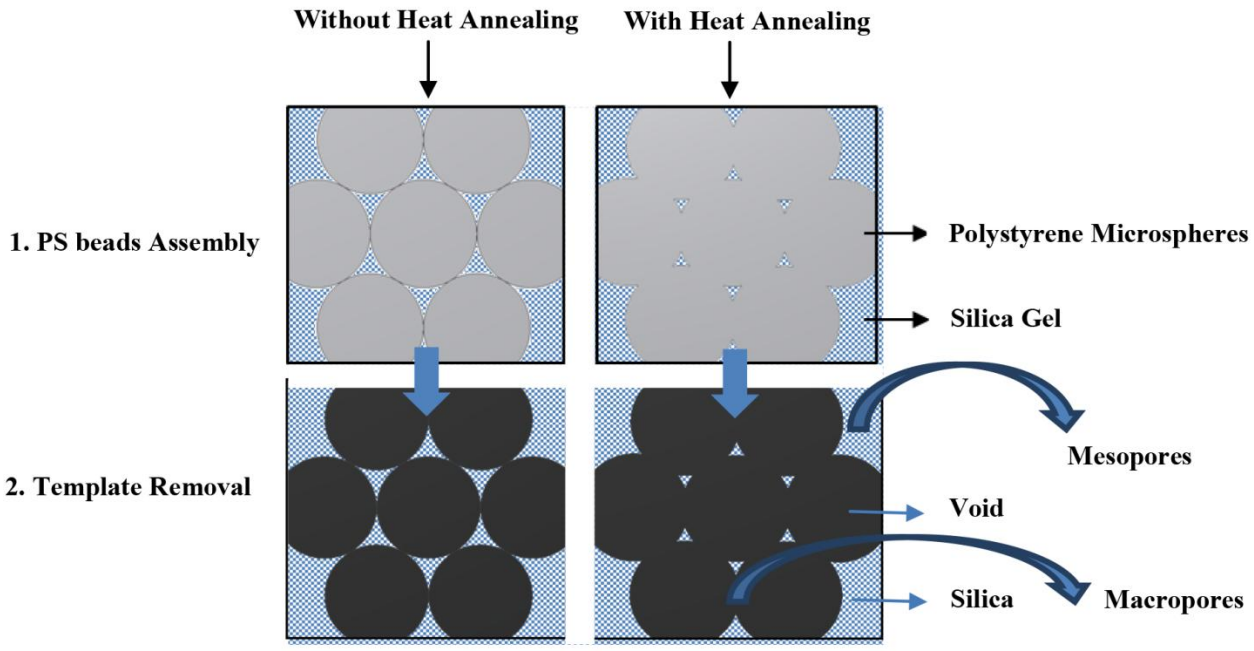

Figure 3-16 Dual macro/mesoporous silica monolith

3.8 Summary

A highly ordered macroporous silica structure to be synthesized by using TEOS sol-gel and soft polystyrene template methodology was designed for DNA extraction module. Fabrication process for integrating the monolith with the microfluidic channel was also developed.

Overall schematics of the microfluidic device are outlined in Figure 3-16. The PDMS mold will be printed using rapid prototyping machine, the through-hole PDMS will be replicated using printed mold and bonded with porous membrane by oxygen plasma and microcontact printing technique. Monodispersed polystyrene particles will be used to form closed packed assembly inside the through-hole PDMS and heat treatment will be used to control interconnection of particles. Silica sol-gel will then fill the voids between microspheres. Finally the microspheres will be removed to achieve the macro/mesoporous structure within silica monolith.

At the same time, the silicon master mold will be made via photolithography patterning, and microfluidic channels will be replicated using PDMS as before using soft-lithography. In the final step, the top microfluidic channel will be bonded with the bottom extraction chamber containing silica monolith to enclose the channel and the silica extraction chamber. The fabrication process will be discussed further in details in Chapter 4.

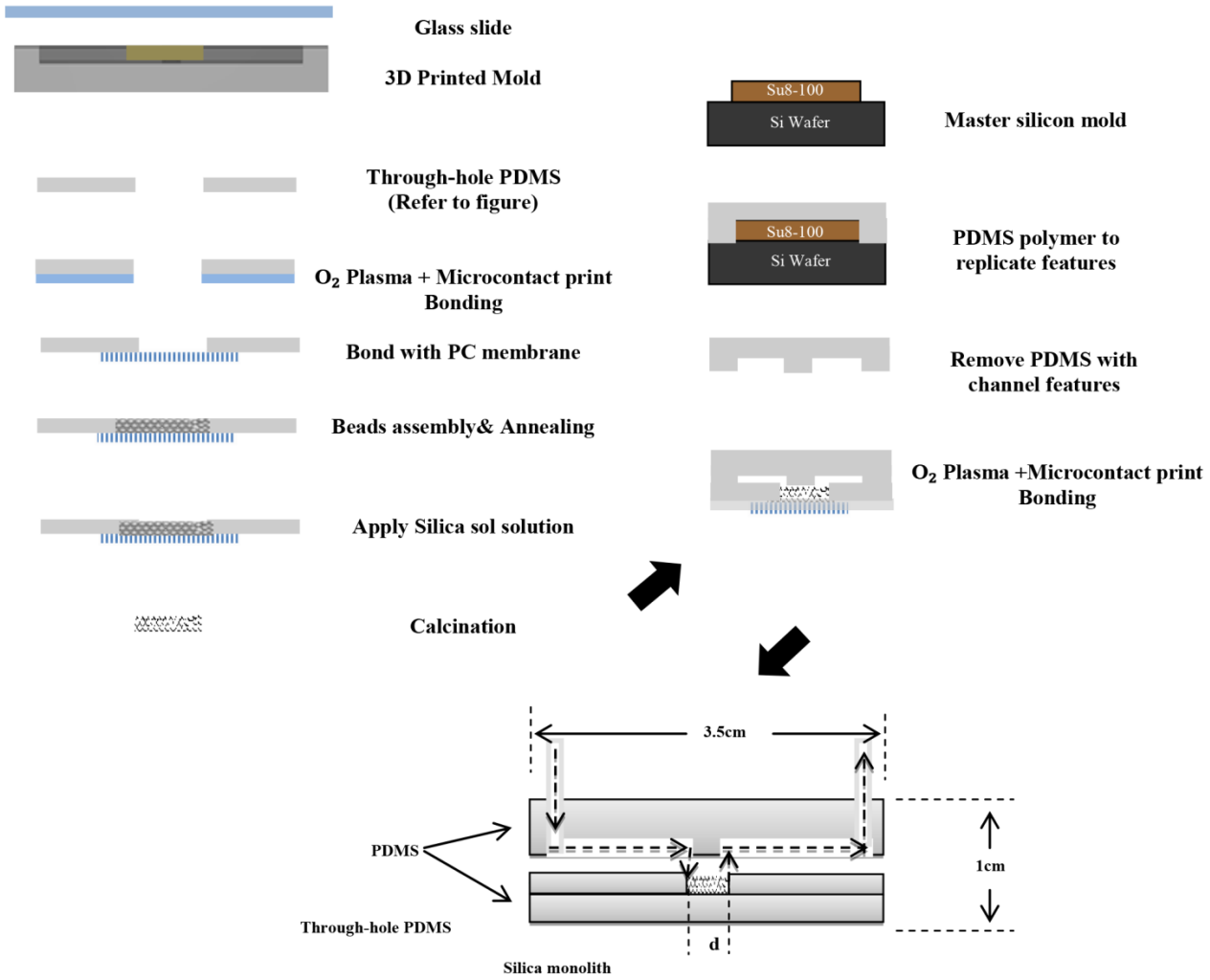

Figure 3-17 Schematics for device fabrication

Chapter 4 Device Fabrication and Experiment Set-up

4.1 Introduction

The overall design and principle were presented in the last chapter, and in this chapter the detail fabrication process of the microfluidic device will be discussed, as well as materials and method used during fabrication of microfluidic device and the macro/mesoporous silica material.

Monodispersed polystyrene microspheres are first synthesized and then assembled inside the extraction chamber. This assembly is used as the soft-template for the fabrication of the porous silica monolith. The size of pores in the monolith is controlled by heat treatment of the polystyrene microspheres. The silica sol-gel is mixed and filled the interstitial space between the polystyrene particles to form macro/mesoporous silica skeleton. Finally, thermal decomposition removes the polystyrene microspheres template and forms macro/mesoporous silica network.

The optimum temperature and duration for heat annealing of polystyrene microsphere monolith is presented at the result section, different methods for removing polystyrene templates are also explored and documented to justify the reason why thermal decomposition method is used for polystyrene template removal. Finally, characterization of the final macro/mesoporous silica structure is done by using N_2 isotherms, Thermogravimetric Analysis and Scanning Electron Microscopy.

4.2 Materials

4.2.1 PDMS (Polydimethylsiloxane)

SYLGARD® 184 PDMS (Polydimethylsiloxane) (Dow Corning, Midland, MI) was used at 1:10 curing agent to prepolymer base ratio. The curing agent is the cross linker used to form long polymer chains of the monomer when mixed with polymer base. The material has been widely used in the field of microfluidics due to its superior properties like transparency, biocompatibility, user defined stiffness [123] and the ability to routinely generate patterns with feature size down to 100nm[124] by using standard soft lithography procedures which do not require access to clean room facilities.

4.2.2 Silica Sol-gel

TEOS (Tetraethyl orthosilicate) was used as a silica source, and triblock copolymer surfactants (Sigma Aldrich), Pluoronic F127, was used as structure directing agent. The silica sol-gel solution was mixed based on recipe reported in the literature, TEOS:n-Butanol:Ethanol:H_2O:HCl molar ratio of 1:3:4:4:0.04 [125]. The triblock copolymer surfactant F127 was dissolved in n-butanol/EtOH to make 30 wt% solutions.

The sol-gel solution was formed through hydrolysis and condensation as explained in the last chapter and it was used to fill the interstitial space between assembled polystyrene microspheres after 24 hours of aging at 50 ℃.

4.2.3 Filter Membranes

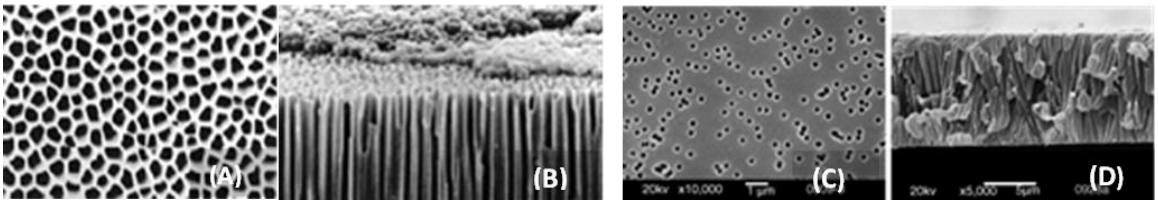

Figure 4-1 A typical Anodic Aluminum Oxide (AAO) membrane[126]**(a) Top view (b) Cross-sectional view and a typical Polycarbonate(PCTE) membrane (c) Top view (d) Cross-sectional view** [127]

There are few different types of membranes that can be integrated with PDMS based microfluidic devices, (i) Anodic Aluminum Oxide (AAO) membrane-Hydrophilic membrane (Figure 4-2 A&B); (ii) Polycarbonate Track Etch (PCTE) membrane-Hydrophobic membrane, and (iii) Polyvinylpyrrolidone (PVP) coated PCTE- Hydrophilic membrane. It was observed that the polystyrene microsphere self-assembly was more uniform on hydrophilic membranes comparing with a hydrophobic membrane. In addition, compared with hydrophilic AAO membrane, hydrophilic PCTE membrane is much thinner (10 μm thickness) and cheaper. Thus PVP coated PCTE membrane was chosen to create a through-hole PDMS piece.

PVP coated PCTE membranes with various pore sizes were purchased from Sterlitech Corporation. The pore density for 2 μm PC membrane used is 2 x 10^6 pores /cm^2, typical water flow rate through the membrane rated up to 300 ml/min/cm^2. And the membrane can be easily bonded with PDMS material by using microcontact printing process with the use of PDMS glue and Oxygen plasma treatment of PDMS surface.

4.3 Fabrication Method

4.3.1 Photolithography

Photolithography is a widly used technique in microfabrication process. In this process, the light-sensitive chemical “photoresist” is first coated on a silicon wafer. UV light transfers a desired pattern onto photoresist through a photomask. With the use of negative photoresist, unexposed regions can be selectively removed by using developer, and for a positive photoresist, exposed pattern can be removed by using developer after exposure [123], [128], [129].

4.3.2 Soft-Lithography: Replica Molding

The term soft-lithography was coined by *Whitesides* and his coworkers[130]. It was first introduced by *Xia et al* [131]. A negative replica of the photoresist master mold can be generated by casting uncured PDMS, and the patterns will transfer from the master mold to PDMS when PDMS is cured. Unlike traditional method such as etching in glass and silicon, soft-lithography dramatically simplified the process of fabrication, reduced time and cost for a cycle of design and testing. It also provided a faster, less expensive and reliable mean to do device fabrication outside of the clean room environment [132].

4.3.3 Rapid Prototyping-3D Printer

Photolithography technique is best suited to define patterns in photoresist that are few micrometers in height. Although features up to few hundred micrometers have been constructed using photolithography, the process becomes very time consuming and labour intensive. The rapid prototyping machine (3D printer) however offers a much easier

process albeit with lower resolution. The fast prototyping mold was first designed in AutoDesk Inventor software, and the 3D printer will then uses the design to inkjet the acrylic polymer to build the part line by line.

Projet HD3000 (Agile Manufacturing Inc., Uxbridge, Ontario) fast prototyping printer was used for creating master molds used for making through-hole PDMS (Polydimethylsiloxane) pieces. The acrylic polymer used in the machine was Visijet EX200 and the high resolution printing mode was used to provide an accuracy of 0.025-0.05 mm of part dimension and 29 micron print resolution [133].

4.3.4 Soft-Lithography: Microcontact Printing

Microcontact printing (or μCP) technique uses a stamp with relief features to transfer an 'inked' material onto a different substrate. Typically a PDMS replicated mold is used as stamp to transfer a thin layer (200-500 nm) of uncured PDMS glue onto a different substrate with certain pattern. With the use of 50W, 50 second of oxygen plasma treatment for PDMS surfaces, this coated substrate can be permanently bonded to another PDMS substrate by bring two flat surface together [134].

Microcontact printing method was used to effectively bond the through-hole PDMS piece with a polycarbonate porous membrane, they were then bonded between top microfluidic channel PDMS and bottom blank PDMS pieces for enclosing the micro-flow channels.

4.4 Fabrication of Microfluidic Channels

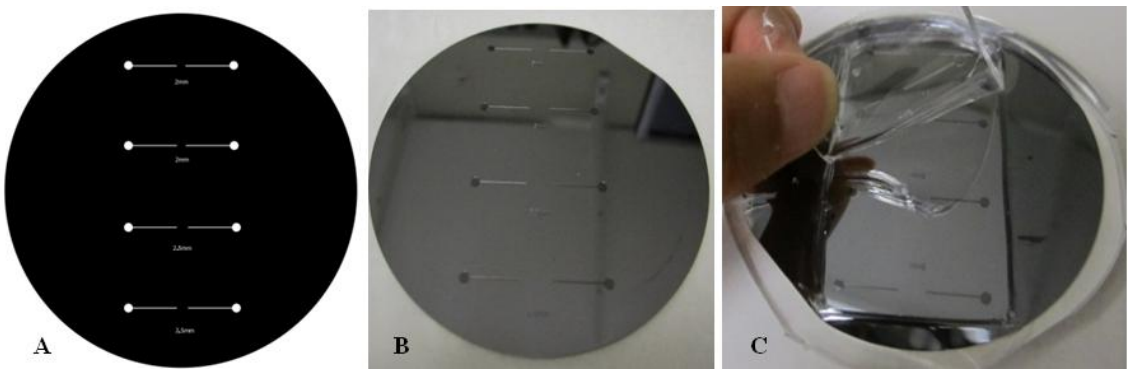

Figure 4-2 A) Photomask design B) Photo lithography: silicon master mold fabrication C) Soft lithography: PDMS channel replication

In order to pattern microchannels on a silicon wafer, photomask was first designed in AutoCAD software (Figure 4-2A), a microfluidic channel pattern with total length of 20 mm, width of 200 μm and a center 2mm stop block was transferred to a 3 inch wafer via photolithography process (Figure 4-2B), the detail parameter and receipe for the photolithography process to fabricate 100 μm height channel features using SU8-100 photoresist is documented in the Appendix II. Finally the microchannel features were transferred to PDMS polymers through soft lithography procedure (Figure 4-2C).

4.5 Synthesis of Mono-Dispersed Polystyrene Microspheres

In order to assemble the polystyrene soft-template, first the monodispersed polystyrene microsphere has been synthesized by dispersion polymerization[121]. A modified drop-wise monomer feeding procedure for synthesizing monodispersed

polystyrene microsphere developed by *Qi et al*. [135] has been adopted in the following synthesizing process to create larger than micrometer sized polystyrene microspheres.

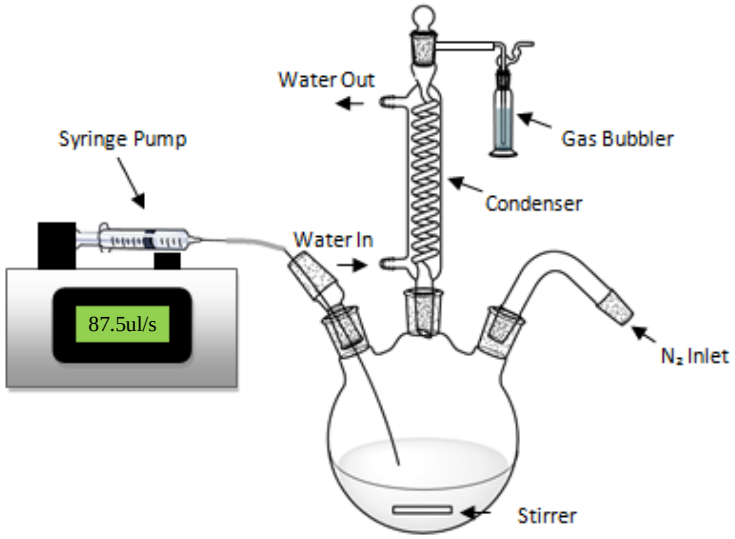

Figure 4-3 Synthesis of monodispersed polystyrene microspheres set-up

Styrene (St) (99%, Sigma-Aldrich) was filtered by using Inhibitor remover (Sigma-Aldrich, 306320) to remove the inhibitor, and the filtered solution was stored in refrigerator before uses. As initiator, peroxide compound, benzoyl peroxide (BPO) (>98%, Sigma-Aldrich), was used as received. Polyvinylpyrrolidone (PVP-40) (Sigma-Aldrich) was used as the stabilizer and anhydrous ethanol was used as the dispersion polymerization medium.

There are few parameters that are the important to successful synthesizing of monodispersed microspheres, namely reaction time, stabilizer concentration and feeding rate:

Reaction Time: the polystyrene particle size is dependent on the reaction time, the size increases deeply at the early stage and then gradually increases until it reaches saturation point[136]. The 12 hours of stirring at the end of reaction ensures all particle size reaches saturation.

Stabilizer Concentration: *Lee et al*. demonstrated that with PVP concentration relatively to the monomer weight of 2*wt*% [118] is best for producing monodispersed polystyrene microspheres when using amphoteric initiator. Polystyrene particle size decreases as the concentration of PVP increases due to the increase of primary nuclei in the beginning of polymerization.[136]

Feeding Rate: Styrene and BPO mixture feeding rate were chosen based on Fig-5 of *Qi's* work[135]. For instance, optimal feeding rate of 87.5ul/s is used when synthesizing 3.45 μm sized polystyrene microspheres.

Ethanol and PVP-40 were mixed and placed inside the three neck flask. The polymerization temperature was precisely controlled at 70 ℃ by using an oil bath. Once the solution was well mixed and reached desired temperature, styrene and BPO mixture then were delivered into the system under nitrogen atmosphere via a syringe pump. The reaction was carried out for 12 hours with constant stirring. The final solution was centrifuged at 3,500 rpm to eliminate any unreacted chemicals, and polystyrene microspheres were then re-suspended in ethanol. Brookhaven Dynamic Light Scattering (DLS) with BI-9000AT auto-correlator and 35 mw laser was used to analyze the size and

the polydispersity index (PDI) of the polystyrene microspheres. The recipe and result are given in Table 4-1 as following.

Table 4-1 Recipe for preparing monodispersed polystyrene microspheres

Size\Ingredients	Styrene(g)	Benzoyl Peroxide(g)	PVP 40(g)	Ethanol(g)	RPM	PDI
1.12 μm	6	0.006	0.18	18	200	0.147
3.45 μm	32	0.472	0.96	68	500	0.11

The polydispersity index effective (PDI) showed in above table is a measure of the size distribution for width of polystyrene particles resulted from DLS test. A low polydispersity value indicated a narrowly distributed particle size, 3.45 μm polystyrene microsphere monodisperse to 0.11 and 1.12 μm polystyrene microsphere monodisperse to 0.147 were synthesized by using this drop-wise dispersion polymerization process.

4.6 Suction Assisted Approach for Assembly

4.6.1 Through-hole PDMS Piece Fabrication Standardization

Figure 4-4A illustrated the process of fabricating a through-hole PDMS feature by using a rapid prototyping mold. PDMS was cast on the rapid prototyped printed mold (Figure 4-2B) and a glass slide was used to cover the top to create a smooth PDMS surface, which can subsequently bonded with a polycarbonate membrane. Two flat aluminum plates were used to clamp the glass slides tightly, and the glass slide on top was closely in touch with the printed feature which resulting a through-hole at the center

of PDMS piece. Finally, the PDMS was cured at 60^{o}C for 3 hours, and the through-hole PDMS piece was peeled off carefully from the rapid prototyping mold.

.

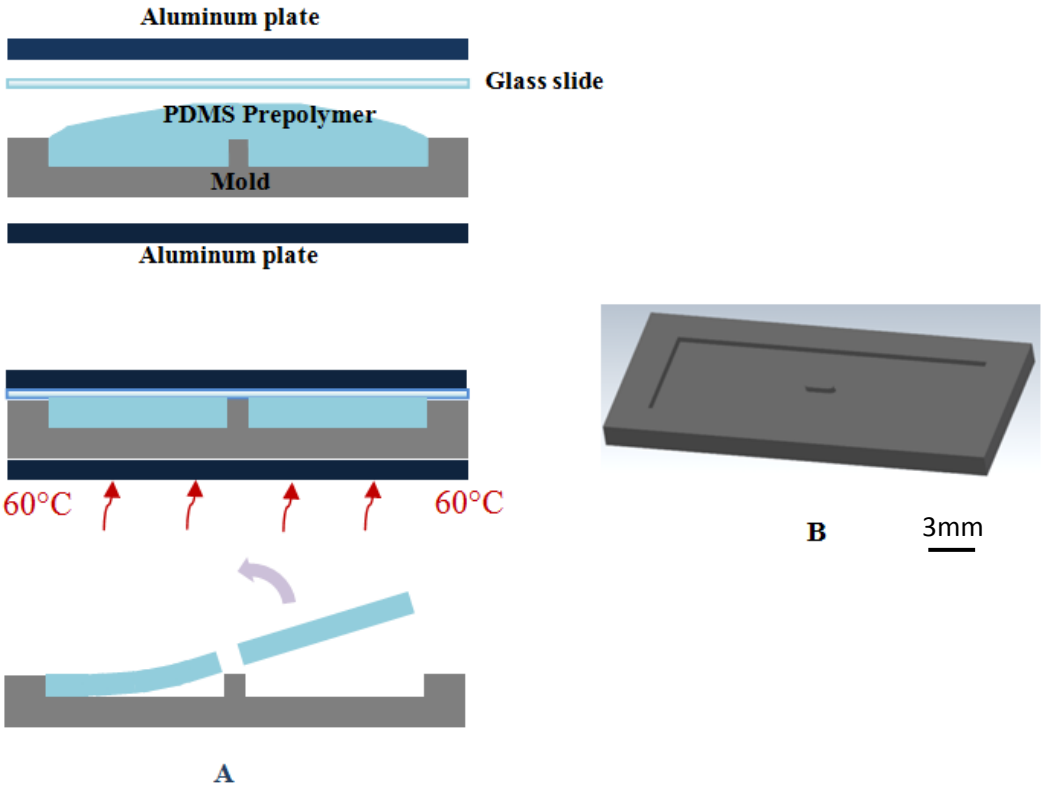

Figure 4-4 A) Fabrication process of PDMS through-hole feature B) Inventor mold design

The PDMS through-hole/extraction chamber is designed to have a 0.65 mm thick through-hole with an openning of 2.79 mm^2 to achieve 1.81 mm^3 chamber volume as specified in Chapter 3. However the top PDMS openings were always partially blocked by a thin PDMS film on the top side (Figure 4-5B). A complete PDMS film can even form if the fast prototyping mold bended due to thermal expansion during the curing

phase (Figure 4-5A). This problem has to be solved in order to create a uniform pressure distribution for polystyrene microspheres assembly.

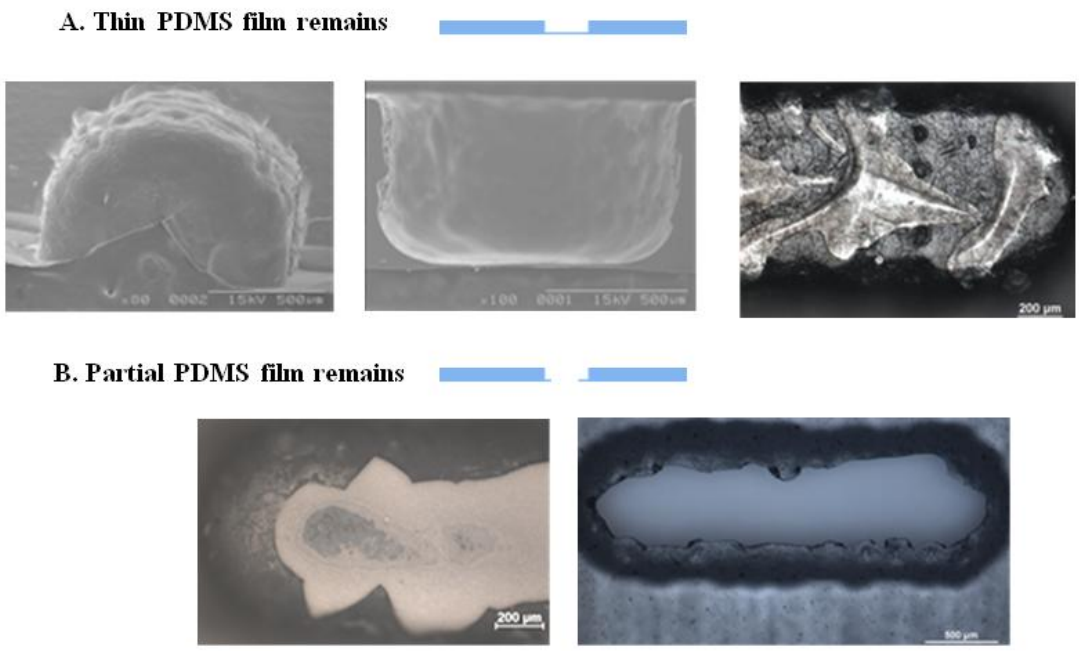

Figure 4-5 **Problems when using 3D printed mold to make through-hole PDMS**

The procedure has been standardized in order to create a better through-hole PDMS part as illustrated in Figure 4-6. A transparency film was introduced in between the glass slide and fast prototyping mold for easier removal of cured PDMS, the center feature of the mold was designed 10-15 μm higher than the edge to ensure the feature will be tightly in contact with transparency and glass slide on top. And the curing temperature was set at 50^{o}C to prevent deformation of acrylic material. In addition a flat glass slide was used to remove excess PDMS from the fast prototyping mold before sandwiching the mold in between two glass surfaces.

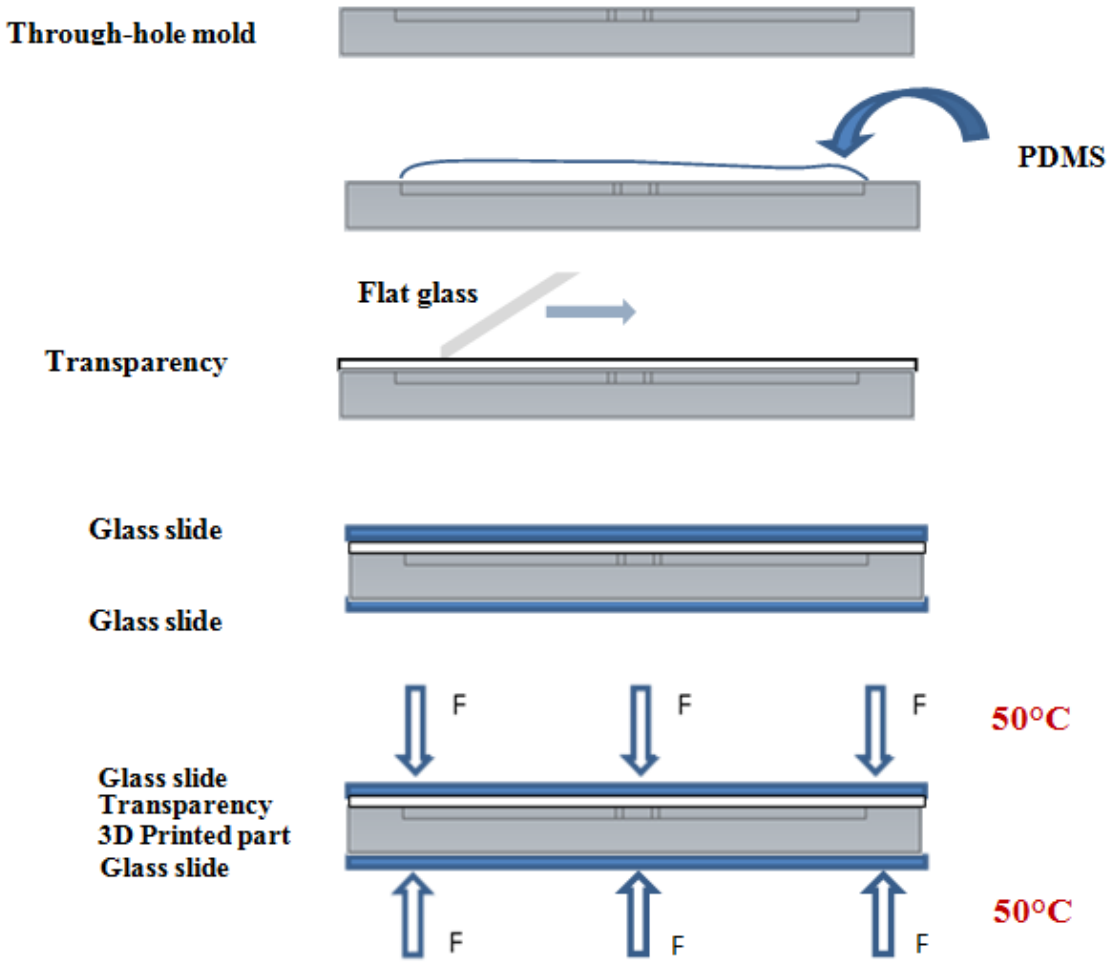

Figure 4-6 Standard procedure of making through-hole PDMS by using a 3D printed part

The new standardized procedure yield significant improvements of the fabricated through-hole PDMS piece. Three new fast prototyping molds were printed and tested to verify the standardized procedure can generate a good and consistent through-hole PDMS piece every time. And three through-hole PDMS pieces were prepared from each mold. Then the feature surface area of the mold and corresponding opening area for each PDMS

replicate were measured and compared (Figure 4-7). It is seen that the opening of through-hole PDMS created using this procedure can match average 95% opening areas from fast prototyping mold (Table 4-2), and the majority of unwanted extra PDMS film was eliminated.

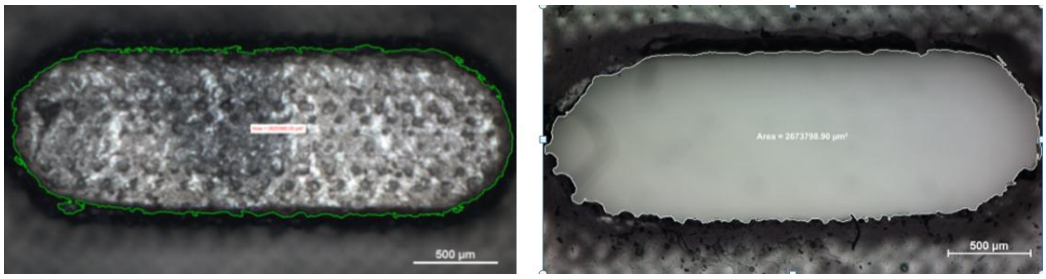

Figure 4-7 Measuring mold feature (left) area and PDMS opening area (right) using ImageJ software

Table 4-2 Consistency of printed mold and PDMS through-hole replicate

	Part1	Part2	Part3	Average
Printed Area (mm^2)	2.6254	2.5368	2.478	
Average PDMS area (mm^2)	2.5309	2.3821	2.3111	
Actual (PDMS)/Printed (%)	96.40%	93.90%	93.26%	94.52%

4.6.2 Experiment Set-Up for Polystyrene Microsphere Assembly

After through-hole PDMS piece was created, microcontact printing was used to attach the 2 μm pore sized polycarbonate membrane (Sterlitech Corporation, PCT2013100) onto the through-hole PDMS piece.

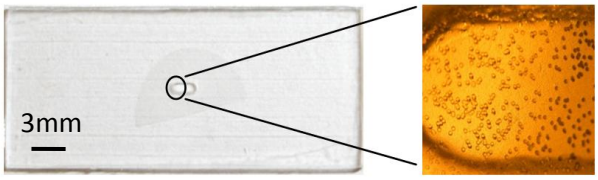

Figure 4-8 Through-hold PDMS part bonded with PC membrane (20 μm pore size polycarbonate membrane)

A thin layer of PDMS was obtained by spinning PDMS pre-polymer (base/curing agent: 10:1) on the silicon wafer at 8000 rpm for 2 minutes, the through-hole PDMS piece was placed on the thin uniform PDMS pre-polymer and lifted off, the polycarbonate porous membrane which has uniformly distributed 2 μm pores was carefully placed on to the through-hole to form the bottom filter membrane for the assembly chamber. The pores that came in contact with PDMS glue during microcontact printing were blocked and only the ones located within the through-hole opening were left open (Figure 4-8). The open region of polycarbonate membrane will be used as filter membrane to accumulate polystyrene particles in the chamber.

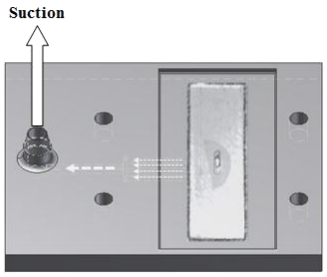

Figure 4-9 Suction mold

As shown in Figure 4-9, a fast prototyping suction mold has been designed and fabricated to supply an uniform negative suction pressure to the openning pore region of the through-hole PDMS piece using a withdraw syringe pump. The syringe was connected to the inlet of suction mold using TYGON tubing, when the syringe pump starts its withdrawing motion, the negative pressure created was distributed to the pore opening evenly through 4 smaller split channels inside the suction mold. A 8.5mg/ml concentrated polystyrene microspheres solution in ethanol was used, and it was sonicated for 5 minutes before using. The additional infusion syringe pump was used to continuously delivering polystyrene particles through a BD 30G1/2" needle positioned on top of assembly chamber using a micro-positioning stage (refer to Figure 4-10), a small stirrer bar has been placed inside the infusing syringe tube and stir plate was used to agitate the solution to avoid the sedimentation of polystyrene particles.

The surface of fast prototyping suction mold was coated with PDMS to make a good contact in between through-hole PDMS substrate and the mold. It ensures the seal in between two parts are good and no pressure leakage in between those two PDMS surfaces when suction is applied.

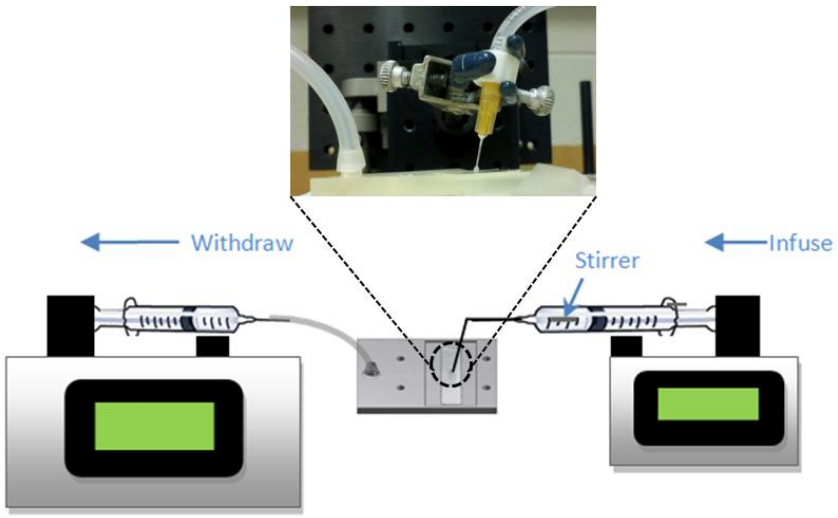

Figure 4-10 Pressure assisted beads assembly experiment set up

Delamination between polycarbonate membrane and PDMS occurs when withdraw rate applied to the system was higher than 0.5ml/min during assembly (Figure 4-11). The polycarbonate membrane can still deform even at a slower withdrawal rate. To eliminate this problem, a small piece of 0.1μm pore sized AAO membrane was added in between PDMS through-hole piece and the suction mold to increase the stiffness of the membrane and prevent any deformation/delamination might occur when applying suction. With this modification, withdraw speed can be increased up to 0.8 ml/min without affecting the bonding and the shape of polycarbonate membrane, and 0.7ml/min withdraw rate were used during all assembly procedures unless otherwise stated.

In addition, infusion syringe pump was stopped every 3 minutes and 2.5μl pure ethanol was manually deposited in the particle assembly chamber to help better assembly.

With the use of 0.7ml/min withdraw rate and 8.5mg/ml polystyrene solution, the filling process normally takes 20 minutes for completion.

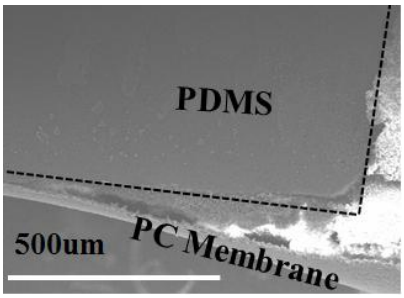

Figure 4-11 Delamination of polycarbonate membrane

Once the polystyrene microspheres filled the whole assembly chamber, a flat glass slide was used carefully to remove excess amount of particles. Finally, additional low concentration (<0.5mg/ml) of polystyrene microsphere solution was applied to make the top surface of the assembly smooth, fill any voids caused by the removal process.

4.7 Thermal Annealing of Polystyrene Monolith

To ensure the monolith is one solid structure and the pores are interconnected throughout the monolith after removal of polystyrene template, the assembled polystyrene monolith was treated in an annealing oven. By varying the annealing time and the temperature, one could control the interstitial spaces between polystyrene particles. As illustrated in Figure 4-12, the interstitial space between polystyrene microspheres becomes smaller when the annealing duration increases. Since the interstitial space between particles will be filled by silica sol-gel material, annealing process can be used to control the macropores in the final silica monolith. The effect of heat treatment on the

polystyrene monolith was investigated by varying the temperature and the time duration. SEM images of top surface, bottom surface after removing polycarbonate membrane and the center of the monolith were taken after the annealing for analysis (three different locations are shown in Figure 4-13). The contact length between adjacent particles and the area of interstitial space in between particles were then measured to characterize the annealing process and its effects.

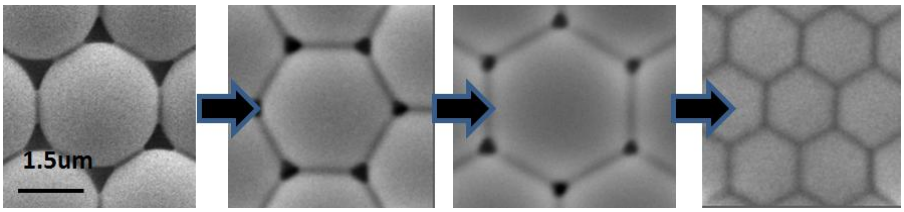

Figure 4-12 Monolayer of PS particle (3.4μm) annealing (107^{o}C) with various time duration (10min, 20min, 30min, 40min)

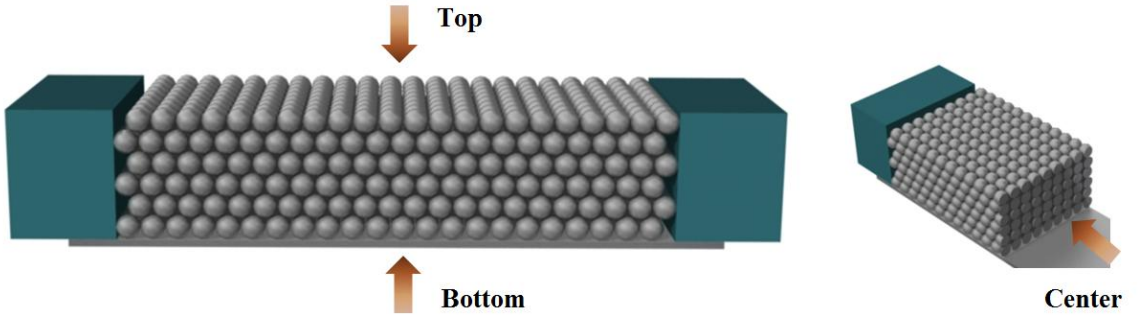

Figure 4-13 SEM imaging locations

The glass transition temperature for polystyrene material is 95^{o}C[122], therefore temperatures ranging from 90 ^{o}C up to 124 ^{o}C were used in experiments to investigate the control of interstitial spaces. This range covers temperature from below the glass

transistion temperature to that well above it. and the temperature difference between heating substrate and the air was measured using thermostats (Appendix I), and it was noticed that the temperature of the heating substrate was on an average of 4.7^{o}C higher comparing with the air temperature.

Samples were subjected to various duration of annealing from 10 minutes to 40 minutes, and ImageJ software was used to measure the contact length between adjacent particles: **d** and the interstitial space area for different samples (Figure 4-14).

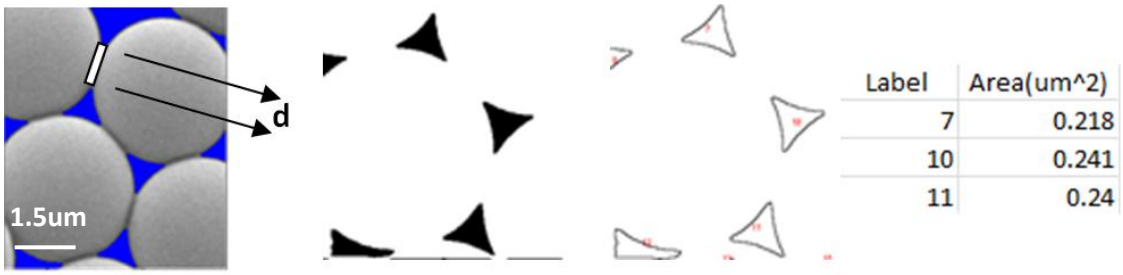

Figure 4-14 Measurement of the contact length between adjacent particles: d and interstitial space areas (7, 10, and 11)

4.7.1 Results

Scanning Electron Microscopy studies of the monolith formed have been conducted and are summarized into Table 4-3. It can be seen that particles remain in contact but have not melted when annealing temperature was below 95^{o}C as shown in Figure 4-15. SEM images were not taken for these temperatures conditions due to the looseness and non-conductivity nature of the particle. Particle in the bottom surface of the polystyrene monolith started melting and bonding with one another when temperature

used slightly above glass transition temperature (98^{o}C), but the particles at the center were still unbonded. Heat was able to penetrate the monolith deeper from the bottom surface towards the top surface at 107^{o}C, and it was seen that the particle at the bottom surface particles all merged together and formed hexagonal patterns when duration increased to 40 minutes, the particle at the center also appeared to have small deformations (white dots) at this condition, which seems to be the location of break off point of bonded particles (Figure 4-16). When temperature was raised further to 116^{o}C, an interconnected particle network was formed throughout the polystyrene monolith even at 10 minutes of heat treatment. Beyond 20 minute duration, further increase of the duration caused the particles to completely merge with one another and form hexagonal patterns which resulting zero interstitial spaces. And the completely merged state can be best illustrated with Figure 4-17, where the polystyrene monolith was treated at 124^{o}C for 10 minutes.

Table 4-3 Time and temperature required for interstitial particle fusion start occurring (F) to the complete merged state(C), symbol "-" means there is no connection formed due to melting of particles

	Top					Center					Bottom				
	90^{o}	98^{o}	107^{o}	116^{o}	124^{o}	90^{o}	98^{o}	107^{o}	116^{o}	124^{o}	90^{o}	98^{o}	107^{o}	116^{o}	124^{o}
10min	–	–	–	F	C	–	–	–	F	C	–	F	F	F	C
20min	–	–	–	F	C	–	–	–	F	C	–	F	F	C	C
30min	–	–	–	C	C	–	–	–	C	C	–	F	F	C	C
40min	–	–	–	C	C	–	–	F	C	C	–	F	C	C	C

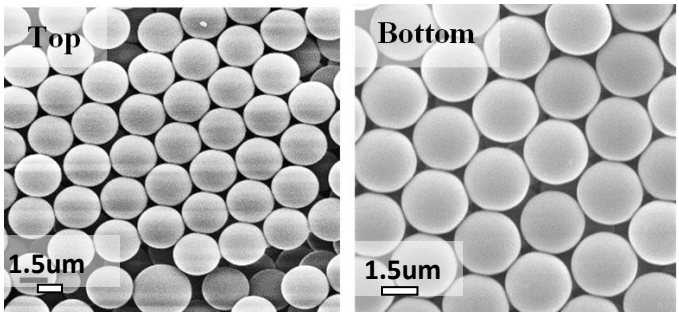

Figure 4-15 SEM images for top and bottom surface of monolith at 90°C, 10min

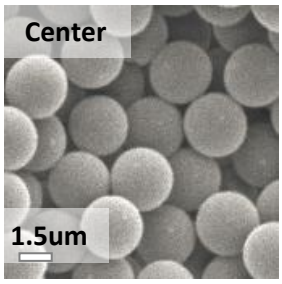

Figure 4-16 Interconnectivity of PS beads at 107°C, 40min

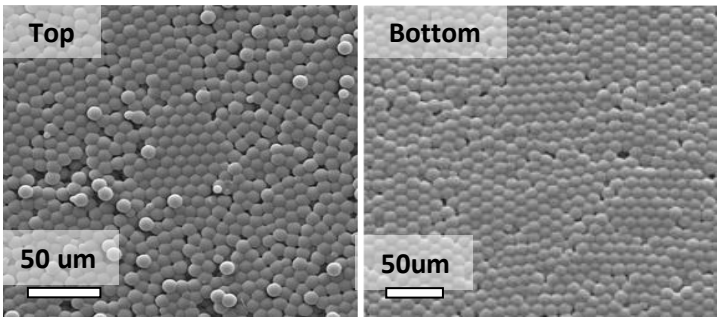

Figure 4-17 Complete merged state at 124°C, 10 min

Duration and Temperature Effect on Polystyrene Monolith

The effect of the annealing duration at different locations on the polystyrene monolith is shown in Figure 4-18. It indicates that at constant temperature of 116°C the particles at various locations on the monolith show increasing interconnectivity with increase in the annealing time. The particles at the bottom surface particles became

completely bonded after 10 minutes, the particles at the center and the top both started bonding after 20 minutes. And it is obviously to see that when annealing temperature is above glass transition temperature of polystyrene, increases in the duration of annealing can result the increase in contact length and the decreases in interstitial space.

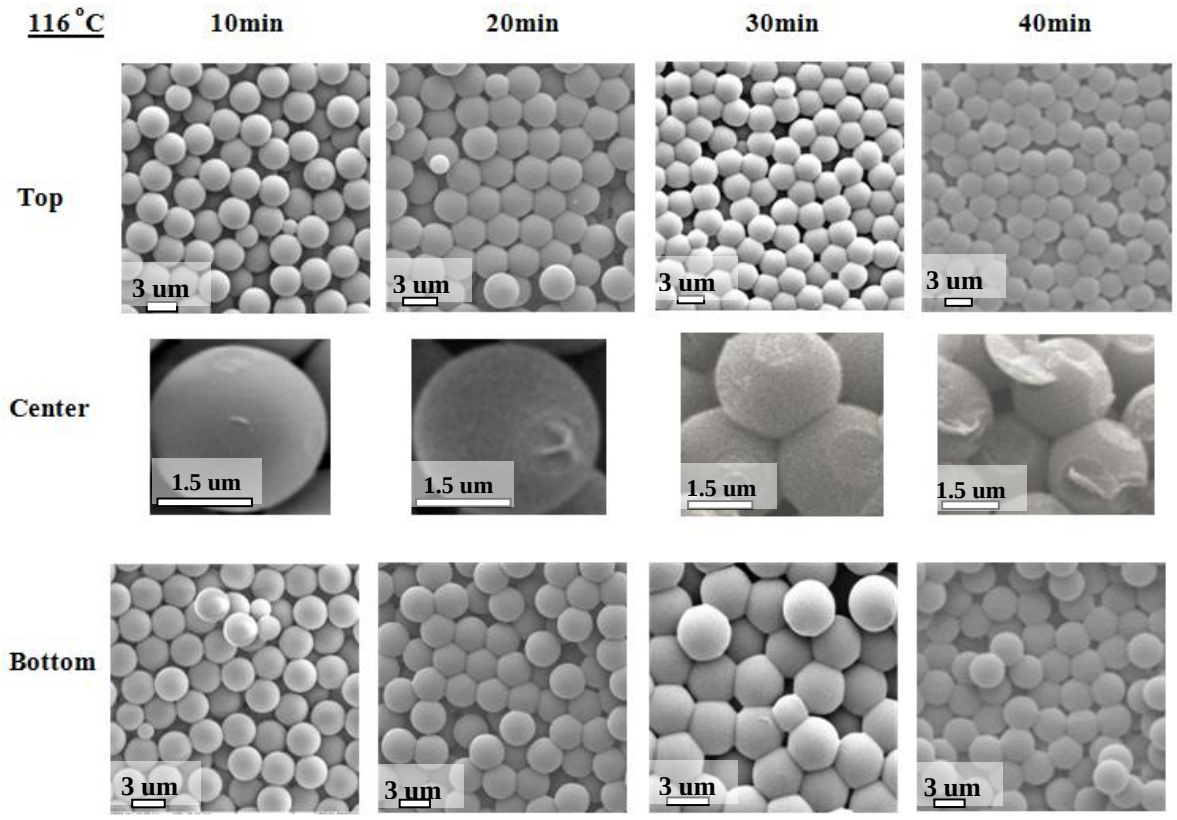

Figure 4-18 Effect of variation in time

The effect of annealing temperature at various locations of the polystyrene monolith is illustrated in Figure 4-19. When the annealing time kept at constant 20 minutes and the temperature increased, both the particles at the bottom and top surface start deforming from a circular cross section to a hexagon as they been to merge at 116 ℃.

The center of monolith also had good interconnectivity at 116 ℃ and 124 ℃. However, in the case of 98 ℃ and 107 ℃, the particles were not bonded with each other at the center of the monolith which made it difficult to obtain SEM images at those conditions. Based on these result it can be concluded that the increase of temperature at a fixed annealing duration will result longer contact length between adjacent particles and smaller interstitial spaces.

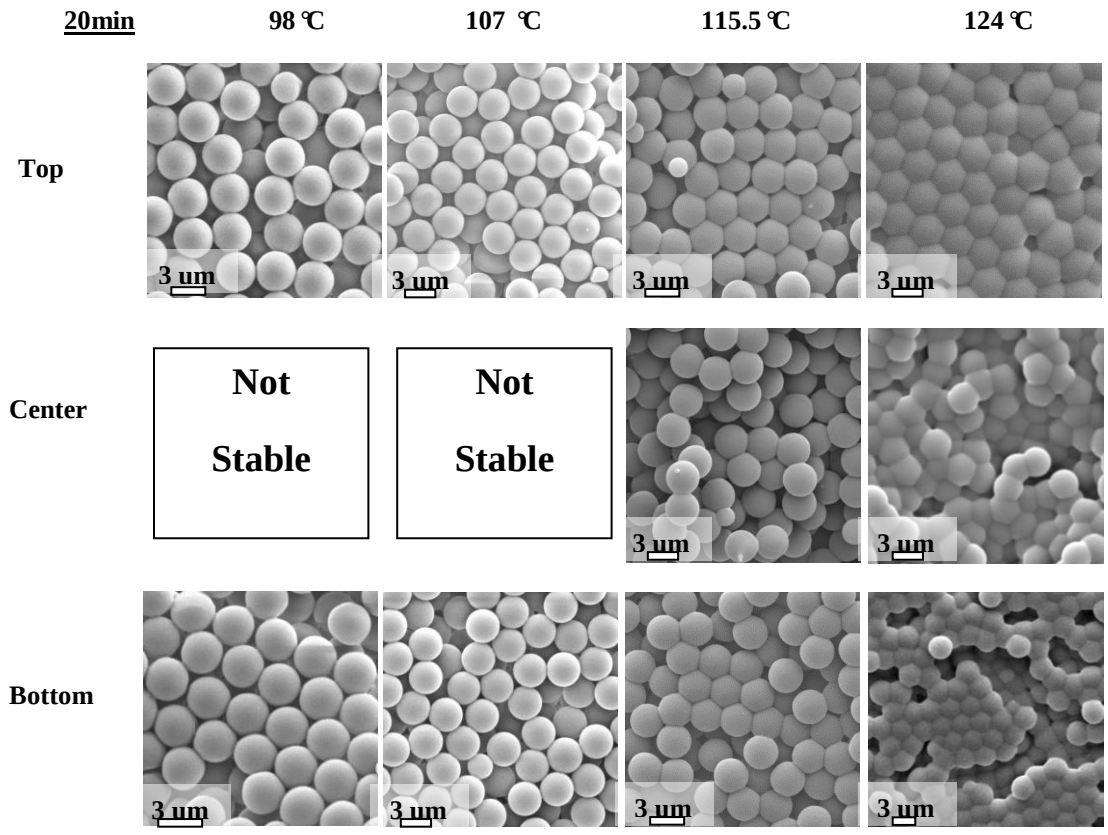

Figure 4-19 Effects of variation in temperature

Maximum Contact Length & Optimal Temperature and Duration

In order to determine the maximum contact length, the contact length attainable between perfectly stacked monodispersed polystyrene microspheres after annealing (the contact length of adjacent particles at the moment of zero interstitial space), the contact length data for both top and bottom surface of monolith at 116^{o}C for 20 minutes is plotted in Figure 4-20, the interstitial spaces were completely sealed at the bottom of the monolith (close to the PC membrane) while small interstitial openings were still present at the top (Figure 4-20). By measuring contact length between adjacent particles at this instance, the maximum contact length between adjacent particles was determined to be between 1.4 μm and 1.5 μm. Which is close to the side length of a hexgon inscribed in a 3 μm polystyrene microsphere.

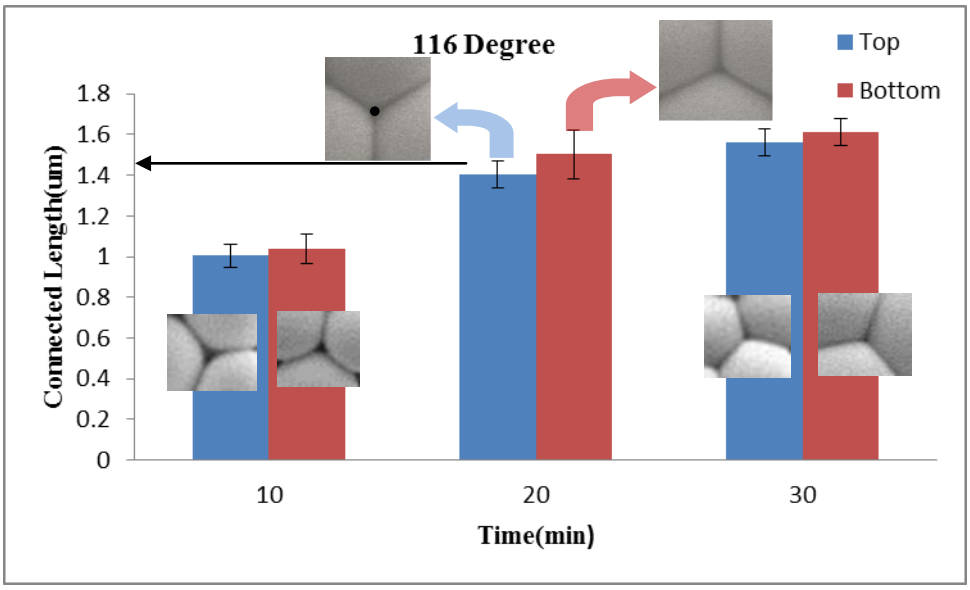

Figure 4-20 Maximum contact-length for forming hexagon pattern

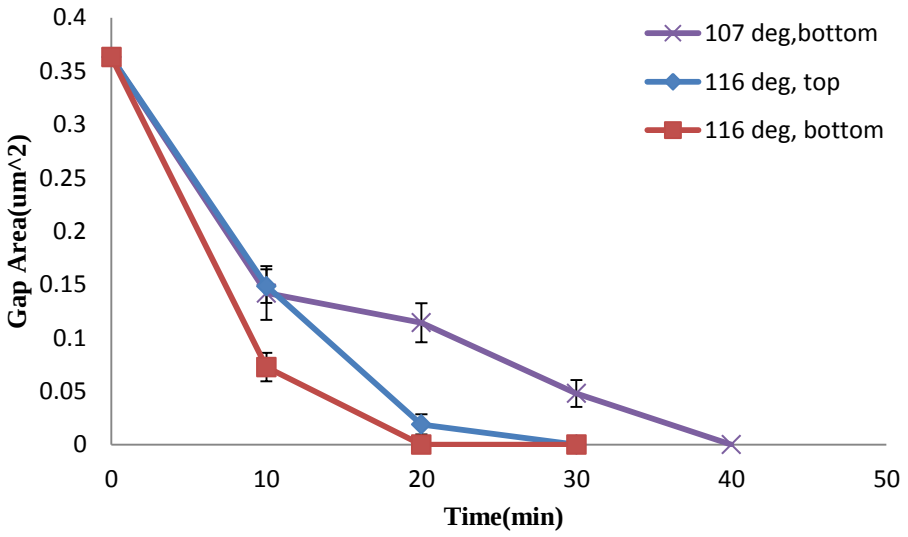

Figure 4-21 Interstitial space areas for all different parameter settings

The interstitial spacing formed between particles in respect to the annealing temperature and the time duration is plotted in Figure 4-21, note that the data for those temperatures that include bonding without complete merger of particles($0.363\mu m^2$>interstitial space>0) were presented. As we can see from the graph, the interstitial space decreases as the annealing duration increases, and the interstitial area decreasing rate increases while temperature increases.

The bottom surface particle contact length data from all different settings is plotted in Figure 4-22. The maximum contact length between adjacent particles is 1.4-1.5 μm and the shaded band shown in the figure is indicating the complete merge of particles.

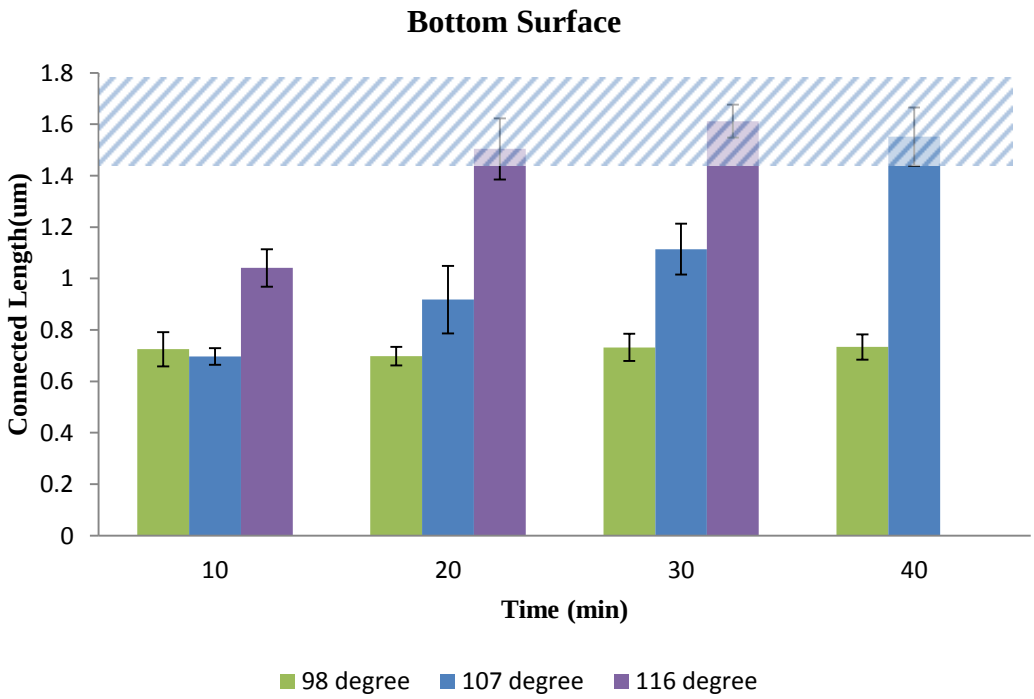

Figure 4-22 Particle contact length with respect to annealing temperature and time

When the temperature approaches glass transition temperature, the contact length of the adjacent particle should start increasing from zero and approach to the side length of the hexagon that circumscribes/inscribes the circular cross section of a particle as iluustrated in Figure 4-23, and the interstitial space should approch to zero. With the use of 3 μm polystyrene microspheres, The particles are expected to completely fuse with one another when the contact length is between 1.5 μm and 1.73 μm, where 1.5 μm is the side length of the hexagon, and 1.73 μm is the side length of circumscribes the circular cross section of a particle with a diameter of 3 μm. Which maches our experimental observation of maximum contact length of 1.4 μm - 1.5 μm.

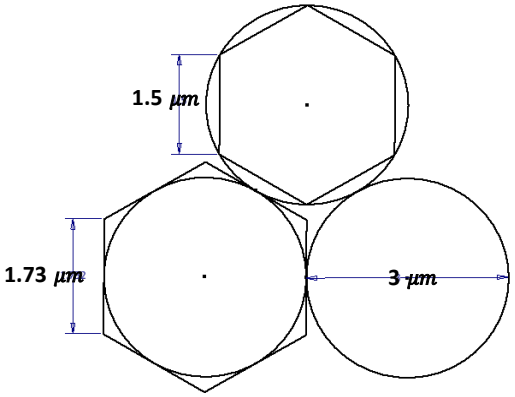

Figure 4-23 Theoretical particle fusion-length for hexagon pattern

Based on all discussion above, to avoid the complete merge of polystyrene particles and to ensure the interconnectivities are presented throughout polystyrene template, one could heat up the monolith to 116^{o}C degree for between 10 minutes in order to create fused connections in all locations without sealing the gaps in between particles and reaching complete merged state.

4.8 Synthesis and Pattern of Macroporous/mesoporous SiO_2 Monolith

Acetone or toluene dissolution was investigated as possible methods to remove polystyrene template inside a PDMS through-hole chamber, result indicated that both solvents dissolved polystyrene microsphere assembly within one minute, but it was found that solidificated silica sol-gel crumbles to poweder after toluene treatment (Figure 4-24C) the toluene also partically disolved the polycarbonate membrane during the dissolution process, thus acetone has been chosen as solvent removing method for comparison with the thermal decomposition method.

Figure 4-24 A: Solidified silica sol-gel, B: Acetone treated silica sol-gel, C: Toluene treated silica sol-gel

Silica sol-gel solution was prepared based on the process and recipe outlined in 4.2.2, it was heated to 50^{o}C for 2 days, and three samples were prepared from this solidified silica monolith for comparisons purposes. The first sample was the solidified sol-gel silica monolith without any treatment (Figure 4-24A, Figure 4-25A), the second sample was the sol-gel silica monolith treated with acetone for 1 minute (Figure 4-24B, Figure 4-25C) and the third solidified sol-gel sample was placed in a programmable

calcination oven and heated up to 550^{o}C for 5 hours with a ramp up rate of 1.5^{o}C /min to simulate the polystyrene thermal decomposition process (Figure 4-25B).

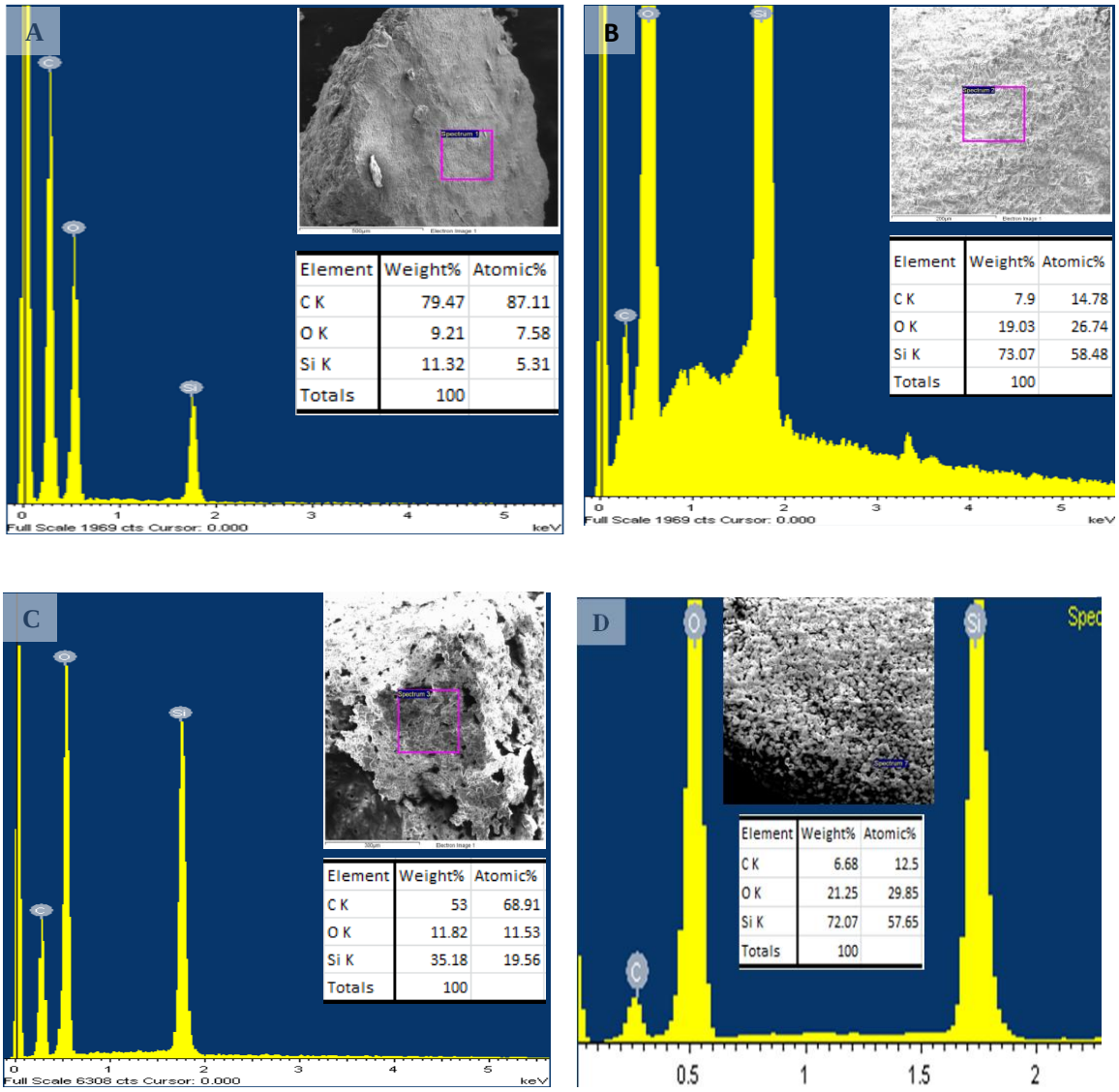

Figure 4-25 comparison of two different methods of dissolving template polystyrene particles, A) Silica monolith B) Silica monolith + calcination C) Acetone treated Silica monolith D) Pure SiO_2

Energy Dispersive X-ray (EDX) spectroscopy was used to analyze the chemical composition of the silica material after thermal decomposition and solvent dissolution. EDX for silica sol-gel solid is shown in Figure 4-25A, the final sol-gel product without any treatment resulted almost 90% of carbon might due to the presence of large amount of triblock copolymer F127.

SEM images revealed the structure integrity has been serverly damaged for acetone treated silica monolith (Figure 4-25C), and the structure still contains almost 70% of carbon. High carbon content might cuased by inefficienct disolving of F127, and one reason why the strucutre was damaged by acetone might be that acetone attacks F127 and dissolved incompletely solidified colloidal silica nanoparticles in the silica-gel.

The EDX result for thermal decomposition silica sol-gel (Figure 4-25B) and pure silica (Figure 4-25D) are very silmilar, both contains roughly 30% of Si and 60% of O element. And the ratio of the chemical element weight percentage obtained are very similar to the composition of silica nanotube reported by *Jo et al* [137]. Compared to the solvent dissolution method, thermal decomposition can preserve the structure integrity of the porous silica monolith, and the chemical composition from EDX indicated that the monolith is silicon rich. Thus thermal decomposition will be used as polystyrene soft-template removal method.

4.8.1 Silica Monolith without Heat Annealing

Silica sol-gel solution was prepared and used to fill interstitial spaces in between particles by using the same suction assisted assembly set up described in 4.6.2, but with much slower withdraw rate 0.3ml/min because the sol-gel solution is more viscous. Once the sol-gel has penetrated through the monolith to the suction device, the syringe pump was then stopped and the system left under pressure for 30 minutes to allow infiltration of sol-gel solution. The sol-gel residual on top of polystyrene monolith was carefully removed by KIMWIPES® Wipers. Finally, the monolith was undergoing thermal decomposition process to remove polystyrene template.

The calcination oven was programed with ramp up rate of 1.5^{o}C /min to 550^{o}C for 5 hours. The decomposition of polystyrene material started at temperature 200^{o}C and complete volatilization was achieved at 450^{o}C [138]. After the complete removal of polystyrene microspheres, temperature was kept at 550^{o}C for 5 hours to remove any organic contaminants.

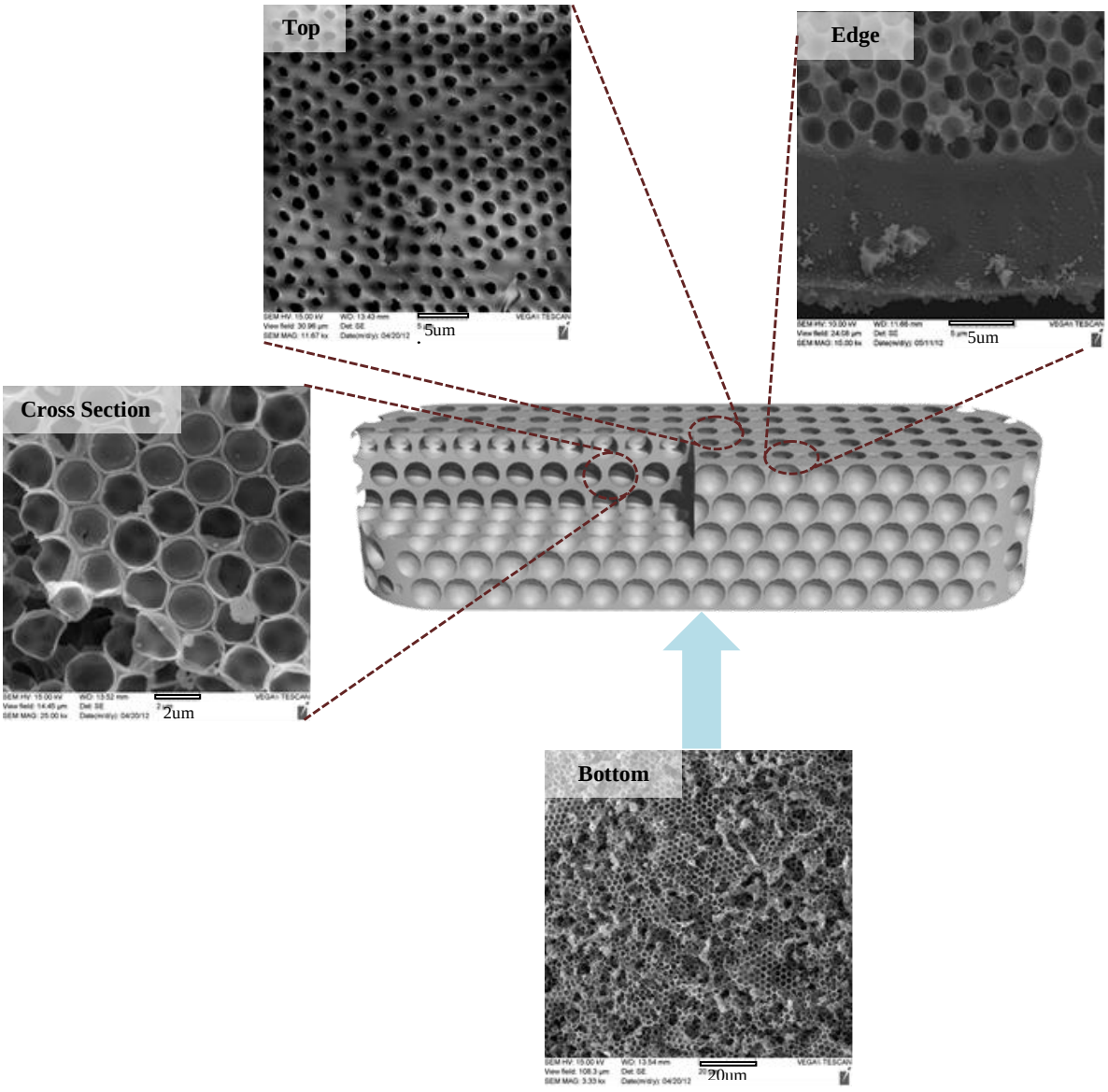

Figure 4-26 Silica mesoporous monolith characteristics without heat annealing process

As shown in Figure 4-26, SEM images for different locations of silica monolith are taken after thermal decomposition removal of polystyrene template. It was observed that most of the pores formed were sealed and only a few were interconnected with each

other through openings as small as 150 nm. The isolated pores will be of no use for DNA extraction as sample solution cannot enter them.

The result also revealed the spherical cavity formations were presented everywhere as expected, since the silica sol-gel will be a negative replica of the original polystyrene colloidal assembly. The hexagonal close-packed lattices of pores were observed at the top surface, cross-section and the bottom surface of the monolith. The hexagonal close packed cavities on top and bottom are most open pores, which means the cavity is expose directly to the air without the sol-gel residual blocking the pores. On the side of the monolith however, there is a thin layer of silica film formed between the original polystyrene microspheres assembly and the PDMS sidewall that completely enclosed all cavities.

It was also observed that the shape of cavities was slightly deformed (Figure 4-26Cross-section& Edge) and became more elliptical. The overall shrinkage of the monolith was 14% in contrast to the shrinkage of 50%-85%[139] in a TEOS derived silica without addition of F127. More importantly, the porous silica monolith synthesized was crack free as illustrated in Figure 4-27.

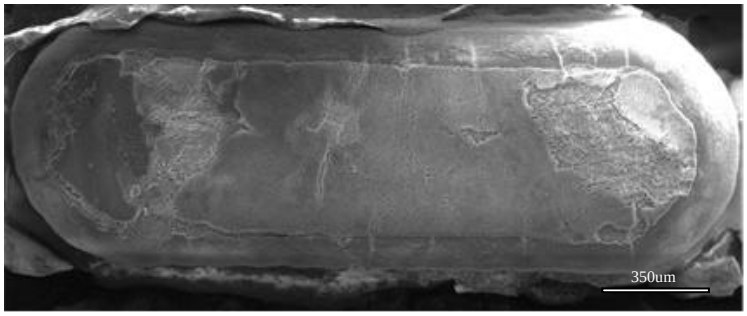

Figure 4-27 Crack-free mesoporous silica monolith, bottom surface

It is critical to ensure the interconnectivity of all pores is presented throughout the silica monolith for DNA extraction purpose, and the synthesis of silica monolith with heat annealing was investigated.

4.8.2 Silica Monolith with Heat Annealing

Silica sol-gel solution was again prepared and used to fill the interstitial spaces in between particles, based on previous polystyrene assembly annealing result, the polystyrene monolith was heated up to 116 ℃ for 10 minutes before silica sol-gel solution infiltration step to control the interconnectivity of all pores. As illustrated in Figure 4-28, the porous silica monolith created appears similar as before, but the interconnected pores were formed everywhere throughout various locations. The interconnecting openings at the cross-section close to the top shows circular shaped pores (0.5 μm to 0.86 μm) presented in different cavities. Instead of one circular shaped pore, interconnect pores comprised of series of small openings that forms a ring shape was observed at the center location, which essentially matched the negative replica of Figure 4-18Center.

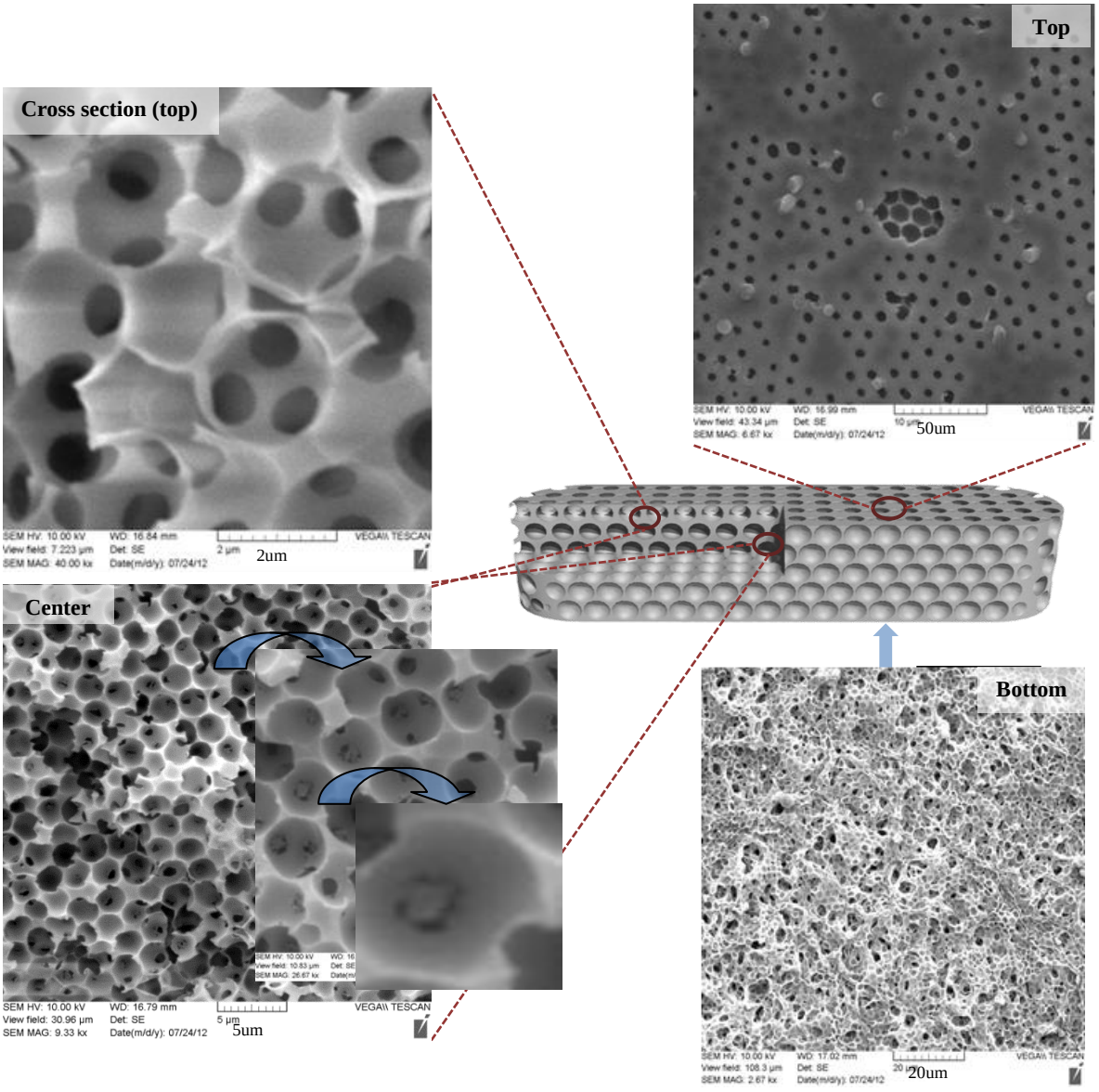

Figure 4-28 Silica macro/mesoporous monolith characteristics with 116 °C, 10min annealing

Pore Size Distribution: N_2 Absorption isotherms

The physical gas adsorption can be used to detect pores up to 100nm [140], and the N_2 adsorption properties of synthesized mesoporous silica structure was obtained by

nitrogen adsorption/desorption tests at 77K using an ASAP 2020 Nitrogen Adsorption Porosimeter. The pore size distributions of representative mesoporous silica monolith, calculated from the desorption branches of the isotherms using the Barrett-Joyner-Halanda (BJH) method, are displayed in Figure 4-24B, and the pore size distributions of the strucutre are centered around 3.65 nm with a relatively narrow pore size distriution, indicating the uniform mesoporous strucutre created via silica sol-gel process. BJH model also indicated total pore volumn of 0.3729 cc/g was presented in the material. And finally the Barrett- Emmett-Teller (BET) calculations for surface area revealed the silica monolith has BET surface area of 333 m^2/g.

The 3.65 nm pore size measured matched with the reported value for SBA-16 material synthesized using triblock copolymer [141]. Compared with BET surface value reported 810m^2/g, the obtained measurement was significant less. This could be because the removal of the polystyrene template significantly reduced the specific area of the monolith.

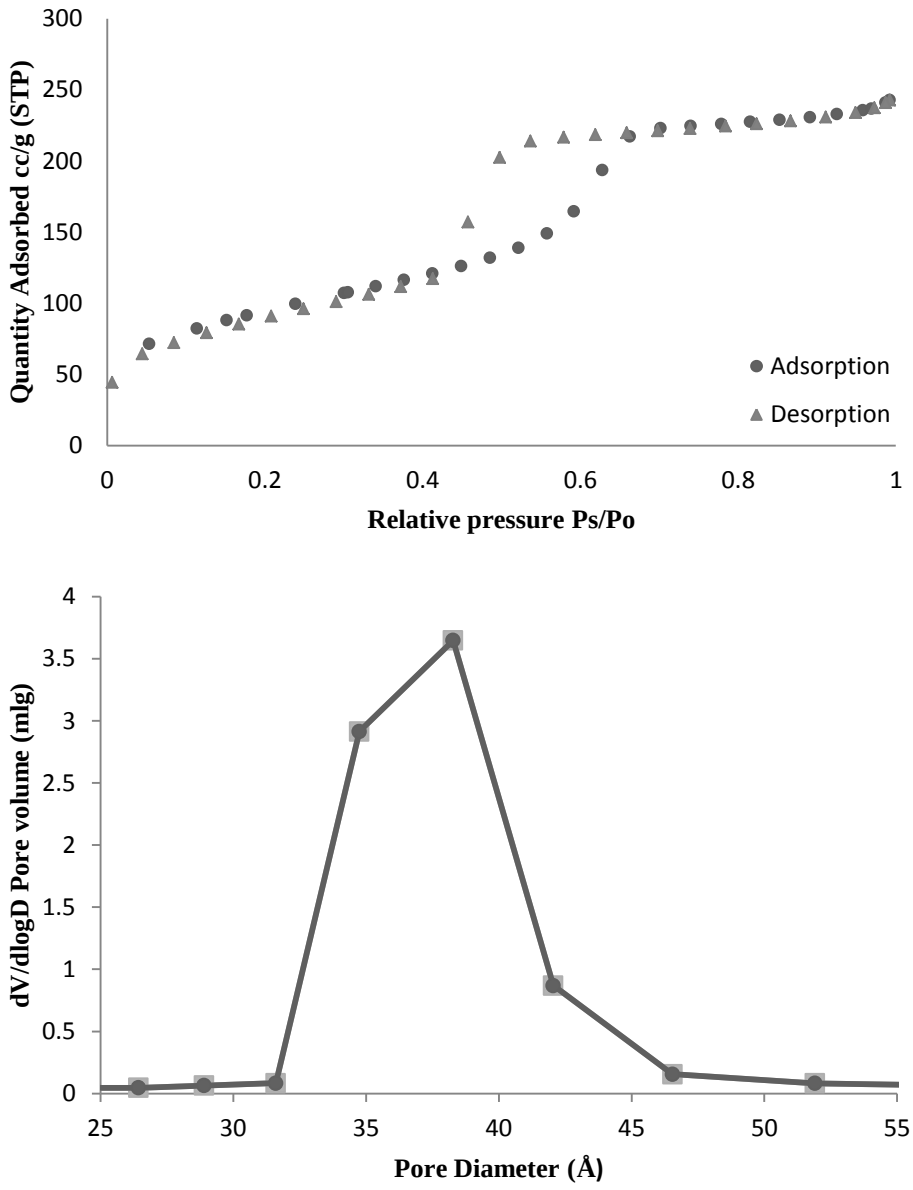

Figure 4-29 Pore size distribution curve obtained from the desorption branch of the nitrogen adsorption–desorption isotherm measurement (Dv(log d) Vs. Pore size). The mean pore diameter is 3.65 nm. The BET surface area and the total pore volume are 333 m^2/g and 0.3729 cc/g, respectively.

Thermogravimetric Analysis

Thermogravimetric analysis (TGA) was used in order to investigate the porosity of the monolith and to examine the weight composition of the polystyrene particles and silica skeleton frame, the weight percentage of polystyrene microspheres and the weight percentage of silica in a typical polystyrene and silica composite material can be calculated by keep tracking of the weight before and after volatilization of polystyrene microspheres. And the porosity can be estimated based on the density of polystyrene, F127 and silica.

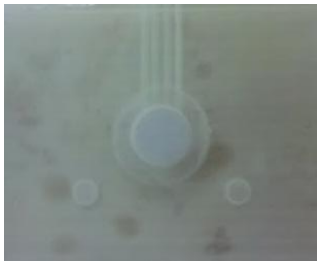

Figure 4-30 Sample preparation for TGA test

Two samples were prepared using the same pressure assisted assembly process as before, with 8.1mm diameter and 1mm depth of assembly chamber, total weight of 45mg polystyrene microspheres were packed in the chamber as shown in Figure 4-30. The first sample was the composite of polystyrene latex spheres and silica, and the second sample was the monolith made out of pure polystyrene microspheres. Water was removed from both systems using hot plate before the TGA test, and both samples were heated to 105 ℃ for one minute at the beginning of TGA test to ensure there wasn't any water residual left

in the system. As indicated in Figure 4-31, temperature was ramped up to 500 ℃ with heating rate of 10^{o}C/min after removing all water residual, and then remains at 500 ℃ to ensure complete removal of polystyrene template. Finally, it is heated up to 700^{o}C with ramp up rate of 10^{o}C/min to finish the test.

The analysis results for comparing the thermal decomposition of polystyrene particle and silica composite and of pure polystyrene are shown in Figure 4-31. Both samples started losing weight rapidly around 400^{o}C, polystyrene monolith sample quickly and completely evaporated at 450^{o}C. Polystyrene template with silica material however had a slower weight loss rate, as due to the mesoporous structure added obstacles and made it harder for vapor to escape. At temperature of 600^{o}C the total weight remains constant, which indicated all polystyrene microspheres and other organic impurities are burned off and only silica structure remained at the end. The total micro/mesoporous silica monolith weight is 6.89% of total weight. And rest of 93.11% weight can be attributed to the Polystyrene and F127.

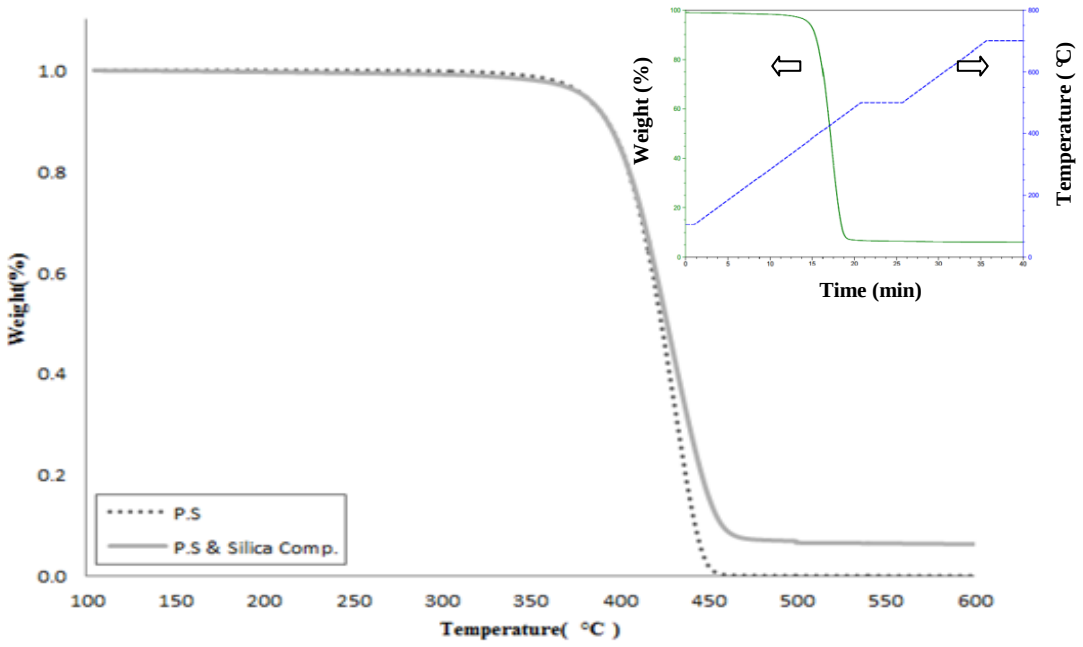

Figure 4-31 **Thermogravimetric plot obtained during calcination of materials formed from 3um latex. The latex-silica composite sample is normalized to 100% after evaporation of the residual water. The inset shows the temperature cycle vs. time.**

Equation 4-1 was used to evaluate the porosity of the final silica monolith, in this equation, ρ_1, ρ_2 and ρ_3 are density of polystyrene microspheres, density of silica [142] and the density of F127 respectively. w_1, w_2 and w_3 are weight of polystyrene microspheres, silica and F127, respectively. Substituting TGA values for silica weight and assuming a polystyrene microsphere density of 1.05g/ml [143], F127 density of 0.5 g/ml [144] and a density of mesoporous silica of 2.198g/ml [142]. The final estimated porosity calculated as 83.6%.

$$\phi = \frac{Vp}{Vt} = \frac{Pore\ Volumn}{Total\ Bulk\ Volumn} = \frac{w1/\rho1}{\frac{w1}{\rho1} + \frac{w2}{\rho2} + \frac{w3}{\rho3}}$$

Equation 4-1, Adopted from [145]

Compare with theoretical porosity calculated 79.1% based on the pore volume measurement of $0.3729 m^2/g$ and the assumption of closed packed polystyrene microspheres with filling fraction of 74%. The result is very close to the theoretical value. Combine with the observation from SEM images of the monolith and it is safe to draw the conclusion that the final porous silica structure is highly ordered and closed packed. Because of its high porosity, the monolith is very fragile and great care was taken when transferring it to the new through-hole PDMS chamber for microfluidic integration.

4.9 Multi-chamber Assembly

In order to prove that the single chamber assembly process can be easily scaled to multiple chamber assembly with minimal modifications, a seven by seven micropillar array multi-chamber fast prototyping mold has been created and used to cast and fabricate the PDMS through-hole part as shown in Figure 4-32. The $500 \times 500\ \mu m$ rectangular micropillars were spaced $500\ \mu m$ apart from one another, and the pillar features were transferred to 0.5mm thick PDMS piece and formed 49 assembly chambers.

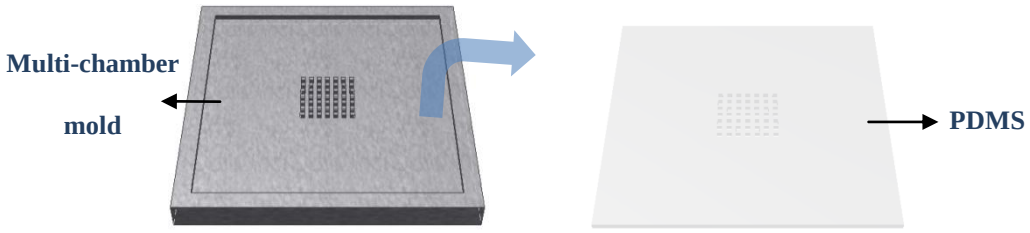

Figure 4-32 **7X7 chamber mold used for casting PDMS through-hole part**

Microcontact printing was used to bond a 13mm diameter polycarbonate membrane with multiple chamber through-hole PDMS piece, and open chambers were formed by the polycarbonate membrane and four PDMS side walls created by the pillars (Figure 4-33). The corresponding fast prototyping suction mold is used to evenly distribute the negative pressure to all assembly chambers. In addition to the old fast prototyping suction mold, a ring shaped protrution and a center star shapped pillar design was added to create a holder to support a full size 13mm AAO membrane as shown in Figure 4-34. Individual bead assembly in each chamber was then observed by using Scanning Electron Microscopy.

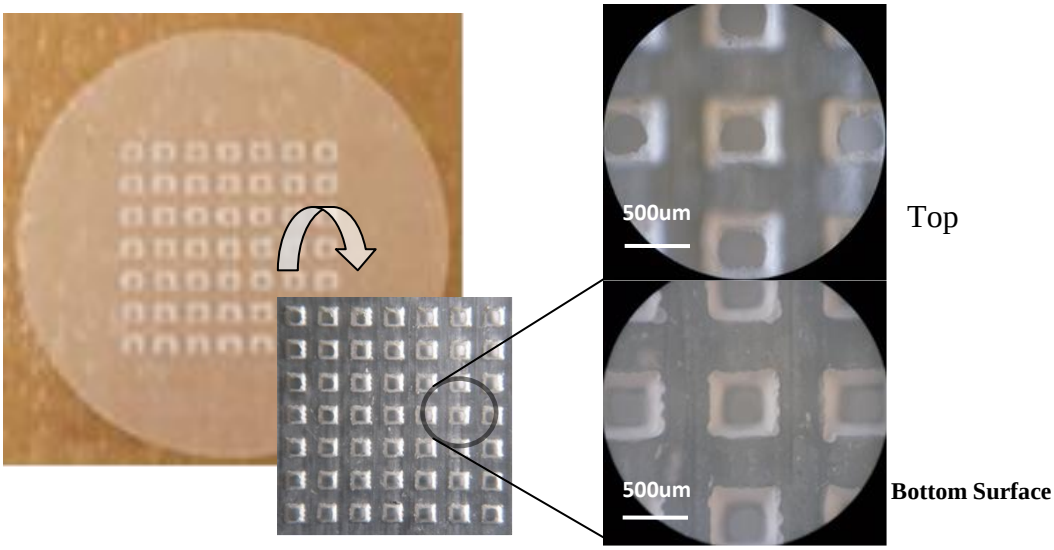

Figure 4-33 Through-hole PDMS from 7X7 array printed by 3D printer, bonded with PC membrane

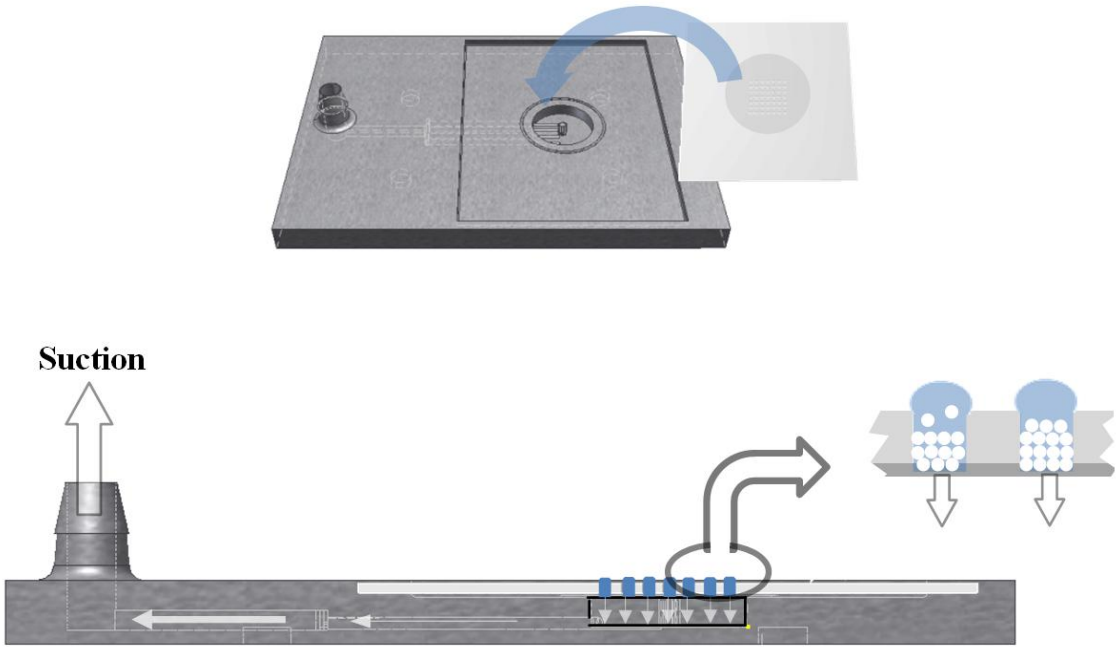

Figure 4-34 Suction assembly of PS microspheres in 7X7 assembly chambers

4.9.1 Results

The polystyrene particles were easily assembled inside all seven by seven arrays of chambers by using withdraw rate of 0.7ml/min as demonstrated in Figure 4-36, It was observed that the through-hole features was harder to create when it comes to 500μm features, with the center pillars' height raised 25μm higher above the edge of the mold, the bottom opening was only up to 300-350μm in diameter (Figure 4-36C). And it was due to the limitation of fast prototyping printer (resolution of 29μm), the edge of rectangular pillar became more rounded for smaller features like 500μm by 500μm (Figure 4-35).

The polystyrene assemblies were then heat treated at 116^{o}C for 10 minutes and the SEM images of monoliths are show in Figure 4-36. This suction assisted assembly process is very robust, even with only 30%-40% of through-opening for the multi-chamber assembly; it still can assemble and pattern polystyrene microspheres closely in a short period of time (10-20 minutes). It opens up the possibility of integrating with multiple microchannels on top and expanding the capacity of the microfluidic DNA extraction chip in the future.

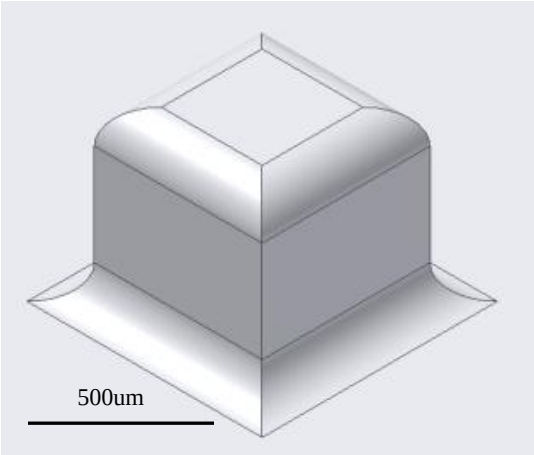

Figure 4-35 Printed 500 μmX500μm pillar feature

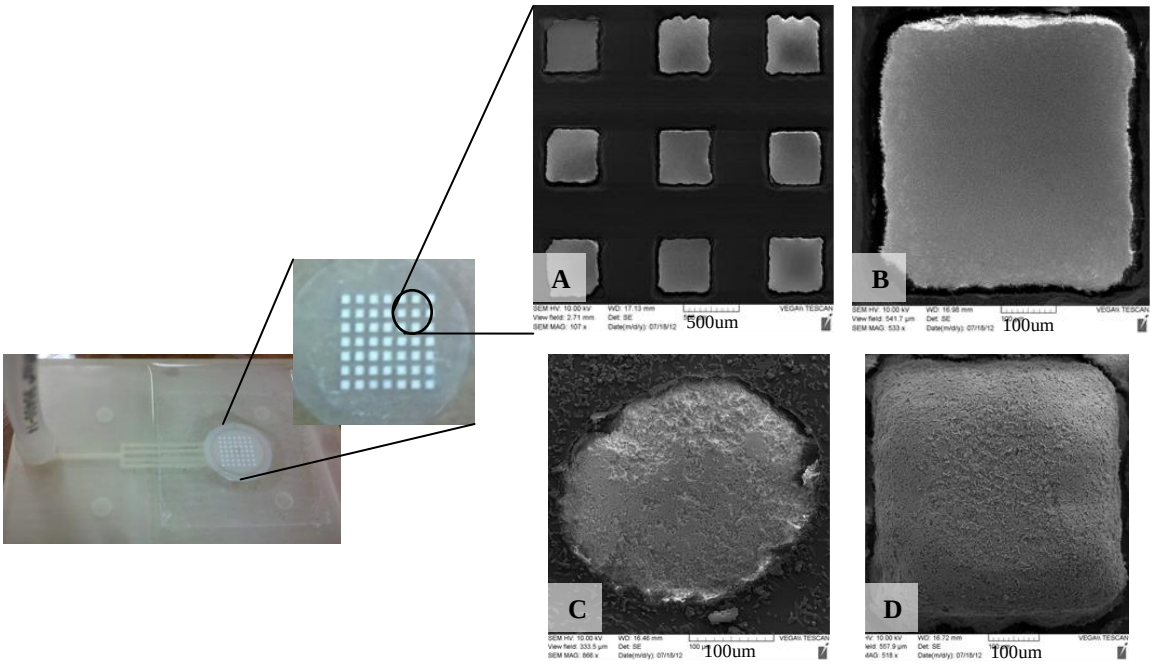

Figure 4-36 Multi-Chamber assembly, annealing at 116°C for 10min

4.10 Microfluidic Device Integration

4.10.1 Flow Visualization

The integration of a top-down configuration microfluidic device was first demonstrated by assemble 3μm plain silica microspheres (50mg/ml, Kisker Biotech) into an extraction chamber and then bonded with a top microfluidic channel and a bottom blank PDMS piece. Fluorescence tagged lipids was used to visualize sample flow inside the assembled media.

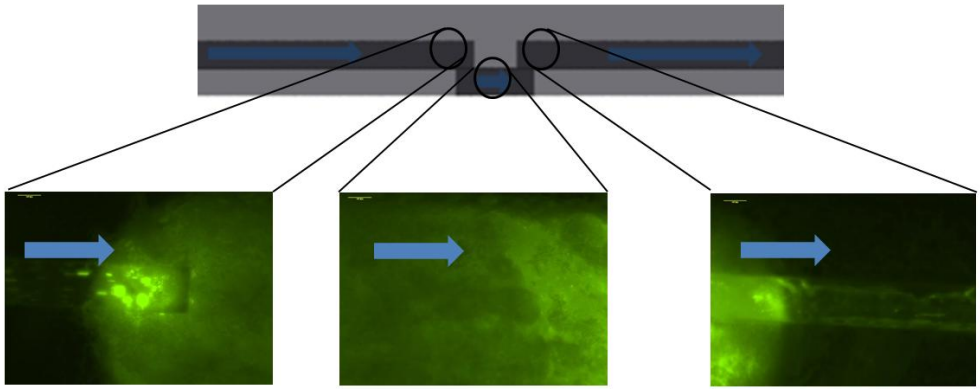

Figure 4-37 Flow visualization in an integrated device

As illustrated in Figure 4-37, the solution was flowing from the left of the microfluidic channel to the right at 1ml/hr. The fluorescent signals were uniformly distributed throughout different locations of silica assembly, which indicated fluorescence tagged lipids were able to penetrate into all particles interstitial spaces, and the sample solution was fully utilizing all available surfaces of the silica assembly.

4.10.2 Porous Monolith Integration

Once the macroporous/mesoporous silica monolith was synthesised, it was then used as a cartridge to fill in another through-hole PDMS piece. Shrinkage makes the monolith smaller than the original through-hole size, and silica sol-gel was used to apply at the chamber inner wall surfaces to 'glue' the porous silica monolith in place and the final device integration is shown in Figure 4-38.

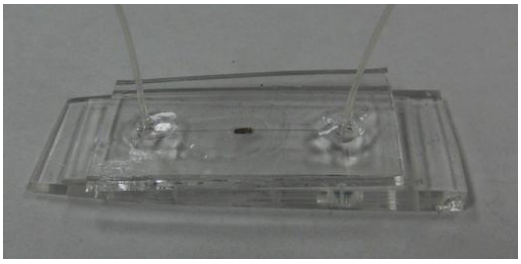

Figure 4-38 Macro/mesoporous silica monolith integration

Chapter 5 Conclusion & Recommendation

5.1 Conclusion

Continuous monitoring of pathogens that may be present in the water is one of the key preventive measures that can be used in rural areas of developed countries and developing countries to reduce chances of the water borne diseases outbreak. The traditional off-site testing of microbiological contamination requires centralized laboratories and labour intensive experimental work, the additional time delay incurred is normally undesired. Molecular biological methods such as DNA based detection based on microfluidic platforms rather than bacterial culture are being currently investigated for the rapid detection of microbiological contaminations.

Such a microfluidic system will include sample processing device that filters and accumulate target pathogens or indicator organisms such as *E. coli*, a cell lysis component that break open the cell membrane and releases nucleic acid, and a DNA extraction and purification phase where DNA are separated from proteins and other cell contaminations present in the lysate. Finally the PCR will be carried out to amplify the concentration of DNA preparing for the BioFET sensors for further identification and analysis.

In this microfluidic sample preparation system, one of the key components is the DNA extraction chip that extracts DNA from lysate solution to avoid interference causes

by lipid, protein and other cell debris in the biosensor. And the focus of the thesis will be on the fabrication of this microfluidic DNA extraction system.

The synthesis of porous silica monolith was chosen as the main technology used to create a high surface-to-volume silica surface for DNA binding column. Such column would have similar high extraction efficiency to silica resins, and the sol-gel silica structure synthesis method can yield better reproducibility comparing with other packed silica column methods. With the addition use of triblock copolymer guiding agent F127 in the sol-gel silica solution, a crack-free mesoporous silica network was created in the monolith. Furthermore, a monodispersed polystyrene microspheres soft-template assembly was used in combination of heat annealing treatment to generate a highly controllable macroporous silica structure that allows a lower pressure resistance for sample flow. The method for fabrication that has been developed is scalable and can be integrated with existing processing methods for microfluidic lab-on-chip systems.

The final macro/mesoporous silica monolith was determined to have a porosity of 83.6%. Mesopores of the silica monolith was determined by BET test to be 3.65 nm, and the macropores ranging from 0.5μm to 0.86μm were observed using SEM based on chosen annealing parameters of 115.3^{o}C for 10 minutes. The high surface-to-volume ratio of the monolith synthesized makes it possible to have a small sized monolith and large DNA molecules extraction capacity.

The TEOS and Pluronic F127 silica monolith synthesis approach was then integrated with a top-down flow configuration microfluidic device to minimize the effect

of crack and shrinkage during solidification of sol-gel process. Additionally, the concept for simultaneous assembly in multiple chambers was tested for the case where there are multiple columns in a single device.

5.2 Contributions

The contribution of this thesis primarily consist of a novel but simple methodology of assemble monodispersed microspheres into single/multiple chambers, which fabricated through fast prototyping printing technology and soft-lithography technology. The synthesis and characterization of highly controllable macro/mesoporous silica structure that can be further integrated for microfluidic DNA extraction chip.

Single Chamber & Multiple Chambers Microsphere Assembly

It was demonstrated in this thesis that assembly chamber/chambers can be fabricated via molds printed in a fast prototyping machine, and long range periodicity of polystyrene microsphere assembly can be achieved in a short period of time for both single and multiple chamber assembly with the use of negative pressure applied uniformly through the porous polycarbonate filter membrane. This method can be easily re-designed and used for other different size/material particle assembly purposes. This process is also easy to integrate with existing fabrication methods for microfluidic LoC devices.

Highly Controllable Macroporous Silica Structure

The interstitial space between adjacent microspheres can be controlled by varying the annealing temperature or duration. The effect of temperature and annealing duration on the polystyrene template was investigated and characterized. And the final size of macropores presented in the silica monolith was controlled by choosing the optimal annealing condition. And this methodology can be further expanded for creating different macropores in other materials using the soft-template technique.

5.3 Future Work

There are a number of aspects of the device that can be improved and enhanced, in order to have a uniformly temperature distribution and a similar contact length between adjacent particles throughout the polystyrene monolith, microwave pulse heating can be considered as an alternative heating method. The method was briefly tested and showed signs of uniform interstitial particle fusion-length distribution on a 2D polystyrene microsphere assembly. The microwave annealing method potentially can replace the conventional annealing oven for heat treatment of polystyrene monolith to achieve uniform macroporous, but a systematic characterization for this method is needed in order to identify the optimal parameter settings.

Although EDX test has revealed the chemical composition of the porous monolith is in fact silica, but additional tests like streaming potential measurement of integrated microfluidic system and Fourier transform infrared spectroscopy (FTIR) can be

conducted to confirm that silica material is the only surface that lysate solution will be in contact with on top surface, within pores of the silica monolith, and there is no other contaminate residual left in the porous monolith structure.

Biological validation tests need to be done on the final integrated microfluidic device to assess the capability and repeatability. Sensitivity and the capability of the device can be determined by testing the DNA recovery efficiencies at different given amount of DNA sample. In theory, the device would be able to recovery 1μg of DNA with efficiency more than 70%, and the experiment should start from recovering of 1μg of DNA and slowly reduces the amount of input DNA, until the recovery efficiency falls below our required minimal efficiency of 70%, that range would be considered as the detection limit and capability of this DNA extraction device. Similarly, the repeatability test can be identified by using a fixed amount of input DNA sample and repeatedly test the recovery efficiency on the same microfluidic chip until it falls below our requirement. Finally, real cell lysate solution which contains nucleic acid, proteins and other cell debris have to be introduced as testing sample in order to examine the real purification efficiency.

Once all these aspects of device are addressed, the device can then be fully automated by adding another cross flow channel controlled by a syringe pump to separate the washing process and the eluting process (Figure3-1). Finally, the improved microfluidic device can be integrated with upstream cell lysis device and downstream PCR and BioFET sensors for pathogen detection in real-life water samples.

REFERENCES

[1] K. Annan, “PRESS RELEASE: WATER-RELATED DISEASES RESPONSIBLE FOR 80 PER CENT OF ALL ILLNESSES, DEATHS IN DEVELOPING WORLD,” 2003. [Online]. Available: http://www.un.org/News/Press/docs/2003/sgsm8707.doc.htm.

[2] A. Prüss, D. Kay, L. Fewtrell, and J. Bartram, “Estimating the burden of disease from water, sanitation, and hygiene at a global level.,” *Environmental health perspectives*, vol. 110, no. 5, pp. 537–42, May 2002.

[3] N. J. Hoxie, J. P. Davis, J. M. Vergeront, R. D. Nashold, and K. a Blair, “Cryptosporidiosis-associated mortality following a massive waterborne outbreak in Milwaukee, Wisconsin.,” *American journal of public health*, vol. 87, no. 12, pp. 2032–5, Dec. 1997.

[4] S. E. Hrudey, P. Payment, P. M. Huck, R. W. Gillham, and E. J. Hrudey, “A fatal waterborne disease epidemic in Walkerton, Ontario: comparison with other waterborne outbreaks in the developed world.,” *Water science and technology : a journal of the International Association on Water Pollution Research*, vol. 47, no. 3, pp. 7–14, Jan. 2003.

[5] J. Bartram and S. Pedley, “Chapter 10 - MICROBIOLOGICAL ANALYSES,” 1996.

[6] K. Lemarchand, L. Masson, and R. Brousseau, “Molecular biology and DNA microarray technology for microbial quality monitoring of water.,” *Critical reviews in microbiology*, vol. 30, no. 3, pp. 145–72, Jan. 2004.

[7] G. J. Netto, R. D. Saad, and P. a Dysert, “Diagnostic molecular pathology: current techniques and clinical applications, part I.,” *Proceedings (Baylor University. Medical Center)*, vol. 16, no. 4, pp. 379–83, Oct. 2003.

[8] S. Herzer, “DNA Purification,” vol. 7, pp. 167–195, 2001.

[9] P. R. Harrison, “Selective precipitation of ribonucleic acid from a mixture of total cellular nucleic acids extracted from cultured mammalian cells.,” *The Biochemical journal*, vol. 121, no. 1, pp. 27–31, Jan. 1971.

[10] D. Lang, “Collapse of single DNA molecules in ethanol.,” *Journal of molecular biology*, vol. 46, no. 1, p. 209, Nov. 1969.

[11] S. Miller, “A simple salting out procedure for extracting DNA from human nucleated cells.,” *Nucleic acids research*, vol. 16, no. 3, p. 55404, 1988.

[12] G. D. N. A. Purification, “DNA isolation methods,” no. 1, pp. 10–13.

[13] P. Chomczynski, “Single-Step Method of RNA Isolation by Acid Guanidinium Extraction,” vol. 159, pp. 156–159, 1987.

[14] Weimin Sun, “Chapter 4 - Nucleic Extraction and Amplification,” in *Molecular Diagnostics — Techniques and Applications for the Clinical Laboratory*, San Diego: Academic Press, 2010, pp. Pages 35–47.

[15] Y. L. Tsai and B. H. Olson, “Rapid method for direct extraction of DNA from soil and sediments.,” *Applied and environmental microbiology*, vol. 57, no. 4, pp. 1070–4, Apr. 1991.

[16] M. Á. Oliva-Llaven, L. Rodríguez-Hernández, P. Mendoza-Nazar, B. Ruiz-Sesma, J. D. Álvarez-Solís, L. Dendooven, and F. a. Gutiérrez-Miceli, “Optimization of worm-bed leachate for culturing of tomato (Lycopersicon esculentum Mill) inoculated with Glomus fasciculatum and Pseudomonas fluorescens,” *Electronic Journal of Biotechnology*, vol. 13, no. 2, Mar. 2010.

[17] D. B. S. and E. J. Shrawder, “Method of isolating and purifying nucleic acids from biological samples,” *US Patent 4,935,342*, 1990.

[18] J. Willard, “Recovery of DNA for PCR amplification from blood and forensic samples using a chelating resin,” *METHODS IN MOLECULAR BIOLOGY …*, 1998.

[19] P. Walsh, D. Metzger, and R. Higuchi, “Chelex 100 as a medium for simple extraction of DNA for PCR-based typing from forensic material.,” *Biotechniques*, 1991.

[20] J. Willard, “Recovery of DNA for PCR amplification from blood and forensic samples using a chelating resin,” *METHODS IN MOLECULAR BIOLOGY …*, 1998.

[21] E. Suenaga and H. Nakamura, “Evaluation of three methods for effective extraction of DNA from human hair.,” *Journal of chromatography. B, Analytical technologies in the biomedical and life sciences*, vol. 820, no. 1, pp. 137–41, Jun. 2005.

[22] M. Lorenteb, A. Valenzuelab, A. Lorenteb, and J. C. Alvarezb, “Increasing DNA extraction yield from saliva stains with a modified Chelex method,” vol. 83, pp. 167–177, 1996.

[23] S. a Greenspoon, M. a Scarpetta, M. L. Drayton, and S. a Turek, “QIAamp spin columns as a method of DNA isolation for forensic casework.,” *Journal of forensic sciences*, vol. 43, no. 5, pp. 1024–30, Sep. 1998.

[24] QIAGEN Inc., “QIAGEN Anion-Exchange Resin,” 2012. [Online]. Available: http://www.qiagen.com/resources/info/qiagen_purification_technologies_1.aspx#binding.

[25] R. Boom, C. J. Sol, M. M. Salimans, C. L. Jansen, P. M. Wertheim-van Dillen, and J. van der Noordaa, “Rapid and simple method for purification of nucleic acids.,” *Journal of clinical microbiology*, vol. 28, no. 3, pp. 495–503, Mar. 1990.

[26] P. E. Mason, G. W. Neilson, C. E. Dempsey, a C. Barnes, and J. M. Cruickshank, “The hydration structure of guanidinium and thiocyanate ions: implications for protein stability in aqueous solution.,” *Proceedings of the National Academy of Sciences of the United States of America*, vol. 100, no. 8, pp. 4557–61, Apr. 2003.

[27] F. J. Castellino and R. Barker, “The denaturing effectiveness of guanidinium, carbamoylguanidinium, and guanylguanidinium salts.,” *Biochemistry*, vol. 7, no. 11, pp. 4135–8, Nov. 1968.

[28] J. M. Chirgwin, a E. Przybyla, R. J. MacDonald, and W. J. Rutter, “Isolation of biologically active ribonucleic acid from sources enriched in ribonuclease.,” *Biochemistry*, vol. 18, no. 24, pp. 5294–9, Nov. 1979.

[29] “QIAquick ® Spin Handbook QIAGEN Sample and Assay Technologies,” *QIAGEN*, no. March, 2008.

[30] B. Yoza, A. Arakaki, K. Maruyama, H. Takeyama, and T. Matsunaga, “Fully automated DNA extraction from blood using magnetic particles modified with a hyperbranched polyamidoamine dendrimer.,” *Journal of bioscience and bioengineering*, vol. 95, no. 1, pp. 21–6, Jan. 2003.

[31] Bioneer Corporation, “AccuBead™ Silica Coated Magnetic Bead.” [Online]. Available: http://eng.bioneer.com/products/Protein/MagneticBeads-technical.aspx. [Accessed: 08-Aug-2012].

[32] Life Technologies Inc., “Surface-Activated Dynabeads®,” 2012. [Online]. Available: http://www.invitrogen.com/site/us/en/home/Products-and-Services/Applications/Protein-Expression-and-Analysis/Protein-Sample-Preparation-and-Protein-Purification/ProteinSPProteinIso-Misc/Protein-Isolation/Surface-activated-Dynabeads.html.

[33] G. F. Steward and A. I. Culley, “Extraction and purification of nucleic acids from viruses,” *Direct*, pp. 154–165, 2010.

[34] D. Rickwood, *Centrifugation: A Practical Approach*, 2nd editio., vol. 7. IRL Press, 1989, p. 352.

[35] V. Glisin, R. Crkvenjakov, and C. Byus, “Ribonucleic acid isolated by cesium chloride centrifugation.,” *Biochemistry*, vol. 13, no. 12, pp. 2633–7, Jun. 1974.

[36] S. C. Tan and B. C. Yiap, “DNA, RNA, and protein extraction: the past and the present.,” *Journal of biomedicine & biotechnology*, vol. 2009, p. 574398, Jan. 2009.

[37] S. R. Noles, T. F. Scientific, and A. P. Manager, “Traditional Methods for CsCl Isolation of Plasmid DNA by Ultracentrifugation,” vol. 3865.

[38] D. Shapiro, “Quantitative ethanol precipitation of nanogram quantities of DNA and RNA.,” *Analytical biochemistry*, vol. 231, no. 1981, pp. 229–231, 1981.

[39] H. G. Martinson and E. B. Wagenaar, “Hydroxylapatite-catalyzed degradation of ribonucleic acid.,” *Biochemistry*, vol. 13, no. 8, pp. 1641–5, Apr. 1974.

[40] J.-H. Wang, D.-H. Cheng, X.-W. Chen, Z. Du, and Z.-L. Fang, “Direct extraction of double-stranded DNA into ionic liquid 1-butyl-3-methylimidazolium hexafluorophosphate and its quantification.,” *Analytical chemistry*, vol. 79, no. 2, pp. 620–5, Jan. 2007.

[41] D. Goldenberger, I. Perschil, M. Ritzler, D. Goldenberger, and M. Ritzler, “A simple ‘ universal ’ DNA extraction procedure using SDS and proteinase K is compatible with direct PCR amplification . A Simple ‘ Universal ’ DNA Extraction Procedure Using SDS and Proteinase K Is Compatible with Direct PCR Amplification,” pp. 368–370, 1995.

[42] D. Laboratoire, B. Moleculaire, and F. Received, “Nucleic Acids Research,” vol. 7, no. 6, pp. 1513–1523, 1979.

[43] T. Mygind, L. Østergaard, S. Birkelund, J. S. Lindholt, and G. Christiansen, “Evaluation of five DNA extraction methods for purification of DNA from atherosclerotic tissue and estimation of prevalence of Chlamydia pneumoniae in tissue from a Danish population undergoing vascular repair.,” *BMC microbiology*, vol. 3, p. 19, Sep. 2003.

[44] a. Manz, N. Graber, and H. M. Widmer, “Miniaturized total chemical analysis systems: A novel concept for chemical sensing,” *Sensors and Actuators B: Chemical*, vol. 1, no. 1–6, pp. 244–248, Jan. 1990.

[45] D. R. Reyes, D. Iossifidis, P.-A. Auroux, and A. Manz, “Micro total analysis systems. 1. Introduction, theory, and technology.,” *Analytical chemistry*, vol. 74, no. 12, pp. 2623–36, Jun. 2002.

[46] T. Vo-Dinh and B. Cullum, “Biosensors and biochips: advances in biological and medical diagnostics.,” *Fresenius’ journal of analytical chemistry*, vol. 366, no. 6–7, pp. 540–51, 2008.

[47] L. Kang, B. G. Chung, R. Langer, and A. Khademhosseini, “Microfluidics for drug discovery and development: from target selection to product lifecycle management.,” *Drug discovery today*, vol. 13, no. 1–2, pp. 1–13, Jan. 2008.

[48] S. C. Jakeway, a J. de Mello, and E. L. Russell, “Miniaturized total analysis systems for biological analysis.,” *Fresenius’ journal of analytical chemistry*, vol. 366, no. 6–7, pp. 525–39, 2000.

[49] D. J. Beebe, G. a Mensing, and G. M. Walker, “Physics and applications of microfluidics in biology.,” *Annual review of biomedical engineering*, vol. 4, pp. 261–86, Jan. 2002.

[50] T. Chován and A. Guttman, “Microfabricated devices in biotechnology and biochemical processing.,” *Trends in biotechnology*, vol. 20, no. 3, pp. 116–22, Mar. 2002.

[51] a J. Tudos, G. J. Besselink, and R. B. Schasfoort, “Trends in miniaturized total analysis systems for point-of-care testing in clinical chemistry.,” *Lab on a chip*, vol. 1, no. 2, pp. 83–95, Dec. 2001.

[52] J. Lichtenberg, N. F. de Rooij, and E. Verpoorte, “Sample pretreatment on microfabricated devices.,” *Talanta*, vol. 56, no. 2, pp. 233–66, Feb. 2002.

[53] V. Linder, “Microfluidics at the crossroad with point-of-care diagnostics,” *The Analyst*, vol. 132, no. 12, p. 1186, 2007.

[54] C. D. Chin, V. Linder, and S. K. Sia, “Commercialization of microfluidic point-of-care diagnostic devices.,” *Lab on a chip*, vol. 12, no. 12, pp. 2118–34, Jun. 2012.

[55] M. J. Cima, “Microsystem technologies for medical applications.,” *Annual review of chemical and biomolecular engineering*, vol. 2, pp. 355–78, Jan. 2011.

[56] V. Reddy and J. D. Zahn, “Interfacial stabilization of organic-aqueous two-phase microflows for a miniaturized DNA extraction module.,” *Journal of colloid and interface science*, vol. 286, no. 1, pp. 158–65, Jun. 2005.

[57] L. Christel and K. Petersen, “Rapid, automated nucleic acid probe assays using silicon microstructures for nucleic acid concentration,” *Journal of biomechanical …*, 1999.

[58] B. Vogelstein and D. Gillespie, “Preparative and analytical purification of DNA from agarose.,” *Proceedings of the National Academy of Sciences of the United States of America*, vol. 76, no. 2, pp. 615–9, Mar. 1979.

[59] N. C. Cady, S. Stelick, and C. a. Batt, “Nucleic acid purification using microfabricated silicon structures,” *Biosensors and Bioelectronics*, vol. 19, no. 1, pp. 59–66, Oct. 2003.

[60] J. Wen, L. a Legendre, J. M. Bienvenue, and J. P. Landers, “Purification of nucleic acids in microfluidic devices.,” *Analytical chemistry*, vol. 80, no. 17, pp. 6472–9, Sep. 2008.

[61] A. Manuscript, “NIH Public Access,” vol. 11, no. 9, pp. 1603–1611, 2012.

[62] H. Tian, a F. Hühmer, and J. P. Landers, “Evaluation of silica resins for direct and efficient extraction of DNA from complex biological matrices in a miniaturized format.,” *Analytical biochemistry*, vol. 283, no. 2, pp. 175–91, Aug. 2000.

[63] M. C. Breadmore, K. a Wolfe, I. G. Arcibal, W. K. Leung, D. Dickson, B. C. Giordano, M. E. Power, J. P. Ferrance, S. H. Feldman, P. M. Norris, and J. P. Landers, “Microchip-based purification of DNA from biological samples.,” *Analytical chemistry*, vol. 75, no. 8, pp. 1880–6, Apr. 2003.

[64] Y.-C. Chung, M.-S. Jan, Y.-C. Lin, J.-H. Lin, W.-C. Cheng, and C.-Y. Fan, “Microfluidic chip for high efficiency DNA extraction.,” *Lab on a chip*, vol. 4, no. 2, pp. 141–7, Apr. 2004.

[65] E. Verpoorte, “Beads and chips: new recipes for analysis.,” *Lab on a chip*, vol. 3, no. 4, p. 60N–68N, Nov. 2003.

[66] H. Andersson, W. van der Wijngaart, P. Enoksson, and G. Stemme, “Micromachined flow-through filter-chamber for chemical reactions on beads,” *Sensors and Actuators B: Chemical*, vol. 67, no. 1–2, pp. 203–208, Aug. 2000.

[67] K. J. Shaw, L. Thain, P. T. Docker, C. E. Dyer, J. Greenman, G. M. Greenway, and S. J. Haswell, “The use of carrier RNA to enhance DNA extraction from microfluidic-based silica monoliths.,” *Analytica chimica acta*, vol. 652, no. 1–2, pp. 231–3, Oct. 2009.

[68] Q. Wu, J. M. Bienvenue, B. J. Hassan, Y. C. Kwok, B. C. Giordano, P. M. Norris, J. P. Landers, and J. P. Ferrance, “Microchip-based macroporous silica sol-gel monolith for efficient isolation of DNA from clinical samples.,” *Analytical chemistry*, vol. 78, no. 16, pp. 5704–10, Aug. 2006.

[69] Q. Wu, J. M. Bienvenue, B. J. Hassan, Y. C. Kwok, B. C. Giordano, P. M. Norris, J. P. Landers, and J. P. Ferrance, “Microchip-based macroporous silica sol-gel monolith for efficient isolation of DNA from clinical samples.,” *Analytical chemistry*, vol. 78, no. 16, pp. 5704–10, Aug. 2006.

[70] X. Chen, D.-F. Cui, C.-C. Liu, and H. Li, “Microfabrication and characterization of porous channels for DNA purification,” *Journal of Micromechanics and Microengineering*, vol. 17, no. 1, pp. 68–75, Jan. 2007.

[71] X. Chen, D.-F. Cui, C.-C. Liu, and H. Li, “Microfabrication and characterization of porous channels for DNA purification,” *Journal of Micromechanics and Microengineering*, vol. 17, no. 1, pp. 68–75, Jan. 2007.

[72] M. Karle, J. Miwa, G. Roth, R. Zengerle, and F. V. Stetten, “A NOVEL MICROFLUIDIC PLATFORM FOR CONTINUOUS DNA EXTRACTION AND PURIFICATION USING,” pp. 276–279, 2009.

[73] G. Roth, R. Zengerle, and G. We, “A NOVEL MICROFLUIDIC PLATFORM FOR CONTINUOUS DNA EXTRACTION AND PURIFICATION USING LAMINAR FLOW MAGNETOPHORESIS,” *Engineering*, pp. 276–279, 2009.

[74] B. J. Hindson, D. M. Gutierrez, K. D. Ness, A. J. Makarewicz, T. R. Metz, U. S. Setlur, W. B. Benett, J. M. Loge, B. W. Colston, P. S. Francis, N. W. Barnett, and J. M. Dzenitis, “Development of an automated DNA purification module using a micro-fabricated pillar chip.,” *The Analyst*, vol. 133, no. 2, pp. 248–55, Feb. 2008.

[75] J. M. Bienvenue, N. Duncalf, D. Marchiarullo, J. P. Ferrance, and J. P. Landers, “Microchip-based cell lysis and DNA extraction from sperm cells for application to forensic analysis.,” *Journal of forensic sciences*, vol. 51, no. 2, pp. 266–73, Mar. 2006.

[76] M. Karwa, D. Hahn, and S. Mitra, “A sol–gel immobilization of nano and micron size sorbents in poly(dimethylsiloxane) (PDMS) microchannels for microscale solid phase extraction (SPE),” *Analytica Chimica Acta*, vol. 546, no. 1, pp. 22–29, Aug. 2005.

[77] “Total, Fecal & E. coli Bacteria in Groundwater,” *The British Columbia Ground Water Association*, 2007.

[78] “Guidelines for Canadian Recreational Water Quality Third Edition,” *Health Canada*, 2010.

[79] B. Matthews, H. Stratton, S. Schreoder, and S. Toze, “Pathogen Detection Methodologies for Wastewater and Reservoirs Urban Water Security Research Alliance Technical Report No . 32,” no. 32, 2010.

[80] M. G. LaMontagne, F. C. Michel, P. a Holden, and C. a Reddy, “Evaluation of extraction and purification methods for obtaining PCR-amplifiable DNA from compost for microbial community analysis.,” *Journal of microbiological methods*, vol. 49, no. 3, pp. 255–64, May 2002.

[81] X. Li, J. Zhang, and H. Gu, “Study on the adsorption mechanism of DNA with mesoporous silica nanoparticles in aqueous solution.,” *Langmuir : the ACS journal of surfaces and colloids*, vol. 28, no. 5, pp. 2827–34, Feb. 2012.

[82] K. a. Melzak, C. S. Sherwood, R. F. B. Turner, and C. a. Haynes, “Driving Forces for DNA Adsorption to Silica in Perchlorate Solutions,” *Journal of Colloid and Interface Science*, vol. 181, no. 2, pp. 635–644, Aug. 1996.

[83] N. Rohland and M. Hofreiter, “Comparison and optimization of ancient DNA extraction,” *BioTechniques*, vol. 42, no. 3, pp. 343–352, Mar. 2007.

[84] P. J. G. Andrei S. Dukhin, “Chapter 2 - Fundamentals of Interface and Colloid Science,” in *Studies in Interface Science*, Volume 24., 2010, pp. 21–89.

[85] L. L. Hench and J. K. West, “The sol-gel process,” *Chemical Reviews*, vol. 90, no. 1, pp. 33–72, Jan. 1990.

[86] D. a. . Bulla and N. . Morimoto, “Deposition of thick TEOS PECVD silicon oxide layers for integrated optical waveguide applications,” *Thin Solid Films*, vol. 334, no. 1–2, pp. 60–64, Dec. 1998.

[87] L. W. Hrubesh, “Aerogel applications,” *Journal of Non-Crystalline Solids*, vol. 225, pp. 335–342, Apr. 1998.

[88] G.-D. Kim, D.-A. Lee, J.-W. Moon, J.-D. Kim, and J.-A. Park, “Synthesis and applications of TEOS/PDMS hybrid material by the sol-gel process,” *Applied Organometallic Chemistry*, vol. 13, no. 5, pp. 361–372, May 1999.

[89] C. Brinker, “Hydrolysis and condensation of silicates: effects on structure,” *Journal of Non-Crystalline Solids*, vol. 100, pp. 31–50, 1988.

[90] J. HWA YOUNG, R. K. GUPTA, S. DONG WON, K. YOO HANG, and W. CHIN MYUNG, “Preparation and characterization of hybrid silica-poly(ethylene glycol) sonogel,” *Bulletin of the Korean Chemical Society*, vol. 23, no. 6, pp. 884–890.

[91] S. Yu, J. Geng, P. Zhou, J. Wang, A. Feng, X. Chen, H. Tong, and J. Hu, “Application of a new hybrid organic-inorganic monolithic column for efficient deoxyribonucleic acid purification.,” *Analytica chimica acta*, vol. 611, no. 2, pp. 173–81, Mar. 2008.

[92] M. Kato, K. Sakai-Kato, T. Toyo’oka, M. T. Dulay, J. P. Quirino, B. D. Bennett, and R. N. Zare, “Effect of preparatory conditions on the performance of photopolymerized sol-gel monoliths for capillary electrochromatography.,” *Journal of chromatography. A*, vol. 961, no. 1, pp. 45–51, Jun. 2002.

[93] A. Prof and S. Kaliaguine, “SBA-16 Materials Synthesis , Diffusion and Sorption Properties,” no. January, 2006.

[94] S. Chemistry, “international union of pure and applied chemistry division of physical chemistry manual of symbols and terminology for physicochemical quantities and units appendix ii,” 2001.

[95] D. Zhao, J. Feng, Q. Huo, N. Melosh, G. Fredrickson, B. Chmelka, and G. Stucky, “Triblock copolymer syntheses of mesoporous silica with periodic 50 to 300 angstrom pores,” *Science (New York, N.Y.)*, vol. 279, no. 5350, pp. 548–52, Jan. 1998.

[96] Y. Yokogawa, T. Toma, a. Saito, a. Nakamura, and I. Kishida, “Biomolecules Loading and Mesoporous SBA-15 Pore Sizes,” *Bioceramics Development and Applications*, vol. 1, pp. 1–3, 2010.

[97] F. Kleitz, T. Kim, and R. Ryoo, “Phase Domain of the Cubic Im3 h m Mesoporous Silica in the,” no. 21, pp. 440–445, 2006.

[98] Y. Sakamoto, M. Kaneda, O. Terasaki, D. Y. Zhao, J. M. Kim, G. Stucky, H. J. Shin, and R. Ryoo, “Direct imaging of the pores and cages of three-dimensional mesoporous materials.,” *Nature*, vol. 408, no. 6811, pp. 449–53, Nov. 2000.

[99] O. Trofymluk, A. a. Levchenko, S. H. Tolbert, and A. Navrotsky, “Energetics of Mesoporous Silica: Investigation into Pore Size and Symmetry,” *Chemistry of Materials*, vol. 17, no. 14, pp. 3772–3783, Jul. 2005.

[100] M. L. K. Hoa, M. Lu, and Y. Zhang, “Preparation of porous materials with ordered hole structure.,” *Advances in colloid and interface science*, vol. 121, no. 1–3, pp. 9–23, Sep. 2006.

[101] G. M. Whitesides and B. Grzybowski, “Self-assembly at all scales.,” *Science (New York, N.Y.)*, vol. 295, no. 5564, pp. 2418–21, Mar. 2002.

[102] B. a. Grzybowski, C. E. Wilmer, J. Kim, K. P. Browne, and K. J. M. Bishop, “Self-assembly: from crystals to cells,” *Soft Matter*, vol. 5, no. 6, p. 1110, 2009.

[103] Y. S. Lee, “PART I: Self-Assembly,” in *Self-assembly and nanotechnology: a force balance approach*, 2008.

[104] V. Shklover and H. Hofmann, “Methods of Self-Assembling in Fabrication of Nanodevices,” vol. 2, pp. 181–214, 2006.

[105] M. Brust and C. J. Kiely, “Some recent advances in nanostructure preparation from gold and silver particles: a short topical review,” *Colloids and Surfaces A: Physicochemical and Engineering Aspects*, vol. 202, no. 2–3, pp. 175–186, Apr. 2002.

[106] L. Isa, K. Kumar, M. Müller, J. Grolig, M. Textor, and E. Reimhult, “Particle lithography from colloidal self-assembly at liquid-liquid interfaces.,” *ACS nano*, vol. 4, no. 10, pp. 5665–70, Oct. 2010.

[107] A. S. Negi and A. K. Sood, “Electric field-enhanced sensitivity of grafted ligands and receptors.,” *Clinical chemistry*, vol. 54, no. 2, pp. 366–70, Feb. 2008.

[108] D. L. Rue, “Electrophoretic assembly of colloidal crystals with optically tunable micropatterns,” vol. 404, no. March, 2000.

[109] I. W. Hamley, “Ordering in thin films of block copolymers: Fundamentals to potential applications,” *Progress in Polymer Science*, vol. 34, no. 11, pp. 1161–1210, Nov. 2009.

[110] P. Jiang, T. Prasad, M. J. McFarland, and V. L. Colvin, “Two-dimensional nonclose-packed colloidal crystals formed by spincoating,” *Applied Physics Letters*, vol. 89, no. 1, p. 011908, 2006.

[111] J. R. Oh, J. H. Moon, H. K. Park, J. H. Park, H. Chung, J. Jeong, W. Kim, and Y. R. Do, “Wafer-scale colloidal lithography based on self-assembly of polystyrene nanospheres and atomic layer deposition,” *Journal of Materials Chemistry*, vol. 20, no. 24, p. 5025, 2010.

[112] C.-M. Hsu, S. T. Connor, M. X. Tang, and Y. Cui, “Wafer-scale silicon nanopillars and nanocones by Langmuir–Blodgett assembly and etching,” *Applied Physics Letters*, vol. 93, no. 13, p. 133109, 2008.

[113] A. R. Tao, J. Huang, and P. Yang, “Langmuir-Blodgettry of nanocrystals and nanowires.,” *Accounts of chemical research*, vol. 41, no. 12, pp. 1662–73, Dec. 2008.

[114] Z. Lu, W. Ruan, N. Ji, L. Ren, Q. Cong, and B. Zhao, “Fabrication of Large-scale Nanostructure by Langmuir-Blodgett Technique,” *Journal of Bionic Engineering*, vol. 3, no. 2, pp. 59–62, Jun. 2006.

[115] S. H. Park, D. Qin, and Y. Xia, “Crystallization of Mesoscale Particles over Large Areas,” *Advanced Materials*, vol. 10, no. 13, pp. 1028–1032, Sep. 1998.

[116] O. D. Velev and A. M. Lenhoff, “Colloidal crystals as templates for porous materials,” *Current Opinion in Colloid & Interface Science*, vol. 5, no. 1–2, pp. 56–63, Mar. 2000.

[117] C. W. Price, D. C. Leslie, and J. P. Landers, “Nucleic acid extraction techniques and application to the microchip.,” *Lab on a chip*, vol. 9, no. 17, pp. 2484–94, Sep. 2009.

[118] J. Lee, J. U. Ha, S. Choe, C.-S. Lee, and S. E. Shim, “Synthesis of highly monodisperse polystyrene microspheres via dispersion polymerization using an amphoteric initiator.,” *Journal of colloid and interface science*, vol. 298, no. 2, pp. 663–71, Jun. 2006.

[119] K.E.J. Barrett, “Dispersion Polymerization in Organic Media.” John Wiley & Sons, Inc., 1975.

[120] C. M. Tseng, Y. Y. Lu, M. S. El-Aasser, and J. W. Vanderhoff, “Uniform polymer particles by dispersion polymerization in alcohol,” *Journal of Polymer Science Part A: Polymer Chemistry*, vol. 24, no. 11, pp. 2995–3007, Nov. 1986.

[121] K. Ouek and K. Ober, “Particle size control in dispersion polymerization of polystyrene,” no. 7, 1985.

[122] C. E. Wilkes, C. A. Daniels, and W. Summers, *PVC Handbook*. 2005.

[123] J. C. McDonald and G. M. Whitesides, “Poly(dimethylsiloxane) as a material for fabricating microfluidic devices.,” *Accounts of chemical research*, vol. 35, no. 7, pp. 491–9, Jul. 2002.

[124] Y. Xia, J. Tien, D. Qin, and G. M. Whitesides, “Non-Photolithographic Methods for Fabrication of Elastomeric Stamps for Use in Microcontact Printing,” vol. 7463, no. 14, pp. 4033–4038, 1996.

[125] S.-H. Kim, C.-K. Shin, C.-H. Ahn, and G.-J. Kim, “Syntheses and application of silica monolith with bimodal meso/macroscopic pore structure,” *Journal of Porous Materials*, vol. 13, no. 3–4, pp. 201–205, Aug. 2006.

[126] SPI Supplies, “ANOPORE^{TM} Inorganic Aluminum Oxide Membrane Filters.” [Online]. Available: http://www.2spi.com/catalog/spec_prep/filter2.shtml.

[127] R. Xie, L. Chu, W. Chen, W. Xiao, H. Wang, and J. Qu, “Characterization of microstructure of poly(-isopropylacrylamide)-grafted polycarbonate track-etched membranes prepared by plasma-graft pore-filling polymerization,” *Journal of Membrane Science*, vol. 258, no. 1–2, pp. 157–166, Aug. 2005.

[128] D. C. Duffy, J. C. McDonald, O. J. Schueller, and G. M. Whitesides, “Rapid Prototyping of Microfluidic Systems in Poly(dimethylsiloxane).,” *Analytical chemistry*, vol. 70, no. 23, pp. 4974–84, Dec. 1998.

[129] J. C. Mcdonald, D. C. Duffy, J. R. Anderson, and D. T. Chiu, “Review General Fabrication of microfluidic systems in poly (dimethylsiloxane),” 2000.

[130] G. S. Fiorini and D. T. Chiu, “Disposable microfluidic devices: fabrication, function, and application.,” *BioTechniques*, vol. 38, no. 3, pp. 429–46, Mar. 2005.

[131] Y. Xia and G. M. Whitesides, “SOFT LITHOGRAPHY,” no. 12, 1998.

[132] J. C. Mcdonald, D. C. Duffy, J. R. Anderson, and D. T. Chiu, “Review General Fabrication of microfluidic systems in poly (dimethylsiloxane),” 2000.

[133] H. P. Parts, “The Highest Defi nition Hard Plastic Parts Functional 3D Printing.”

[134] H. Wu, B. Huang, and R. N. Zare, “Construction of microfluidic chips using polydimethylsiloxane for adhesive bonding.,” *Lab on a chip*, vol. 5, no. 12, pp. 1393–8, Dec. 2005.

[135] H. Qi, W. Hao, H. Xu, J. Zhang, and T. Wang, “Synthesis of large-sized monodisperse polystyrene microspheres by dispersion polymerization with dropwise monomer feeding procedure,” *Colloid and Polymer Science*, vol. 287, no. 2, pp. 243–248, Dec. 2008.

[136] S. T. Ha, O. O. Park, and S. H. Im, “Size control of highly monodisperse polystyrene particles by modified dispersion polymerization,” *Macromolecular Research*, vol. 18, no. 10, pp. 935–943, Nov. 2010.

[137] W. Jo, K. J. Freedman, D. K. Yi, and M. J. Kim, “Fabrication of tunable silica-mineralized nanotubes using flagella as bio-templates.,” *Nanotechnology*, vol. 23, no. 5, p. 055601, Feb. 2012.

[138] J. L. Gurman, L. Baier, and B. C. Levin, “Polystyrenes : A Review of the Literature on the Products of Thermal Decomposition and Toxicity,” vol. 11, no. January, pp. 109–130, 1987.

[139] Y. Chen, Z. Zhang, X. Sui, J. D. Brennan, and M. a. Brook, “Reduced shrinkage of sol–gel derived silicas using sugar-based silsesquioxane precursors,” *Journal of Materials Chemistry*, vol. 15, no. 30, p. 3132, 2005.

[140] J. C. Groen, “Porosity and Surface Area- Assessment by physical characterization techniques.”

[141] T. Yamada, H. Zhou, K. Asai, and I. Honma, “Pore size controlled mesoporous silicate powder prepared by triblock copolymer templates,” vol. 56, no. September, pp. 93–96, 2002.

[142] W. A. James F . Shackelford, Ed., *CRC Materials Science and Engineering Handbook, Third Edition*, vol. 232, no. 4757. 1986, p. 1485.

[143] S. Aldrich, “Polystyrene Latex Beads: Product Information,” 1947.

[144] Brenntag Canada Inc., “MSDS: Basf pluronic f 127,” no. 604, 2007.

[145] Paul Glover, “Chapter 5 : Porosity,” *Formation Evaluation MSc Course Notes*, vol. V, no. xiii, pp. 43–53.

APPENDIX I: TEMPERATURE DIFFERENCE BETWEEN SUBSTRATE AND AIR

Tdisp ^{o}C	100	105.1	110.0	115.0	120.0	125.0	130.0	135.0	140.0	145.0
Tair ^{o}C	86.4	89.5	93.5	98.0	102.0	107.0	110.7	116.3	120.2	124.3
Track ^{o}C	90.0	94.3	98.3	102.9	107.2	112.3	115.5	122.2	124.2	128.5

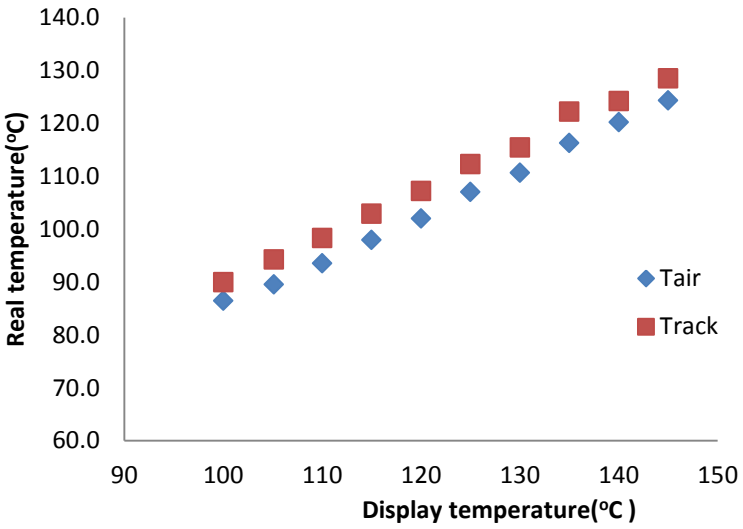

APPENDIX II: SU8-100 MOLD FRABRICATAION

- Wash silicon wafer in acetone solution for one minute
- Methanol wash and blow dry with nitrogen
- Place wafer in plasma etcher at 50Watt for 1 minute
- Spin Su-8-100 photoresist on the wafer at 500 rpm for 20 second
- Ramp up the speed to 2750 rpm at an acceleration of 100 rpm/s and spin at final speed for 40 second
- Prebake the wafer at 65 ℃ for 15 minutes
- Increase the pre-baking temperature to 95 ℃ in 5 minutes
- Bake the wafer at 95 ℃ for the period of 30 minutes
- Align the wafer and photomask on mask aligner
- Expose the wafer to UV light for a total exposure energy of 600 mJ/cm^2
- Post bake at 65 ℃ for 1 minute
- Increase post bake temperature to 95 ℃ and maintain the temperature for 10 minutes
- Submerge wafer into developer solution and slowly stir until the features are clear
- Isopropyl alcohol check for complete removal of unexposed photoresist
- Re-submerge wafer back in developer solution if white residual appears
- DI water rinse and blow dry with nitrogen